DEVELOPMENT OF LASER-INDUCED FLUORESCENCE DETECTION DEVICES FOR ASTROBIOLOGICAL AND PLANETARY SCIENCE APPLICATIONS

A Dissertation
Presented to
The Academic Faculty

by

Zachary Duca

In Partial Fulfillment
Of the Requirements for the Degree
Doctor of Philosophy in Chemistry

Georgia Institute of Technology

August 2020

DEVELOPMENT OF LASER-INDUCED FLUORESCENCE DETECTION DEVICES FOR ASTROBIOLOGICAL AND PLANETARY SCIENCE APPLICATIONS

Approved by:

Dr. Amanda M. Stockton, Advisor
School of Chemistry and Biochemistry
Georgia Institute of Technology

Dr. Britney E. Schmidt
School of Earth and Atmospheric Sciences
Georgia Institute of Technology

Dr. Loren D. Williams
School of Chemistry and Biochemistry
Georgia Institute of Technology

Dr. Facundo M. Fernandez
School of Chemistry and Biochemistry
Georgia Institute of Technology

Dr. Bridgette A. Barry
School of Chemistry and Biochemistry
Georgia Institute of Technology

Date Approved: July 23, 2020

ACKNOWLEDGEMENTS

I thank Aaron Noell from the Jet Propulsion Laboratory for providing insight into the parts selection during the early development of this system. His support was integral to the initial design phase of my benchtop μCE-LIF detection system. I recognize Alison Skelley, William Grover, and Robin Ivester for their efforts in developing and fabricating the devices used in this work. I also acknowledge Anna Butterworth and the SSL team for their conversations regarding this work and its applications to Planetary Organic Analyzers in development there, including the MOA and EOA.

I thank Morgan Cable from the Jet Propulsion Laboratory for serving as my NSTRF advisor and my group members at Georgia Tech for their support and assistance throughout the years. Particularly, I distinguish Giorgio Morbioli, Nicholas Speller, Scot Sutton, Michael Cato, and George Tan for their daily conversations, often relieving much of the strain associated with particularly challenging days in lab. I acknowledge my committee members Prof. Loren Williams, Prof. Bridgette Barry, Prof. Britney Schmidt, and Prof. Facundo Fernandez for their project insight, and I thank my advisor Prof. Amanda Stockton for her unwavering guidance during my tenure at Georgia Tech. Lastly, I thank my family for their continued support during my pursuit of a doctorate in Chemistry.

This work was supported by a NASA Space Technology Research Fellowship, the state of Georgia, and Georgia Institute of Technology, jointly by NSF and the NASA Astrobiology Program, under the NSF Center for Chemical Evolution, CHE-1504217, and NASA ROSES under NNH16ZDA001N-MATISSE via subcontract from Berkeley Space Sciences Laboratory.

TABLE OF CONTENTS

LIST OF TABLES

LIST OF FIGURES

LIST OF SYMBOLS AND ABBREVIATIONS

AED	Automated external defibrillator
APD	Avalanche photodiode
ASD	Analytical Spectral Devices
aSi	Amorphous polysilicon
BCE	Before common era
BP	Bandpass
CAD	Computer-Aided Design
CCE	Center for Chemical Evolution
CDA	Cosmic Dust Analyzer
cDAQ	Compact Data Acquisition
CE	Common era
CEC	Capillary electrochromatography
CGE	Capillary gel electrophoresis
CIEF	Capillary isoelectric focusing
CITP	Capillary isotachophoresis
Cl^-	Chloride ion
CLD	Compact laser diode
cm	Centimeter
CZE	Capillary zone electrophoresis
d	Distilled
DI	Deionized
DMF	Dimethylformamide
DNA	Deoxyribonucleic acid
DNA	Deoxyribonucleic acid
DO	Digital output
E	Electric field strength
EDTA	Ethylenediaminetetraacetic acid
ELISA	Enzyme-linked immunosorbent assay
EOA	Enceladus Organic Analyzer

ESA	European Space Agency
f	Drag force of solvent
G	Earth-g
g	Gram
+G	Right-side up, directly in line with Earth's gravitational field
-G	Upside down, directly opposing Earth's gravitational field
GC	Gas chromatography
GLUE	Green Low-cost User-friendly Expedient
H_2CO_3	Carbonic acid
H_2SO_4	Sulfuric acid
HCl	Hydrochloric acid
HEPA	High-efficiency particulate air
HF	Hydrofluoric acid
hr	Hour
HV	High voltage
IMPOA	Impact Penetrator Organic Analyzer
InGaN	Indium-Gallium-Nitride
INMS	Ion Neutral Mass Spectrometer
INMS	Ion and Neutral Mass Spectrometer
JUICE	JUpiter Icy Moon Explorer
LabVIEW	Laboratory Virtual Instrument Engineering Workbench
LED	Light-emitting diode
LHD	Lee's High Density Interface
LIF	Laser-induced fluorescence
LOD	Limit of detection
LP	Longpass
LUCA	Last universal common ancestor
m	Meter
M	Molar
MATISSE	Maturation of Instruments for Solar System Exploration
mbar	Millibar
M_c	Size of the active chain between cross-linking points

MECA	Microscopy, Electrochemistry, and Conductivity Analyzer
MEKC	Micellar electrokinetic capillary chromatography
Mg^{2+}	Magnesium ion
$MgSO_4$	Magnesium sulfate
min	Minute
mM	millimolar
mm	Millimeter
MOA	Mars Organic Analyzer
MOAB	Microfabricated Organic Analyzer for Biosignatures
ms	Millisecond
MS	Mass spectrometry
MSL	Mars Science Laboratory
MTBSTFA	*N*-methyl-*N*-*tert*-butyldimethylsilyl-trifluoroacetamide
MΩ	Megaohm
N	Separation efficiency in theoretical plates
NA	Numerical aperature
Na^+	Sodium ion
Na_2CO_3	Sodium carbonate
NaOH	Sodium hydroxide
NASA	National Aeronautics and Space Administration
NIR	Near infrared
nM	Nanomolar
NSF	National Science Foundation
NSTRF	NASA Space Technology Research Fellowship
PAH	Polycyclic aromatic hydrocarbon
PB	Pacific Blue
PCR	Polymerase chain reaction
PD	Silicon photodiode
PDMS	Polydimethylsiloxane
pH	Power of hydrogen
PICASSO	Planetary Instrument Concepts for the Advancement of Solar System Observations
pM	Picomolar

PMA	Programmable microfluidic architecture (or array)
PMT	Photomultiplier tube
POC	Point of care
ppth	Parts-per-thousand
pptr	Parts-per-trillion
PSTAR	Planetary Science and Technology through Analog Research
PWR	Power
q	Net charge of molecule
r	Radius of molecule
R	Resolution
RIE	Reactive-ion etching
ROSES	Research Opportunities in Space and Earth Science
RT	Room temperature
s	Seconds
S/N	Signal-to-noise
SAM	Sample Analysis at Mars
SE	Succinimidyl ester
SiO^-	Deprotonated silanol
SiPM or PM	Silicon photomultiplier
SM	Single mode
SO_4^{2-}	Sulfate ion
SPD	Speed
SSL	Space Sciences Laboratory
STR	Short tandem repeat
TEC	Thermoelectric cooler
t_r	Retention time
t_{r1} and t_{r2}	Retention times of two adjacent peaks
TV	Thermal volatilization
U	10x10x10 cm single unit of CubeSat
UV	Ultraviolet
V	Volts
v_{eof}	Electroosmotic flow

v_{ep}	Electrophoretic flow
VIS	Visible
v_t	Total velocity
w	Width of peak
w_1 and w_2	Width of two adjacent peaks
WCL	Wet Chemistry Laboratory
WD	Working distance
ϵ	Dielectric constant of buffered solution
µCE	Microcapillary electrophoresis
μ_{ep}	Electrophoretic mobility
µL	Microliter
µM	Micromolar
µm	Micrometer
µTAS	Micro-total analysis system
η	Viscosity of solution
ζ	Zeta potential

SUMMARY

Microcapillary electrophoresis (μCE) enables high-resolution separations in miniaturized, automated microfluidic devices. Pairing this powerful separation technique with laser-induced fluorescence (LIF) enables highly-sensitive, quantitative, and compositional analysis of organic molecule monomers and short polymers, which are essential, ubiquitous components of life on Earth. Improving methods for their detection has applications to multiple scientific fields, particularly those related to medicine, industry, and space science. This research focuses on the latter of these fields through advancement of organic molecule detection techniques for biosignature detection missions to celestial bodies within our Solar System, such as Europa. Plume activity and evidence supporting a global subsurface ocean have made Europa a high-priority target for future NASA outer-planetary missions. *In situ* quantitative and compositional analysis of organic molecules in the plumes or subsurface ocean of Europa would provide relevant, detailed information on formation, habitability, and on-going planetary processes of these celestial bodies and could provide the first evidence of the potential for extant life beyond Earth.

A modular benchtop microcapillary electrophoresis with laser-induced fluorescence (μCE-LIF) detection system was constructed and tested by analyzing standard amino acid samples of valine, serine, alanine, glycine, glutamic acid, and aspartic acid in multiple borate buffered solutions of increasing concentrations from 10-50 millimolar (mM), all pH 9. The 35 mM borate buffer solution generated the highest resolution before Joule heating dominated. The limits of detection (LODs) of alanine and glycine using 35 mM borate buffer were found to be 2.12 nanomolar (nM) and 2.91 nM, respectively,

comparable to other state-of-the-art μCE-LIF instruments using a spectrometer as a detector. Furthermore, the microdevice is easily exchanged to fit the desired application of the system and optical components within the central filter cube can be easily replaced to target alternative fluorescent dyes.

Using the benchtop μCE-LIF detection system, high-resolution separations of an amino acid standard solution, including valine, serine, alanine, glycine, glutamic acid, and aspartic acid, contained within icy moon analogue solutions of sulfuric acid, carbonic acid, sodium carbonate, and magnesium sulfate were obtained. Separations were improved by diluting the salts in solution, regulating the pH, and sequestering cations with ethylenediaminetetraacetic acid (EDTA). Using these methods, an icy moon (Enceladus/Europa) analogue sample taken from Champagne Geyser at Chaffin Ranch in Utah was analyzed for amino acids and found to contain leucine, valine, serine, alanine, and glycine by direct comparison to spiked standards. Alanine and glycine were quantified via standard curve at 80.1 ± 0.8 μM and 900 ± 100 nM, respectively, while leucine, valine, serine, and glycine again were quantified at 4.4 ± 0.8 μM, 830 ± 80 nM, 780 ± 60 nM, and 1.0 ± 0.2 μM, respectively.

To begin developing the μCE-LIF technique for an outer-planetary mission setting, a pneumatically-actuated monolithic membrane microdevice fabricated in 2005 was functionally tested after 10 years of storage under ambient conditions. Using a square wave with a 500 millisecond (ms) actuation pulse width and a 1000 ms period and operating under vacuum at -980 millibar (mbar) from ambient pressure, all microvalves opened in less than 1 hour. The vacuum required to actuate an open valve ranged from -218 to -175 mbar from ambient pressure. The microvalves were then programmed to transfer fluid

through the microdevice for flow rate characterization. Fluidic transfer occurred at a flow rate of 122 ± 8 microliters/minute (μL/min) right-side up in Earth's gravitational field and 110 ± 10 μL/min upside down in Earth's gravitational field. These results addressed (1) a concern that these systems may have a limited shelf-life and (2) a concern that performance depends specific device orientation in a gravitational field, indicating likely successful implementation in an orbital microgravity environment after an extended period in storage.

To further develop the μCE-LIF technique for an outer-planetary mission setting, the effect of drying 10+-year-old Pacific Blue (PB) dye with amino acids was examined by performing a set of three experiments: a liquid control where every solution was mixed normally in its liquid form, a partial-liquid control where each solution was dried using a spin vacuum and resuspended to mix before adding liquid PB, and a dry test where each solution was dried using a spin vacuum and resuspended to mix after adding dry PB. The partial-liquid control showed a similar signal-to-noise (S/N) intensity when compared to the liquid control, while S/N of the organics for the dry test displayed a reduction in intensity. However, statistical analysis revealed that only the aspartic acid dry test was significantly different than the liquid and partial-liquid controls. A likely cause of this decreased signal for aspartic acid was the hydrolysis of PB. A 2x excess of PB when stored with amino acids would alleviate any potential loss in S/N. These results indicate that PB dye can retain sufficient reactivity when stored dry with amino acid standards.

To minimize mass, size, and power, a portable lens tube LIF detection prototype was developed to quantify bulk organics in a liquid sample. A limit of detection (LOD) analysis was performed by reacting various concentrations of leucine with fluorescamine dye in 35 mM borate buffer, pH 8.5. The LOD was found to be 11.8 μM, an excellent

benchmark for a prototype LIF detection system of its unique design. Automated analyses were performed using a fast-prototyped microfluidic processor and showed no statistically-significant differences when compared to the manual analyses. A sample (Y31B) collected from the Atacama Desert in Yungay, Chile, was analyzed manually and found to contain 300 ± 50 μM of bulk amines. When analyzed using the automated microfluidic processor, the sample was found to contain statistically equivalent 289 ± 4 μM of bulk amines. These results show the promise of using automated microdevices and portable lens tube LIF detection systems in more restricting environments, like those on Europa and Enceladus.

Quantitative, compositional, and chiral analysis of small organic molecules *in situ* provides important information for studying planetary formation and evolution, and, more excitingly, also can provide signatures of past or present life. MicroCE-LIF detection is a unique technique currently ready for further development for space flight that has the resolution, selectivity, and sensitivity to provide these analyses. While lander or fly-by missions have largely been the focus for the development of μCE-LIF, as proposed in the Mars Organic Analyzer (MOA) and Enceladus Organic Analyzer (EOA), there has been limited development of LIF detection systems for more extreme environments, like the surfaces of the icy moons Europa and Enceladus. This demonstration that microdevices retain full functionality after over 10 years of storage, the successful separation and detection of organic molecules contained within an icy moon analogue sample using a μCE-LIF benchtop system, and the quantification of organics in a planetary analogue sample using a miniaturized lens tube LIF detection system represent a significant step forward for the liquid-based analysis of small organic molecules and biopolymers for future space missions to icy bodies like Europa and Enceladus.

CHAPTER 1. INTRODUCTION

1.1 Background

1.1.1 Historical Motivation of Astrobiology

The field of astronomy has held a firm position in society for millennia, dating as far back as ancient Mesopotamia. In fact, a particularly important development during this period was a concept pioneered by the Babylonians known as astrometry, the mathematical mapping of the night sky. Other civilizations benefitted greatly from this scientific advancement and many established astrological beliefs based on their individual surveying of the stars and planets. As these civilizations developed and changed, so did their views of astronomy. One of the most significant turning points in the field came with Ptolemy's creation of the Almagest in the second century common era (CE) [1]. While a geocentric model of the universe was the general theory among much of the known world at the time, the concept became universally accepted with this document. It was not until the radical free-thinking environment of the Renaissance in the sixteenth century CE when scientists began to alter their views on the topic. During this time, Nicholaus Copernicus presented "On the revolution of heavenly spheres," a mathematical model of a heliocentric universe [2]. This concept had existed since the third century before common era (BCE) but was not widely accepted. However, with major advancements in technology, including more powerful telescopes, precise mapping techniques, and improved cataloging, other scientists began to support his claims. After more than a century and with the support of Johannes Kepler's elliptical orbit theory of the planets and Sir Isaac Newton's laws of motion, the Copernican model was adopted [3, 4].

While Copernicus' understanding of a Sun-centered Solar System was correct, the idea of a Sun-centered universe has since been rebutted. Over the course of the eighteenth and nineteenth centuries, scientists gradually realized there was no one true center of the universe and that the universe is constantly expanding [5]. In the early twentieth century, Edwin Hubble played a critical role in providing definitive proof of galaxies outside of our own. The technological advancements and discoveries made during this time bolstered the world's interest in the cosmos, and new questions about our Solar System and the surrounding universe arose, resurfacing the idea of cosmic pluralism. Dating as far back as the sixth century BCE in the teachings of the Greek philosopher Anaximander, the notion of extraterrestrial life began to reemerge around the time of Copernicus with the radical beliefs of Giordano Bruno. While whisperings of the concept remained, research within the area did not gain traction until the Miller-Urey experiment of 1953, which demonstrated the first spontaneous creation of some of the necessary molecules of life as we know it [6]. These experiments paved the way for the creation of the "exobiology" program, later dubbed "astrobiology" in 1995.

The field of astrobiology is intended to seek answers to the mysteries of life within the context of the universe as a whole [7, 8]. Specifically, the program aims to answer three main questions: (1) How does life begin and evolve? (2) Does life exist elsewhere in our Solar System or surrounding universe? (3) How do we search for and detect life in the universe? Attempts to answer these questions require leading scientists from a range of fields, including astronomy, biology, chemistry, physics, geology, aerospace and mechanical engineering, etc…, making astrobiology one of the most interdisciplinary sciences. From the Urey-Miller experiments to the present, scientists have made

exceptional strides towards a more complete understanding of life in the cosmos, including constructing cutting-edge telescopes on Earth and in space, sending dozens of advanced scientific instrument-filled spacecraft to the far reaches of the Solar System and beyond, and expanding efforts to discover and classify the organisms living on Earth. However, even with what we have discovered about our Solar System and the universe, much is still shrouded in mystery, and a finalized understanding of life in the universe will likely take generations to achieve.

1.1.2 Life on Earth

To begin to answer the questions of life in the universe, scientists must first gain a firm understanding of life and its essential processes on Earth. Since Earth is our only confirmed location to harbor life, using our planet as a template for experiments is our only starting point. From what we know, life here requires an energy source and liquid water to survive and, in fact, tends to thrive in water-rich environments. In addition, life has shown a propensity to adapt and survive in extreme environments, such as those with limited water supplies, extreme temperatures, high salinity, etc… [9]. These organisms are known as extremophiles and have largely been considered models for what we may expect when searching for life elsewhere. Their characteristics have shaped much of the science of past and future life discovery missions on Earth and within our Solar System, including the planetary protection rules in place so that no craft or technique contaminates a target of interest [10]. In addition to extremophiles, scientists have even traced much of the lineage of the origins of life on Earth through the expansion of the ribosomal subunit in an attempt to find the last universal common ancestor (LUCA) [11-13]. Although a definitive LUCA has not been identified, the search for Earth-based life in extreme or extraterrestrial

locations will likely involve probing for the most basic elements of organisms, such as the 20 common amino acids, an energy source, and possibly even evidence of a system for transferring biological information.

1.1.3 Mission Development

1.1.3.1 Early Stage

Searching for biosignatures within our Solar System, especially with the goal of sample return, can incur high costs and take years to accomplish. Therefore, the use of automated, *in situ* techniques and in-depth studies perfecting the search methods are imperative. Programs like that of Planetary Instrument Concepts for the Advancement of Solar System Observations (PICASSO) promote early development of potential mission instruments, while the Maturation of Instruments for Solar System Exploration (MatISSE) program supports the later-stage development of techniques specifically geared towards future planetary science missions. In addition to instrument development programs, NASA's Planetary Science and Technology through Analog Research (PSTAR) program emphasizes testing of scientific methods in Earth-analogue environments relevant to outer-planetary missions. While these programs are not exhaustive to what is available, they serve as an example of the steps necessary for undergoing a successful mission to another planetary body within the Solar System.

1.1.3.2 Late-Stage

Functional demonstration of an instrument or a scientific method in a planetary analogue environment is not the final step in preparing for an outer-planetary mission. Low

gravity testing often follows in-field testing in some capacity. Whether via the CubeSat initiative or by way of a free-falling airplane, the instrument or method must function in a low gravity environment like that of space [14]. In addition to this requirement, the technology must survive thermal, vibrational, and vacuum conditions that may be experienced during lift-off or in transit to the destination of choice within the Solar System. After functional testing, planetary protection laws dictate sterilization of all components of the space craft to prevent potential false positives and panspermia of microorganisms from Earth to another outer-planetary body [15, 16]. Although this process of progressing science for space travel seems abundantly challenging, every step is necessary to ensure the technology readiness level of the space craft and a successful outcome for the mission [17].

1.1.4 Main Targets within our Solar System

1.1.4.1 Overview

Not all locations of interest within the Solar System are equal. Each target presents its own unique science goal and corresponding mission challenge. While some may only require a few months of transit time, others can necessitate years of flight requiring multiple precise maneuvers to remain on course. Similarly, requirements for the onboard science equipment can vary drastically. These requirements depend on the class of mission (i.e. orbiter, lander, impactor, or rover) and heavily shape the structure of the scientific payload. For example, a mapping infrared spectrometer will excel within an orbiter mission profile, but a wet chemistry technique requires material from the surface to accomplish its goals and, therefore, would be contained within an impactor, a lander, or a rover payload. While

not all techniques are explicitly defined to one mission class, each certainly has its own advantages and drawbacks. A science payload is not necessarily defined by a single technique but is rather a range of instruments that can offer the greatest benefits given certain mission criteria, which can significantly vary with the location of interest in the Solar System [18-20].

1.1.4.2 Mars

For decades, Mars has been a primary target of interest in the search for life elsewhere in the Solar System. Its proximity to Earth compared to other planets, as well as evidence suggesting a potentially once-habitable surface [21, 22], make it an excellent candidate for outer-planetary missions. In fact, 1976 saw the initial search for organic chemical signatures on the Martian regolith by way of the Viking missions [23-27]. The payload for this mission included a thermal volatilization gas chromatography mass spectrometer (TV-GS-MS) to detect traces of organic matter. While the instrument did not directly detect native carbon-containing compounds, chlorinated hydrocarbons and other organic chemicals used to clean the spacecraft prior to launch were identified [23, 25, 26]. The biological suites included in the Viking payload provided promising but ambiguous data [24, 27], so the results of these missions were largely interpreted as a negative indication of life on Mars [23, 25, 26].

Since the Viking missions, the only other organic analysis system sent to Mars was also a pyrolysis-based GC-MS system included on the Mars Science Laboratory Sample Analysis at Mars (MSL SAM) instrument suite. Similarly to that of the Viking lander, this instrument detected largely chlorinated hydrocarbons and contaminants resulting from

leakage in the *N*-methyl-*N*-*tert*-butyldimethylsilyl-trifluoroacetamide (MTBSTFA) derivatization system, along with some sulfur-containing compounds [28]. The Phoenix lander Microscopy, Electrochemistry, and Conductivity Analyzer (MECA) Wet Chemistry Laboratory (WCL) experiment measured parts-per-thousand (ppth) levels of perchlorates [29, 30]. Upon heating to 300-600 °C, perchlorates oxidize *in situ* organic matter to chlorinated hydrocarbons and other species, which were likely those detected by both Viking and MSL SAM [31, 32]. The combined data from these missions indicate that an alternate method using wet chemical extraction will be necessary for quantitative, compositional characterization of native *in situ* organic molecules on Mars [23, 25, 33].

1.1.4.3 Europa

Mars' proximity to Earth and potential for a once-habitable environment have made it a primary target of interest in the Solar System. However, other more distant planets, like the largest gas giant Jupiter, have been gaining attention. While Jupiter does not possess conditions likely to harbor life, its moons may provide better prospects. Specifically, the icy Galilean moon Europa has become a high-priority target for future outer-planetary missions due to suggested plume activity and evidence supporting the presence of a global subsurface ocean [34-37]. While no craft has ever landed on the surface of Europa, Earth-bound imaging instruments, such as the Hubble Space Telescope, have provided information from afar [37]. In addition, multiple fly-by missions were conducted to provide a closer picture of the Jovian moon. Of the fly-bys, the Galileo mission to orbit Jupiter and study its surrounding bodies provided the bulk of our chemical information of Europa and has been extensively analyzed as a result [38, 39].

The data from Hubble and Galileo show that Europa's surface is largely defined by streaking ridges and cracks referred to as chaos regions [40]. These deformations are mainly comprised of salt minerals and are thought to be a result of the interaction between the subsurface ocean and the outer ice layer caused by tidal heating [41-43]. Knowledge of the salts contained within these features could assist in estimating the concentrations and chemistries of those in the subsurface oceans. In addition, the presence of salts on the surface may imply an interaction between a rocky core and liquid ocean [44], and on Earth, these interactions at the sea floor create conditions that support life [45, 46].

Salt composition on the surface of Europa is a particularly relevant characteristic when defining habitability. The type of salts on the surface could dictate the suite of wet chemistry techniques for a potential lander mission in search of organic molecules. Since Mg^{2+}, Na^{+}, Cl^{-}, and SO_4^{2-} are believed to be among the most abundant ions residing on the surface of Europa [47, 48], any chosen technique must be robust to minerals comprised of these ions. Several fly-by missions are projected to launch in the early 2020's and will provide an improved survey and characterization the moon's exterior. The information gained from the on-board instruments of the National Aeronautics and Space Administration's (NASA's) Europa Clipper and the European Space Agency's (ESA's) JUpiter Icy Moon Explorer (JUICE) should generate an indirect characterization of the interior of the moon, including the ice crust thickness, the concentration of salts, the ocean size, etc… [49, 50]. These characteristics will aid in selecting appropriate techniques for future *in situ* quantitative and compositional analysis of organic molecules on the surface or even in the plumes or subsurface ocean of Europa. Information of this nature would provide relevant, detailed information on formation, habitability, and on-going planetary

processes of these icy, celestial bodies and could provide the first evidence of the potential for extant life beyond Earth.

1.1.4.4 Enceladus

Similar to that of Jupiter, Saturn maintains its own icy moon Enceladus. Much of what we have discovered about Enceladus originates from the Cassini-Huygens mission to study Saturn and its surrounding bodies [18, 51-66]. The Cassini spacecraft discovered plumes emanating from the moon's south pole, and data analysis has provided evidence of ongoing hydrothermal activity [67, 68] and has suggested the presence of a global subsurface ocean [69]. The hydrothermal systems that may exist at the liquid water/rock interface at the bottom of the subsurface oceans of Enceladus could provide an energy source to fuel organic chemical reactions, potentially giving rise to and supporting extant life [70]. The unique opportunity to directly sample particles from the subsurface ocean via fly-by missions through the plumes makes Enceladus an excellent target for future habitability studies in the outer Solar System. Much like Europa, quantitative and compositional analysis of organic and inorganic molecules in these plumes would provide detailed information on formation, habitability, and on-going planetary processes of Enceladus, an indication of the potential for extant life, and a direction for future outer-planetary missions.

1.1.5 Biosignature Detection Methods

1.1.5.1 Capillary Electrophoresis

The idea of electrophoresis came about in the early 1800's. However, full utilization of the technique did not arise until 1937 when Swedish scientist Arne Tiselius described a moving boundary method for protein separation using a U-shaped tube [71]. Tiselius' breakthrough pushed other scientists to take advantage of this technology and further advance the field of separations. Over the next several decades, multiple groundbreaking developments arose, such as electroblotting for protein transfer into membranes [72], gel electrophoresis for protein fingerprinting [73, 74], and capillary electrophoresis (CE) for Sanger deoxyribonucleic acid (DNA) sequencing and short tandem repeat (STR) typing [75-77]. These innovations lead the way for various CE separation methods [78], including capillary zone electrophoresis (CZE) [79-82], capillary gel electrophoresis (CGE) [83], capillary isoelectric focusing (CIEF) [84-86], capillary isotachophoresis (CITP) [87], micellar electrokinetic capillary chromatography (MEKC) [88], and capillary electrochromatography (CEC) [89, 90]. The CE technique is amenable to many different detection systems, including mass spectrometry, ultraviolet/visible (UV/VIS) absorbance, electrochemical sensors, refractive index, and laser-induced fluorescence (LIF), all of which offer their own unique contributions to separation science [91, 92].

While there are many CE methods, the most commonly used mode, CZE, separates molecules in solution by a combinatory effect of their electrophoretic flow (EP), v_{ep}, and

the electroosmotic flow (EOF), v_{eof}, of the medium, as shown in Equation (1.1.5.1.1). EOF is defined as the velocity at which a molecule migrates in response to an electric field:

$$v_{ep} = \mu_{ep} E \qquad (1.1.5.1.1),$$

where μ_{ep} is the electrophoretic mobility of the molecule and E is the electric field strength [93]. Electrophoretic mobility is further defined by the product of the charge of the molecule and the inverse of the drag force of the solvent, f, which directly relates the solution viscosity to the charge of the molecule, resulting in Equation (1.1.5.1.2):

$$\mu_{ep} = \frac{q}{6\pi\eta r} \qquad (1.1.5.1.2),$$

where q is the net charge of the molecule, η is the dynamic viscosity of the solution, and r is the hydrodynamic radius of the molecule, assuming spherical dimensions using Stoke's law [93]. Using this property, in an electric field negatively-charged molecules will migrate towards the positively-charged anode and positively-charged molecules will migrate towards the negatively-charged cathode. Typical electrophoresis would only separate positively-charged molecules in this system, with the greater charge/size molecules reaching the cathode first.

The addition of EOF circumvents this problem and allows species to migrate towards the electrode with the same charge state. EOF is generated in a glass capillary by applying a high voltage to an electrolyte with a pH greater than 3. The deprotonated silanol (SiO^-) groups of the capillary wall generate a stacked layer of cations and anions, resulting in a loosely bound top layer of cations [94]. These positively-charged ions are free to

migrate down the capillary in the direction of the electric field, generating a constant bulk fluid flow greater than that of the electrophoretic flow of any molecules in solution [93]. This effect is defined by Equation (1.1.5.1.3):

$$v_{eof} = \mu_{eof} E \qquad (1.1.5.1.3),$$

where μ_{eof} is the electroosmotic mobility of the molecule and E is the electric field strength [93]. Electroosmotic mobility is further defined by the Equation (1.1.5.1.4):

$$\mu_{EOF} = \frac{\varepsilon}{4\pi\eta} E\zeta \qquad (1.1.5.1.4),$$

where ε is the dielectric constant of the buffered solution, η is again the dynamic viscosity of the solution, E is the electric field strength, and ζ is the zeta potential of the capillary wall [93]. These factors can influence the overall velocity and separation efficiency of molecules in solution. The total velocity, v_t, of any given molecule in a solution affected by high voltage (HV) is defined by Equation (1.1.5.1.5):

$$v_t = (\mu_{eof} + \mu_{eof})E \qquad (1.1.5.1.5),$$

in which decreasing the power of hydrogen (pH) of the buffer, increasing the applied voltage, or increasing the zeta potential of the capillary would increase the velocity of molecules in solution, decreasing the overall migration time required to separate all molecules. By exploiting these features, both capillary length and width can be reduced while maintaining acceptable separation efficiency, *N*, in theoretical plates/meter, and resolution, R.

Separation efficiency and resolution can express the overall quality of the electropherogram. Separation efficiency is typically defined by Equation (1.1.5.3.6):

$$N = 16\left(\frac{t_r}{w}\right)^2 \qquad (1.1.5.3.6),$$

where N is the number of theoretical plates, t_r is the retention time, and w is the width of the peak [93]. This value quantifies the overall dispersion of individual chromatographic peaks in a separation. Resolution measures how well two peaks separate from each other within an electropherogram and is defined by Equation (1.1.5.3.7):

$$R = \frac{t_{r2} - t_{r1}}{\frac{1}{2}(w_{2-}w_1)} \qquad (1.1.5.3.7),$$

where R is resolution, t_{r1} and t_{r2} are the retention times of two adjacent peaks, and w_1 and w_2 are the widths of the two adjacent peaks [93]. While both are important factors to consider, one may be more critical than the other depending on the objective of the separation. If the goal of the separation is to distinguish between two overlapping peaks, then obtaining a higher resolution should be a priority. If improving the LOD is desired, then maximizing the separation efficiency is imperative. In general, good separation techniques strive to achieve high separation efficiencies while maintaining good chromatographic resolution between peaks.

1.1.5.2 Microcapillary Electrophoresis

Compared to traditional capillary electrophoresis, μCE utilizes microfabricated glass channels in place of lengthy, pulled glass capillaries to achieve high resolution

separations. This simple difference can offer many advantages. For example, miniaturization of equipment is easily achievable due to the small, flat nature of the microdevice [80, 95-98]. This flat structure of the glass wafer can reduce the effects of Joule Heating by allowing heat to dissipate more quickly throughout the device [99]. Separation time can be reduced from tens of minutes with traditional CE to minutes or even seconds with μCE. Optical coupling is simpler due to the planar glass-air and glass-fluid interface of the device and optical components. Furthermore, with the recent advancement of cleanroom technology, the creation of complex channel patterns is possible, making μCE an exceptionally powerful separation method [100, 101].

1.1.5.3 Laser-Induced Fluorescence

As mentioned, μCE has been paired with a variety of unique detection methods, such as MS, UV/VIS absorbance, electrochemical sensors, refractive index, and LIF [91, 92]. While MS can potentially offer direct identification of chemical species without the use of standards and UV/VIS absorbance takes advantage of short analysis times, LIF shines with its ultra-low limit of detection (LOD), specifically for biomolecule detection and quantification [95, 102, 103]. When paired with μCE, LIF can attain a picomolar (pM) LOD at a signal to noise (S/N) ratio of 3 to 1 for certain organic molecules [97]. Highly sensitive detectors like a silicon photomultiplier (SiPM), an avalanche photodiode (APD), or a photomultiplier tube (PMT) are required to achieve this ultra-low LOD [104]. In addition, targeting specific excitation/emission wavelengths corresponding to a specific molecule or dye of interest requires specialized optical components. A spectrometer can be used as a detector to sweep over a broad range of wavelengths at the expense of signal

response at low concentrations [105]. Although the LOD of the system would increase, the overall complexity of the optical system would be reduced, which can be a highly desirable trait in an optical system.

1.1.5.4 Programmable Microfluidic Arrays (PMAs)

Miniaturizing an instrument for spaceflight is a critical yet challenging task. Advancements of lens and laser technologies have enabled extreme reduction in size of LIF devices [106-109], and the improvements of cleanroom procedures and techniques have allowed complex channel designs to be patterned into a microdevice [110]. Thankfully, these same cleanroom advances have furthered the progression of microvalve technology as well, leading to the creation of programmable microfluidic arrays (PMAs). A PMA is a grid of microvalves connected by microchannels for precise routing of fluids, such as mixing, metering, diluting, etc… [110]. This structure can eliminate the need for large vacuum pumps and opens the possibility for automation and portability, which are essential qualities for areas that require compact, modular, and energy efficient equipment [111, 112].

The microdevices at the heart of some miniaturized μCE-LIF instruments integrate a μCE separation channel with an automated microfluidic sample processor that uses pneumatically-actuated normally-closed microfabricated monolithic membrane microvalves, like those first developed in 2003 [113]. In order to minimize contamination between mixing cycles, the microdevice utilizes specially designed bus valves in addition to standard (stop) valves [96]. Bus valves allow fluid flow through the primary input/output bus channel without actuation, while standard stop valves require actuation for fluid

routing. Sequential operation of multiple valves in series forms a peristaltic pump, and when structured as a PMA, complex microfluidic processing is achievable [110]. These complex mixing architectures and routines are essential for microfluidic systems. Since the size and structure of these devices dictate a low Reynolds number, fluid flow within the microchannels is laminar. Therefore, turbulent flow can only be achieved via microfluidic mixing using the microvalves. Multiple microfluidic systems have been developed to generate turbulent flow for mixing within the microdevice [110, 114, 115], demonstrating an independence from macrofluidic mixing systems that are resource-heavy and require bulky equipment.

Mars Organic Analyzer (MOA) prototypes have demonstrated the power of fully automated sample analyses via field tests in the Atacama Desert, Chile [116], and the Panoche Valley, CA [96]. In addition, these systems conducted high resolution analyses of trace organic species in multiple relevant planetary analogue samples, including those from the Rio Tinto [80], hydrothermal sites [82, 117], and the Murchison meteorite [88]. This method of automated sample analysis is ideal for applications where size and power are limited and a low LOD is required, like those to the outer Solar System. In fact, multiple μCE-LIF systems based on these prototypes, such as the Enceladus Organic Analyzer (EOA), the Impact Penetrator Organic Analyzer (IMPOA), and the Microfabricated Organic Analyzer for Biosignatures (MOAB), have been proposed for missions to Mars, Enceladus, and Europa [118-121]. These instruments could provide the selectivity and sensitivity needed to detect small organic molecules and biopolymers at these high-priority targets, potentially leading to the discovery of extraterrestrial life and altering our understanding of habitability within the Solar System and beyond.

1.2 Thesis Organization

Chapter 1 serves as an all-encompassing background to the data presented in Chapters 2-6. Main project motivations and technical concepts are discussed in detail. Contributions to the field are also noted.

Chapter 2 describes the design, assembly, and characterization of a modular benchtop CE-LIF detection system. The system was qualified using a series of buffer concentration and LOD tests. Due to the modularity in design, this system can be adapted to any wavelength excitation/emission required for multiple targets, including enhanced chiral analysis, polycyclic aromatic hydrocarbons (PAH's), etc…, and serves as an excellent test bed for the fabrication of specialized portable or laboratory-based μCE-LIF systems for trace organic molecule detection.

Chapter 3 outlines an application of the benchtop μCE-LIF system. A series of icy moon analogue standards is analyzed to evaluate the performance of the device towards an icy moon environment. Organic molecules are identified and quantified in a relevant Earth-based icy moon analogue sample taken from Champagne Geyser at Chaffin Ranch, Utah. The results represent a significant step forward for the liquid-based μCE-LIF analysis of small organic molecules and biopolymers for future space missions to icy bodies.

Chapter 4 assesses the storability of a μCE-LIF microdevice for an outer-planetary mission. The pneumatically-actuated monolithic membrane microvalves within the device are opened successfully after 10 years of storage under ambient conditions. The device is shown to transfer fluid both with and against gravity at rates comparable to similar devices,

validating the importance of microdevices based on these microvalves for fluidic manipulation and sample handling in outer planetary missions.

Chapter 5 examines the thermal ruggedness of microdevices and the storage capabilities of Pacific Blue (PB) dye for outer-planetary space missions. Microdevices are thermocycled for extreme high temperatures to extreme low temperatures, and PB dye reactivity is analyzed when stored dry and compared to traditional in-lab wet storage reactivity.

Chapter 6 highlights the design, assembly, and testing of a miniaturized lens tube LIF system for organic molecule detection. Using a SiPM as a detector, the device is characterized through a series of manual and automated LOD analyses, and bulk amino acid content is a Mars analogue sample from the Atacama Desert in Yungay, Chile, is determined. These results have shown promising usability of automated microdevices and portable lens tube LIF detection systems for analysis of samples from extreme environments.

Chapter 7 presents concluding remarks and potential future directions for the continuation of multiple efforts.

1.3 Contributions to the Field

The μCE-LIF benchtop system constructed and functionally tested in these studies generated a sub-pptr LOD and high-resolution separations of relevant amino acid molecules for future habitability studies in the Solar System. The modularity of the instrument demonstrates that a μCE-LIF detection system can be constructed using largely

pick-and-place commercially-available components, an option that may be more favorable than purchasing an expensive, complex commercial instrument or a more economical single-purpose system. The successful identification and quantification of amino acids in an icy moon analogue sample taken from Champagne Geyser at Chaffin Ranch, Utah, represents a significant step forward for the liquid-based μCE-LIF analysis of small organic molecules and biopolymers for future space missions to icy bodies like Enceladus and Europa. The microfluidic processing system, based on monolithic membrane microvalves, was shown to function efficiently after 9-10 years in storage, demonstrating the usability of programmable microfluidic architectures utilizing these microvalves for future outer-planetary missions. PB dye was stored dry with a standard mixture of amino acids and exhibited reactivity similar to that of a standard liquid labeling protocol, indicating that this labeling process is an acceptable method for future automated μCE-LIF analyses after extended storage of the microdevice in dry conditions. The successful detection of bulk organics in a Mars analogue sample displays the adaptability of the LIF detection system towards more restricting mission criteria where size and power are extremely limited, like those for missions to the icy moons of the outer Solar System.

CHAPTER 2. A MODULAR MICROCAPILLARY ELECTROPHORESIS SYSTEM WITH LASER-INDUCED FLUORESCENCE FOR QUANTITATIVE COMPOSITIONAL ANALYSIS OF TRACE ORGANIC MOLECULES

Current work in progress:

2.1 Abstract

Microcapillary electrophoresis enables high-resolution separations in miniaturized, automated microfluidic devices. Pairing this powerful separation technique with laser-induced fluorescence enables highly-sensitive, quantitative, and compositional analysis of organic molecule monomers and short polymers, which are essential, ubiquitous components of life on Earth. Improving methods for their detection has applications to multiple scientific fields, particularly those related to medicine, industry, and space science. Here, a modular benchtop system using microcapillary electrophoresis (μCE) with laser-induced fluorescence (LIF) detection was constructed and tested by analyzing standard amino acid samples of valine, serine, alanine, glycine, glutamic acid, and aspartic acid in multiple borate buffered solutions of increasing concentrations from 10-50 millimolar (mM), all pH 9. The 35 mM borate buffer solution generated the highest resolution before Joule heating dominated. The limits of detection (LODs) of alanine and glycine using 35 mM borate buffer were found to be 2.12 nanomolar (nM) and 2.91 nM, respectively, comparable to other state-of-the-art μCE-LIF instruments. This benchtop system is amenable to a variety of detectors, including a photomultiplier tube (PMT), a

silicon photomultiplier (SiPM), or a spectrometer, and currently employs a spectrometer for facile multi-wavelength detection. Furthermore, the microdevice is easily exchanged to fit the desired application of the system, and optical components within the central filter cube can be easily replaced to target alternative fluorescent dyes. This work represents a significant step forward for the analysis of small organic molecules and biopolymers using μCE-LIF systems.

2.2 Introduction

The concept of electrophoresis has existed as a tool for separation since the early 1800's but was not realized until 1937 when Swedish scientist Arne Tiselius published an article describing a moving boundary method for protein separation using a U-shaped tube [71]. This development sparked interest and development in the field over the next several decades, leading to many advances that have been incorporated into multiple varied common scientific practices, including gel electrophoresis for protein fingerprinting [73, 74], electroblotting for protein transfer into membranes [72], and capillary electrophoresis (CE) for Sanger deoxyribonucleic acid (DNA) sequencing and short tandem repeat (STR) typing [75-77]. The CE technique has further developed into a broad-ranging technology with many modes of analysis [78], including capillary zone electrophoresis (CZE) [79, 81, 82], capillary gel electrophoresis (CGE) [83], capillary isoelectric focusing (CIEF) [84-86], capillary isotachophoresis (CITP) [87], micellar electrokinetic capillary chromatography (MEKC) [88], and capillary electrochromatography (CEC) [89, 90], and has been coupled to various detection systems, including mass spectrometry, ultraviolet/visible (UV/VIS) absorbance, electrochemical sensors, refractive index, and laser-induced fluorescence (LIF) [91, 92].

Thanks to the pioneering efforts in the early 1990's led by Manz, Widmer, Harrison, and others, microcapillary electrophoresis (μCE) using microfabricated glass channels in place of lengthy, pulled glass capillaries has increased in popularity over the past few decades and now offers many advantages to traditional CE [122-124]. Miniaturization of equipment is easily achievable with μCE [80, 95-98], and with the recent advancement of cleanroom technology, more complex patterns can be utilized, making this process exceptionally powerful for the creation of miniaturized analysis systems on planar glass devices [100, 101]. The smaller form factor of the glass microdevice also reduces effects from heating due to high voltage [99]. Heat generated during a separation can dissipate much more quickly across the device, and temperature control is facile due to the small, flat structure of the glass wafer. Optical coupling is simpler due to the planar glass-air and glass-fluid interface.

The fabrication of μCE channels on glass wafers opens the possibility of automation using programmable microfluidic arrays (PMAs) and other micro-total analysis systems (μTAS) [94, 110, 125-128]. Automation combined with miniaturization make μCE an excellent option for areas that desire specialized or field-portable instrumentation, like digital heart monitors [129], blood glucose monitors [130], and automated external defibrillators (AEDs) [131] in the medical field, portable gas detection sensors for industry [132], and space instruments designed to fit within one or more standard 10 X 10 X 10 cm single unit (U) CubeSat sizes [14]. Miniaturized equipment is no longer a niche segment of the market, and more fields are shifting research towards compact, modular, and energy-efficient equipment to save cost and increase efficiency in the workplace [111, 112, 133]. For fields centered around microfluidics, these systems are typically designed around a

single-purpose microdevice. This approach enables repeatability of simple, singular tasks but limits research where multiple iterations of devices are required for various concurrent projects. Therefore, research systems must be designed to incorporate many versions of devices to maximize their potential.

A powerful detection technique to combine with μCE is laser-induced fluorescence (LIF). While LIF has various useful applications, including thermometry [134] and optical imaging [135, 136], its primary use when integrated with μCE is biomolecule detection and quantification [95, 102, 103, 137]. When paired together, these techniques can attain picomolar (pM) limits of detection (LODs) at a signal-to-noise (S/N) ratio of 3 to 1 [97]. Achieving this ultra-low detection limit requires the use of highly sensitive detectors, such as a silicon photomultiplier (SiPM), avalanche photodiode (APD), or a photomultiplier tube (PMT) [104]. If targeting specific excitation/emission wavelengths, these detectors require tailored optical components, which can be made to be modular if mounted in the appropriate housing. Wavelength selection can be made even easier when utilizing a spectrometer as a detector. Instead of using a specific series of filters to select for a wavelength range of interest, the spectrometer can filter for those wavelengths, which is a highly desirable trait in an optical system.

The advancements to optical detection systems have been made incrementally over decades of tireless research. To the benefit of those in need of these systems, many instruments have been developed into commercial products, such as the Microfluidic Toolkit for highly-sensitive organic molecule detection (Micralyne, Edmonton, Alberta, Canada) [138, 139], the Wideband Integrated Bioaerosol Sensor 4A and 5/NEO (WIBS-4A and 5/NEO) for detection of bioaerosols (Droplet Measurement Technologies,

Longmont, CO) [140-142], and the Zetalif light-emitting diode (LED) induced fluorescence (LEDIF) detector for organic molecule identification and quantification (formerly Picometrics Technologies, now Adelis Technologies, Labège, France) [143]. These systems are typically configured for single wavelength and single device configuration, and, therefore, there are limitations when research requires more flexibility to test multiple parameters. Here, we showcase a logical step forward with µCE-LIF technology and propose an updated modular take on a system using a spectrometer as a detector. Select machine-room fabricated, custom-designed adapter plates were used to affix some components, but major optical, mechanical, and optomechanical components were purchased commercially to enable simplicity in modulation. Standard amino acid samples of valine, serine, alanine, glycine, glutamic acid, and aspartic acid were analyzed in multiple borate buffered solutions of increasing concentrations from 10-50 millimolar (mM), all pH 9. The borate buffer solution generating the highest resolution before Joule heating occurred was determined. The limits of detection (LODs) of alanine and glycine were determined as well and found to be comparable to other state-of-the-art µCE-LIF instruments [144].

2.3 Materials and Methods

2.3.1 Reagent Preparation

Reagents were used as received except where noted. Deionized (DI) Millipore water (18 MΩ, megaohms) was distilled (d) 10x in a high-efficiency particulate air (HEPA)-filtered environment and used to make all aqueous solutions. HCl (BDH Chemicals, Darmstadt, Germany) and NaOH (Sigma-Aldrich Co., St. Louis, MO) were

prepared as 100 mM aqueous stock solutions. Borate running buffer, pH 9 (Sigma-Aldrich Co.) was recrystallized 10x and prepared as a 100 mM stock aqueous solution. A stock standard amino acid solution (valine, serine, alanine, glycine, glutamic acid, aspartic acid – each 20 mM) (Sigma-Aldrich Co.) was made for multiple concentrations of borate running buffer (10 mM, 20 mM, 30 mM, 35 mM, 40 mM, and 50 mM). A 20 mM stock solution of 3-carboxy-6,8-difluoro-7-hydroxycoumarin (Pacific Blue [PB]) dye (Invitrogen, Carlsbad, CA) was dissolved in dimethylformamide (DMF) (EMD Millipore Co., Billerica, MA). Three independent dilution series (3.33 μM to 33.3 mM) of both alanine and glycine were made in 35 mM borate buffer. All aqueous solutions were stored at 4 °C when not in use, and all DMF solutions were stored at -20 °C when not in use.

2.3.2 Detection System Fabrication

The modular fluorescence detection system utilizes an off-axis optical profile for epifluorescence (Figure 2.1). Commercial components were selected where possible, and custom parts and the structured assembly of the system were designed using SolidWorks (Figure 2.2 A). A CLD1010 compact laser diode controller (Thorlabs, Newton, NJ) was used to regulate a LP406-SF20 404.5 nm, 0-40 mW single mode (SM) fiber-pigtailed InGaN laser diode (Thorlabs) operated at 20 mW laser optical power and collimated using a F671FC-405 Fiber Collimation Package (Thorlabs). A KC1-S 3-axis kinematic mount (Thorlabs) directed the laser through an ET405/10x 10 nm bandpass (BP) optical filter centered at 405 nm (Chroma Technology, Brattleboro, VT) to a DMLP425R 45°-angled, 425 nm longpass (LP) dichroic mirror (Thorlabs). Light reflected from the mirror was gathered and focused into the microcapillary channel of the microdevice for fluorophore excitation by a MPLFLN100X 0.9 numerical aperture (NA), 1 mm working distance (WD),

M Plan FL 100x objective lens (Olympus Co., Tokyo, Japan) mounted on a KC1-S 3-axis kinematic mount (Thorlabs). Fluorescence collected and collimated by the objective lens passed through both the LP dichroic mirror and a FGL420 420 nm LP optical filter (Thorlabs), which are conveniently held in an easily removable and replaceable DFM kinematic fluorescence filter cube (Thorlabs) along with the BP filter. A variable SM1D12D 0.8-12 mm diameter iris diaphragm (Thorlabs) spatially filtered the focused fluorescent light on to a DFM-E02 45°-angled, 400-750 nm dielectric-coated mirror (Thorlabs). Light reflected off the mirror was directed through a LA1422 1 in diameter N-BK7 plano-convex lens (Thorlabs) and focused on to a QP400-2-VIS-NIR 400 µm diameter, 400-2100 nm fiber optic cable (Ocean Optics, Dunedin, FL) housed in a SM1NR1 2" travel-adjustable lens tube (Thorlabs) mounted on a KC1-S 3-axis kinematic mount (Thorlabs). Light guided through the fiber optic was detected by a FLAME-T-VIS-NIR-ES 350-1000 nm Flame spectrometer (Ocean Optics) for analysis.

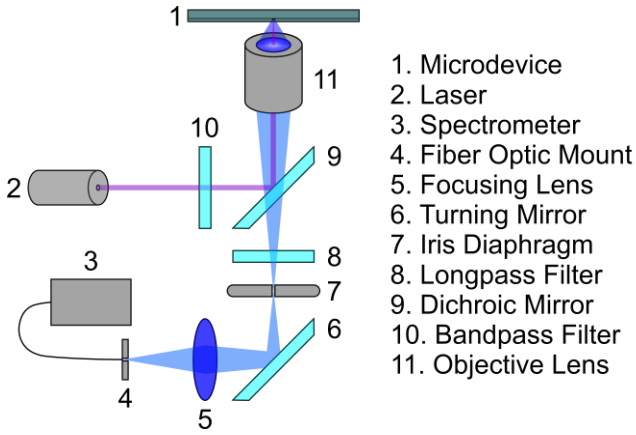

Figure 2.1. Optical schematic of the benchtop µCE-LIF system. Light displayed is intended to guide the eye and does not represent exact scaled, calculated beam diameters.

The optical components were mounted to a MTS50-Z8E 50 mm travel motorized translational Z-axis stage (ThorLabs) using a custom-designed adapter plate fabricated in-house. The Z-axis stage was attached to a LTS150 150 mm travel motorized translational Y-axis stage (ThorLabs) using a custom-designed and fabricated L-bracket (Xometry, Gaithersburg, MD) and adapter plate (Protolabs, Maple Plain, MN) combination. The Y-axis stage was mounted to a LTS300 300 mm travel motorized translational X-axis stage (Thorlabs) to enable complete 3-dimensional (3D) movement for exact laser focusing and ease-of-part replacement. An after-construction image of the completed system is shown in Figure 2.2 B.

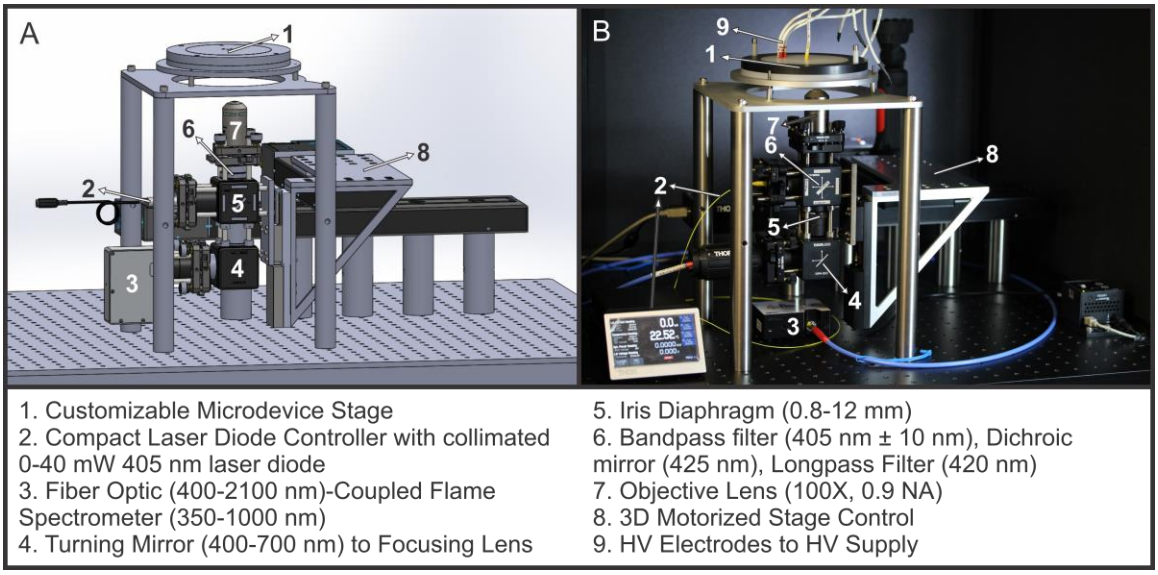

Figure 2.2. (A) Computer-Aided Design (CAD) of the benchtop µCE-LIF detection system labeled with major components. (B) Photograph of the benchtop µCE-LIF detection system labeled with major components, including the addition of HV leads.

2.3.3 Microfluidic Device Fabrication

The microdevices used in this study were custom-designed at Georgia Tech and sent for fabrication at Micronit Microfluidics (Enschede, Netherlands) using standard

isotropic HF etching procedures [95, 103, 122, 145, 146]. Each device featured a perpendicular 1 cm cross injection channel [147] and an 8.2 cm separation channel, both with tapered 1.7 ± 0.1 to 0.75 ± 0.15 mm diameter inlet/outlet holes at each end (Figure 2.3 A-B). Straight channel features were etched to a final 70 ± 8 μm wide and 30 ± 3 μm deep into a 700 ± 70 μm thick planar glass wafer [124] with a 45.0 x 18.0 ± 0.3 mm footprint. Tapered turns were patterned into the separation channel to reduce device size [97, 148] and were etched 65 ± 8 μm wide and 30 ± 3 μm deep to lessen potential band broadening effects, as demonstrated by the Mathies, Ramsey, and Štědrý groups and others [149-151]. The etched wafer was covered and bonded to a 1.1 ± 0.1 mm blank glass wafer to generate an overall thickness of 1.8 ± 0.2 mm. The device was aligned to the focused laser beam 0.2 mm from the end of the separation channel, generating an effective separation distance of 7.5 cm from the cross section.

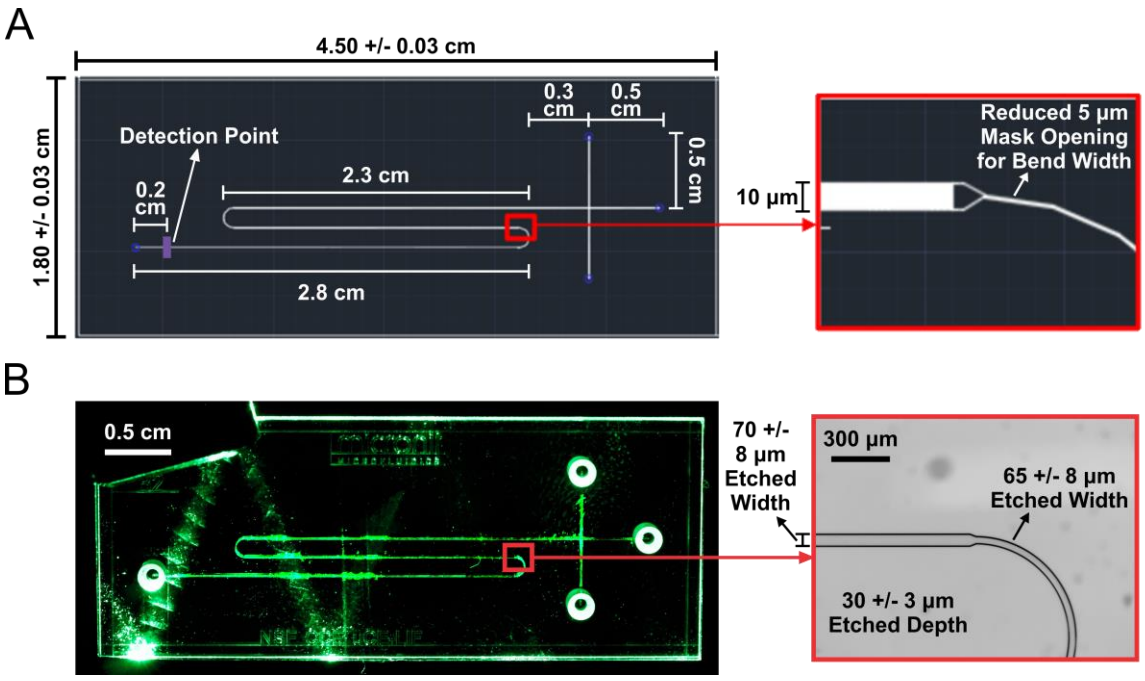

Figure 2.3. (A) Mask design of microdevice labeled with major dimensions, including a zoom-in of a bend in the separation channel incorporating tapered turns. The detection point was placed 0.2 cm from the end of the separation channel, generating an effective separation distance of 7.5 cm from the cross section. (B) Photograph of the benchtop µCE-LIF detection system microdevice with a zoom-in of a bend in the separation channel.

2.3.4 Microdevice Cleaning and Electrophoretic Conditions

With the custom-fabricated microdevice aligned to the focused laser beam, 3x alternating rinses of HCl and NaOH were pulled through the capillary channels by vacuum to clean the device. Vacuum was then applied to fill all channels with borate running buffer. A blank run with running buffer was conducted to ensure the electroosmotic flow (EOF) in the separation channel was enabled using a HVS448 6000 D high voltage (HV) power supply (LabSmith, Inc., Livermore, CA). First, a potential was applied across the sample well (ground) and the waste well (-1500 Volts [V]) while keeping the anode and cathode grounded for 10 seconds (s) to induce a cross-injection. The potential was changed and

applied to the anode (3000 V), cathode (-3000 V), and sample/waste wells (2400 V each) to achieve an electric field strength of 732 V/cm along the capillary during the separation.

2.3.5 Optimization of Buffer Concentration

For each concentration of borate buffer, 1 µL of the stock amino acid solution was pipetted into a microcentrifuge tube (Eppendorf, Hauppauge, NY) and mixed with 20 µL of borate buffer and a 4x molar ratio excess of PB stock solution. The solutions were stored in the dark for 2 hours (hr) to react and diluted 1000x from their starting concentrations for analysis with their respective borate buffer.

2.3.6 LODs of Alaine and Glycine

For each concentration of alanine or glycine, 1 µL of each stock amino acid dilution series solution was pipetted into a microcentrifuge tube and mixed with 20 µL of 35 mM borate buffer and a 4x molar ratio excess of PB stock solution. The solutions were stored in the dark for 2 hr to react and diluted 1000x from their starting concentrations for analysis with 35 mM borate buffer. The final diluted concentrations of alanine and glycine were used for the limit of detection (LOD) analyses.

2.3.7 Data Manipulation and Analysis

Resulting electropherograms were baseline-corrected and fitted using a 0.2 % Loess filter via the chromatographic analysis program PeakFit (Systat Software, Inc., San Jose, CA). Fitted electropherograms were extracted to the graphical data analysis program OriginPro (OriginLab Co., Northampton, MA) for further characterization of signal-to-noise and resolution data extracted from the fitted files. Noise for each electropherogram

was calculated as the standard deviation of the baseline electropherogram in a region without eluting peaks.

2.4 Results and Discussion

2.4.1 Benchtop μCE-LIF System Design

The main consideration in the design of this benchtop μCE-LIF detection system was modularity. One component that emphasized this quality was the customizable microdevice stage. This part was not commercially available and was designed so that minimal modification was necessary to house various microdevice designs. The stage features a stacked, three-piece structure, for which the top two layers tightly house the microdevice, and the bottom section aligns with the optical assembly. The bottom layer connects to a rigidly mounted platform with tip/tilt alignment to easily create a perpendicular cross-section to the optical beam path emanating from the optical assembly. This bottom layer serves as an intermediate to the microdevice assembly, which was individually fabricated to fit each specific microdevice design. Therefore, the only alteration when changing to a different microdevice design is the two-layer microdevice assembly. Parallelism with the optical assembly is maintained even when replacing this assembly with a new design, and realignment with the optical beam path was achieved via X, Y, Z control of the optical assembly, greatly simplifying optical alignment of any new microdevice.

Modification of optical and optomechanical components is simple and cost-effective. All optical components were mounted together using Thorlabs' 30 mm cage cube system and 1" diameter lens tubes. This consistency in design shifted the laser beam to

centerline throughout the optical assembly, simplifying optical alignment. A fixed-power 405 nm 20 mW laser was initially selected for fluorescence excitation of PB but was eventually replaced for a tunable 405 nm 0-40 mW laser for ease of flexibility in testing. This new laser offered a greater optical power range, a programmable thermoelectric cooler (TEC) for an increased lifespan, and controllability via touchscreen and USB connection to a computer. The laser slotted into a KC1-S 3-axis kinematic mount to allow tip/tilt alignment of the beam. The original N40X-PF 0.75 NA Nikon Plan Fluorite 40x imaging objective lens was replaced with a MPLFLN100X 0.9 NA, 1 mm WD M Plan FL 100x objective lens. The 100x objective lens simultaneously increased the NA and the WD, increasing the total captured fluorescent light while making focused-beam alignment to the microchannel much easier. This simple alteration demonstrates the flexibility and further modularity of the design of the system.

Fixed at the center of the optical assembly is a DFM kinematic fluorescence filter cube with an easily removable and replaceable magnetic inner component that houses a LP dichroic mirror, a LP optical filter, and a BP filter, each selected specifically for the laser wavelength and captured fluorescent light from the fluorophore of interest. This study targeted PB dye, a well-established 405 nm excitable amine-reactive probe for μCE-LIF [88, 97, 152, 153] with an emission spectrum between 410 nm - 455 nm [154, 155]. A 10 nm BP optical filter centered at 405 nm was selected to filter undesired wavelengths of laser light. A 45°-angled, 425 nm LP dichroic mirror was chosen to reflect this laser light 90° off-axis and filter the captured fluorescent light through a sequential 420 nm LP filter. Targeting an alternate fluorophore with a different excitation or emission spectra simply requires replacing the removable portion of the DFM cube, which can be purchased

individually and outfitted with the proper filters in advance. The magnetic supports reposition components at exact angles so that final alignment of the beam path towards the detector remains on centerline.

Fluorescent light passing through the DFM cube was spatially filtered using an iris lens to reduce background signal. This filtered fluorescent light was directed 90° and focused towards a fiber-coupled Ocean Optics Flame spectrometer for analysis. An Ocean Optics spectrometer was selected as a detector for two main reasons: compatibility with the visual-based programming language Laboratory Virtual Instrument Engineering Workbench (LabVIEW) and the potential to analyze multiple fluorescent dyes at once without changing the detector. Ocean Optics provides the drivers necessary to control their spectrometers through LabVIEW, making the integration of the Flame spectrometer into the program straightforward. Integration of light intensity under specific wavelengths is possible with the spectrometer, allowing simultaneous analysis of two or more fluorescent dyes with different emission spectra (Supplementary Figure A.1.1), but the spectrometer can be easily exchanged for other detectors, such as a PMT or a SiPM, when higher-sensitivity, single-wavelength band detection is required. For this study, only PB dye was used to maintain simplicity when characterizing the microdevice and the optical capabilities of the system.

2.4.2 Microdevice Characterization

The custom-designed microdevice used in this study was characterized through a series of buffer concentration tests. Buffer optimization is a critical first step in characterizing a new μCE device and is commonly shared in first reports of new devices

due to the value of this information to the community [93, 96, 103, 156-158]. Borate buffer has been shown to provide excellent flexibility and robustness to a range of potential sample matrices [80]. A buffer concentration range of 10 mM to 50 mM was chosen to examine the effect of ionic strength on resolution and peak efficiency. The results of buffer optimization on our new microdevice are shown in (Figure 2.4). Amino acids with different charge/mass ratios were separated successfully using each concentration of borate buffer. Peak identification was performed by the external spiking of individual amino acids. Serine and alanine, two amino acids with similar charge/hydrodynamic radius ratios, began to resolve when using 35 mM borate buffer. Resolution improved with higher concentrations of borate buffer, but successful separations were more difficult to achieve. Joule heating from an increase in heat generated by a higher ionic strength buffer was a likely cause. The amount of heat produced in the channel directly increases with the electric current, which increases with a more concentrated electrolyte.

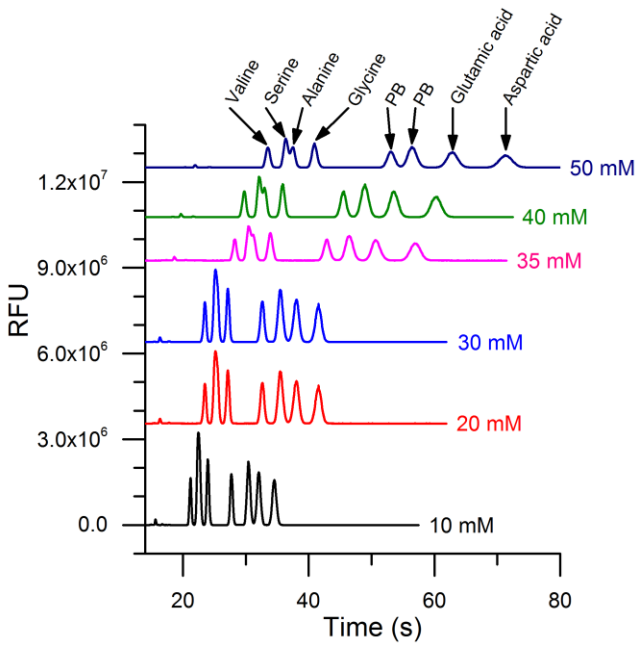

Figure 2.4. Electropherograms for analyses of a 20 µM amino acid standard solution containing valine, serine, alanine, glycine, glutamic acid, and aspartic acid at a 732 V/cm separation potential using indicated borate buffer concentrations.

Comparing the resolution and peak efficiency of the alanine and glycine peaks at various buffer concentrations, a running buffer of 35 mM borate was empirically determined to give the highest peak efficiency without sacrificing resolution (Figure 2.5 A-B). The peak efficiency for alanine and glycine continued to increase for 40 mM and 50 mM borate buffer, but significant Joule heating occurred, increasing run variability and analysis times. Therefore, 35 mM borate buffer was chosen for the LOD experiments of alanine and glycine. Table 2.1 shows the separation results for each amino acid with 35 mM borate buffer. The separation efficiency for each amino acid is above 100,000 theoretical plates per meter (N/m), except for glutamic acid and aspartic acid with the higher concentrations of borate buffer (Supplementary Table A.1.1). MicroCE-LIF systems have been shown to achieve separation efficiencies greater than 1,000,000 *N*/m [88]. However, these systems used HV power supplies that generated up to 30,000 V in

similarly sized devices. Increasing the electric field strength directly increases the electroosmotic flow within the microchannel, resulting in shorter separations and higher peak efficiencies. Signal-to-noise is a standard figure of merit in instrument characterization [93] and is also included in Table 2.1.

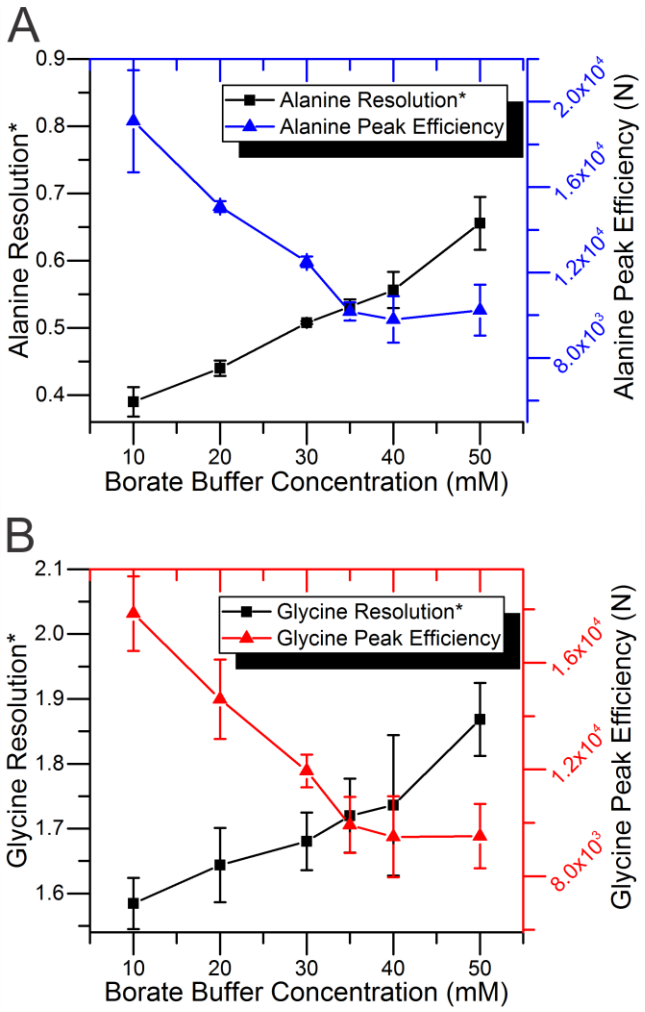

Figure 2.5. Resolution and peak efficiency versus buffer concentration for (A) alanine and (B) glycine. *Resolution for each alanine and glycine peak is calculated with respect to that peak's most adjacent previously eluted peak (serine and alanine, respectively).

Table 2.1 - Key figures of merit of the optimized separation*

Amino Acid	Signal-to-Noise (RFU)	Theoretical Plates (N)/m	Resolution	FWHM (s)
Valine	3800 ± 200	120000 ± 10000	-	7.2 ± 0.5
Serine	5900 ± 300	131000 ± 3000	1.571 ± 0.005	7.5 ± 0.1
Alanine	4200 ± 400	136000 ± 6000	0.53 ± 0.01	7.6 ± 0.1
Glycine	4900 ± 400	130000 ± 10000	1.72 ± 0.06	8.3 ± 0.4
Glutamic Acid	3700 ± 300	81000 ± 3000	7.09 ± 0.2	15.8 ± 0.3
Aspartic Acid	3100 ± 300	72000 ± 6000	1.83 ± 0.02	18.7 ± 0.5

**Signal-to-noise (S/N; relative fluorescence units - RFU), theoretical plates (N)/m, resolution, and full width at half max (FWHM; seconds - s) of electropherograms from analyses done at 732 V/cm using 35 mM borate buffer with an amino acid standard solution containing valine, serine, alanine, glycine, glutamic acid, and aspartic acid each at 20 µM.*

2.4.3 Optical Characterization

The amino acids alanine and glycine were chosen to characterize the LOD of this system. By calculating the signal-to-noise ratio of each alanine and glycine peak from the three independent dilution series and plotting the log of the results versus the log of their respective concentrations, linear regressions for both L-alanine (Figure 2.6, black squares) and glycine (Figure 2.6, red circles) were modeled. LODs of both alanine and glycine were calculated to be 2.12 nM and 2.91 nM at a S/N of 3, respectively, falling within the range of expected LODs for spectrometer-based µCE-LIF detection systems [88, 152, 159].

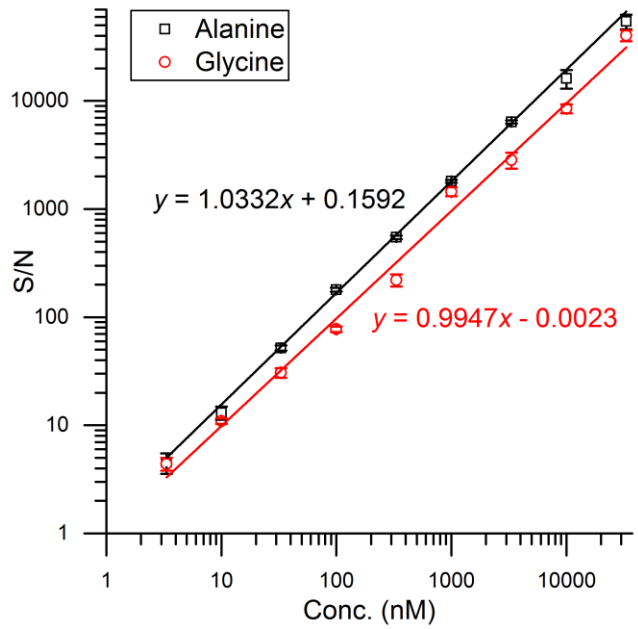

Figure 2.6. Limit of detection (LOD) plot of alanine (2.12 nM) and glycine (2.91 nM) reacted with Pacific Blue (PB) succinimidyl ester dye in 35 mM borate buffer, pH 9. Electropherograms were generated using a 10 s 1500 V injection followed by a 90 s 6000 V separation at 732 V/cm. Error bars represent the standard deviation of triplicate technical replicates of glycine and alanine electropherograms.

2.5 Conclusions

A benchtop µCE-LIF detection system was constructed using easily exchangeable components and achieved LODs of 2.12 nM and 2.91 nM for alanine and glycine, respectively. The LODs of these representative amino acids compare to those of other µCE-LIF detection systems [144] and allow for detection of organic molecules in a variety of applications, including space exploration [152, 160], environmental sampling [80, 88], particle detection [161], etc…. The simplicity in replacing and modifying the optical components of this system improves targeting of alternate fluorophores with different excitation and emission spectra. Implementation of a more sensitive detector, like a PMT or SiPM, would decrease the LOD by 1-2 log orders, as demonstrated with other µCE-LIF

systems [97]. However, use of one of these detectors would require a more complex optical assembly to filter unnecessary stray light and would eliminate tunability for the wavelength of interest, an inherent feature of the spectrometer.

The data presented demonstrates that a modular μCE-LIF detection system can be constructed using largely pick-and-place commercially-available components. Wherever possible, major optical, mechanical, and optomechanical components were purchased commercially to enable simplicity in modulation and operation. For many labs, this option may be more favorable than purchasing an expensive, complex commercial instrument or a more economical single-purpose system. Construction of a miniaturized version of this system is also possible with the addition of custom-designed components, but these modifications to the instrument would reduce the ease of adaptability to novel applications and would increase the cost. Future work will seek to design, build, and test a fully integrated, miniaturized μCE-LIF system for automated amino acid analysis based on components characterized in this modular testbed system. Due to the modularity in design, this system can be adapted to any wavelength excitation/emission required for multiple targets, including enhanced chiral analysis [159], polycyclic aromatic hydrocarbons (PAH's) [117], etc…, and serves as an excellent test bed for the fabrication of specialized portable or laboratory-based μCE-LIF systems for trace organic molecule detection.

CHAPTER 3. QUANTITATIVE, COMPOSITIONAL ANALYSIS OF TRACE AMINO ACIDS IN ICY MOON ANALOGUES WITH A BENCHTOP MICROCE-LIF SYSTEM

Current work in progress:

3.1 Abstract

Enceladus's and Europa's plume activity and evidence supporting a global subsurface ocean have made them high-priority targets for future NASA outer-planetary missions. In situ analysis of organic molecules in the plumes or subsurface oceans of these icy moons would provide relevant, detailed information on formation, habitability, and on-going planetary processes of celestial bodies and could provide the first evidence of the potential for extant life beyond Earth. Microcapillary electrophoresis with laser-induced fluorescence (μCE-LIF) enables highly sensitive, automated, quantitative, compositional analysis of organic molecule monomers and short polymers. Its potential for miniaturization and sub-parts-per-trillion (pptr) limit of detection (LOD) make it an enticing candidate for future planetary missions. Mars Organic Analyzer (MOA) portable μCE-LIF prototypes using μCE-LIF have been built and field tested in the Panoche Valley, CA, and in the Atacama Desert, Chile, and the Enceladus Organic Analyzer (EOA) and the Microfabricated Organic Analyzer for Biosignatures (MOAB) prototypes are currently under development as instruments for future biosignature discovery missions. Here, high-resolution separations of an amino acid standard solution, including valine, serine, alanine, glycine, glutamic acid, and aspartic acid, contained within icy moon analogue solutions of

sulfuric acid, carbonic acid, sodium carbonate, and magnesium sulfate were obtained using μCE-LIF detection. Separations were improved by diluting the salts in solution, regulating the pH, and chelating cations with Ethylenediaminetetraacetic acid (EDTA). A sample taken from Champagne Geyser at Chaffin Ranch in Utah was analyzed for amino acids and found to contain leucine, valine, serine, alanine, and glycine by direct comparison to spiked standards. Alanine and glycine were quantified via standard curve at 80.1 ± 0.8 μM and 900 ± 100 nM, respectively. This work represents a significant step forward for the liquid-based μCE-LIF analysis of small organic molecules and biopolymers for future space missions to icy bodies like Enceladus and Europa.

3.2 Introduction

Life as we know it on Earth requires liquid water to survive and, in fact, tends to thrive in water-rich environments. However, life has also shown a propensity to adapt and endure in extreme environments, such as those with limited water activity, extreme temperatures, high salinity, etc… [9]. Given these realities and the significant advancements made in outer-planetary space travel, the icy moons in our Solar System have been garnering increasing attention over the past few decades [36, 162]. One of the most commonly discussed targets is Enceladus, Saturn's main E-ring provider [163-167]. Much of what we have discovered about Enceladus originates from the Cassini-Huygens mission to study Saturn and its surrounding bodies [18, 51-66]. During the mission, the Cassini spacecraft discovered plumes emanating from the moon's south pole. Data analysis of these striking features has since provided evidence of ongoing hydrothermal activity [67, 68] and has suggested the presence of a global subsurface ocean [69]. The Ion and Neutral Mass Spectrometer (INMS) on board Cassini detected in these plumes the presence

of molecules commonly associated with biological processes, including methane, carbon dioxide, nitrogen, and others [168]. Recent analysis of data provided by Cassini's Cosmic Dust Analyzer (CDA) has shown the presence of macromolecular organic molecules in Saturn's E-Ring, suggesting these molecules originate from hydrothermal systems that exist at the liquid water/rock interface at the bottom of the subsurface oceans of Enceladus [169]. These hydrothermal systems could provide an energy source to fuel organic chemical reactions, potentially giving rise to and supporting extant life [70]. The unique opportunity to directly sample particles from the subsurface ocean via fly-by missions through the plumes makes Enceladus an excellent target for future habitability studies in the outer Solar System.

Europa, Jupiter's smallest Galilean moon, has also become a high-priority target for future outer-planetary missions with the evidence supporting the presence of a global subsurface ocean and suggested plume activity [34, 35, 37, 170, 171]. While no craft has ever landed on the surface of Europa, multiple fly-by missions have been conducted [172-176]. The Galileo mission provided the bulk of our chemical information via reflectance spectroscopy, leading to a better understanding of the surface composition [38, 39], which is largely defined by streaking ridges, cracks (lineae), and chaos territories. These deformations are thought to be caused by tidal heating of the interior of the moon and through interaction of a subsurface ocean with both the rocky core and the outer ice layer [41-43]. Since the material in these lineae has lower water-ice content and appears to be comprised mainly of salt minerals [38, 39], these deposits likely originated from the interior of the moon [44]. The type of salts on the surface could dictate the performance of wet chemistry techniques for a potential lander mission in search of organic molecules, which

have yet to be identified on Europa. Mg^{2+}, Na^{+}, Cl^{-}, and SO_4^{2-} are believed to be among the most abundant ions residing on the surface [47, 48]; any chosen technique must be robust to analysis of water solutions comprised of these ions.

While Europa's surface is relatively young compared to other bodies within the Solar System [177], it is subjected to harmful ionizing radiation from Jupiter's magnetosphere [178]. However, the effects of this radiation vary throughout the surface [179]. The leading and trailing hemispheres experience higher dosages than the mid- to high-latitudes [180]. In addition, the prominent chaos regions show active resurfacing of material [40, 181, 182], and areas with tenuous plume activity are consistently depositing material from the subsurface ocean [183], suggesting these locations likely have been exposed to less radiation. When taken together, locations with more recently deposited subsurface material in the mid to high latitudes would serve as the most promising sites for future biosignature discovery missions. However, these data have also suggested that organic species can survive in the high-dosage regions at depths as little as 10 cm below the surface [180]. While many locations on Europa's surface may be sufficient for biosignature discovery, more knowledge is needed to more accurately select instrumentation for future lander missions [184]. Several fly-by missions, including the National Aeronautics and Space Administration's (NASA's) Europa Clipper and the European Space Agency's (ESA's) JUpiter Icy Moon Explorer (JUICE), are projected to launch in the early 2020's and will provide an improved survey and characterization the moon's exterior [49, 50]. Though indirect, the information gained from the on-board instruments should provide more physical characterization of the interior of the moon, including the concentration of surface salts, ocean size, ice crust thickness, etc…. Much

like Enceladus, *in situ* quantitative and compositional analysis of organic molecules on the surface of Europa would provide relevant, detailed information on formation, habitability, and on-going planetary processes of these icy, celestial bodies and could provide the first evidence of the potential for extant life beyond Earth [185].

One technique that would provide highly sensitive, automated, quantitative, and compositional analysis of organic molecule monomers and short polymers is microcapillary electrophoresis with laser-induced fluorescence (μCE-LIF). Its potential for miniaturization and sub-parts-per-trillion (pptr) limit of detection (LOD) make it an enticing candidate for future planetary missions, like those to Enceladus and Europa [110, 160]. MicroCE-LIF enables analysis of a variety of organic compound classes, including amines, amino acids, aldehydes, ketones, carboxylic acids, thiols, and polycyclic aromatic hydrocarbons [81, 82, 88, 98, 117, 144]. Portable Mars Organic Analyzer (MOA) prototypes have been field tested in the Atacama Desert, Chile [116], and the Panoche Valley, CA [96]. These systems have conducted high resolution analyses of trace species in multiple relevant planetary analogue samples, including those from hydrothermal sites [82, 117], the Murchison meteorite [88], and the Rio Tinto [80]. MicroCE-LIF systems based on these prototypes, such as the Enceladus Organic Analyzer (EOA), the Impact Penetrator Organic Analyzer (IMPOA), and the Microfabricated Organic Analyzer for Biosignatures (MOAB), have been proposed for missions to Mars, Enceladus, and Europa [118-121].

Figure 3.1 outlines a potential μCE-LIF analysis protocol for an icy moon mission platform. An abrasive saw will dig roughly 10 cm below the surface ice and a scooping device will extract a subsurface ice sample. This sample will be heated and delivered as a

liquid to the organic analysis system. A fluorophore will be mixed with the liquid sample and bound to organic molecules of interest using an automated mixing routine in a microfluidic device. The reacted sample will be transferred to the microcapillary for injection and separation using electrophoresis. The laser system will detect the fluorophore-bound organics, which will be identified and quantified using a set of predetermined standards spiked into the sample. Organics present in the sample but not included in the standard will be identified via a collected bank of electropherograms.

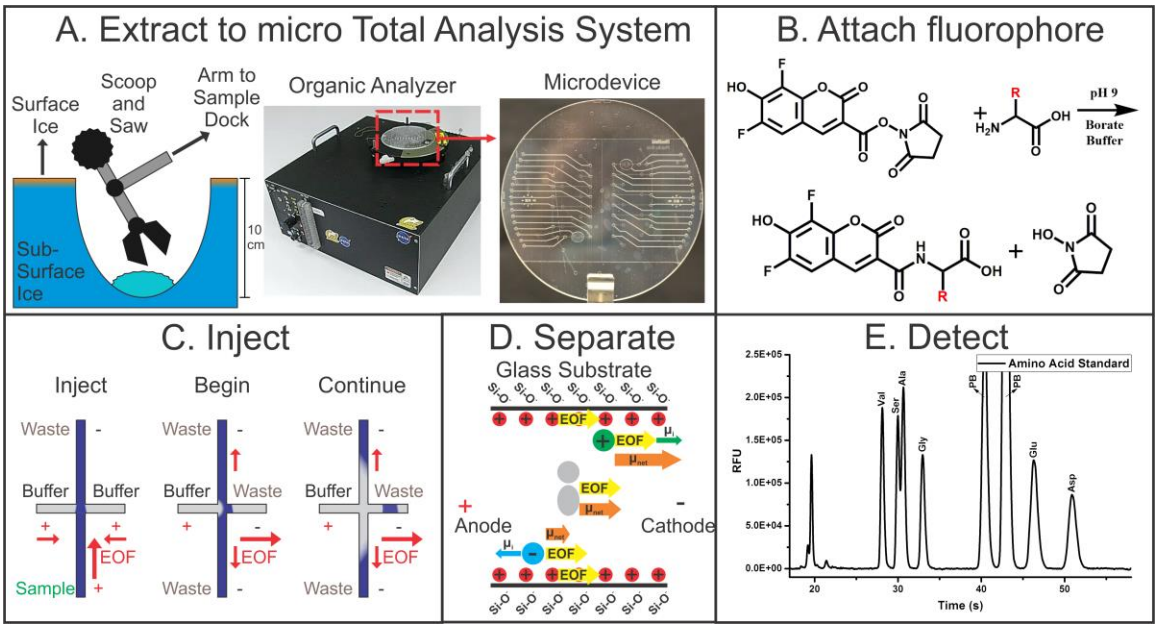

Figure 3.1. Outline of an analysis protocol for a Europa mission platform. (A) Extract a subsurface ice sample and deliver to the organic analysis system. (B) Bind the fluorophore of interest to organic molecules in the extracted liquid sample using a microfluidic device [96]. (C) Inject the sample into the microcapillary channel and (D) separate organic molecules based on their mass to charge ratio. (E) Detect the fluorophore and identify the attached organic molecules.

Here, we selected amino acids as our organic molecule of interest. To demonstrate the robustness of μCE-LIF towards an icy-moon-like environment, we tested four different salt solutions: H_2CO_3 (carbonic acid), Na_2CO_3 (sodium carbonate), H_2SO_4 (sulfuric acid),

and $MgSO_4$ (magnesium sulfate). We chose these compounds to simulate the possible effects of salts found in the plume of Enceladus or likely on the surface of Europa. Separations of amino acids using a benchtop μCE-LIF detection system were improved by diluting the salts in solution, regulating the pH, and chelating cations with Ethylenediaminetetraacetic acid (EDTA). We then analyzed a sample taken from Champagne Geyser at Chaffin Ranch in Utah for amino acids and found it to contain leucine, valine, serine, alanine, and glycine by direct comparison to spiked standards. This work presents important progress for the liquid-based analyses of small organic molecules and biopolymers for future space missions to high-priority targets in our Solar System.

3.3 Experimental

3.3.1 Reagent Preparation

Reagents were used as received except where noted. Millipore deionized (DI) water (18 MΩ, megaohms) was distilled (d) 10x in a high efficiency particulate air (HEPA)-filtered environment and used to make all aqueous solutions. NaOH (Sigma-Aldrich Co., St. Louis, MO) and HCl (BDH Chemicals, Darmstadt, Germany) were prepared as 1 M stock aqueous solutions and diluted where necessary. Borate running buffer (Sigma-Aldrich Co.), pH 9, was recrystallized 10X using 10x d DI water and prepared as a 200 mM stock aqueous solution. Two stock standard amino acid solutions were made: standard stock solution 1 contained valine, serine, alanine, glycine, glutamic acid, and aspartic acid (Sigma-Aldrich Co.), each 20 mM, and standard stock solution 2 added leucine (Sigma-Aldrich Co.) to the previous combination of amino acids, each 4 μM. A 20 mM stock solution of 3-carboxy-6,8-difluoro-7-hydroxycoumarin (Pacific Blue [PB]) dye

(Invitrogen, Carlsbad, CA) was dissolved in dimethylformamide (DMF) (EMD Millipore Co., Billerica, MA). Dilution series of H_2CO_3 (2-2000 nM), Na_2CO_3 (1-1000 mM), H_2SO_4 (1-1000 mM), and Mg_2SO_4 (1-1000 mM) containing valine, serine, alanine, glycine, glutamic acid, and aspartic acid (each 100 nM) were made in 10X d DI water. All aqueous solutions were stored at 4 °C when not in use, and all DMF solutions were stored at -20 °C when not in use.

3.3.2 Detection System and Microdevice Fabrication

Capillary zone electrophoresis (CZE) experiments were conducted using the previously characterized benchtop μCE-LIF system with a fully integrated optical set-up, microdevice stage, and high-voltage power supply. Briefly, the instrument includes a controllable 0-40 mW, 404.5 nm laser diode with an excitation intensity set to 20 mW. Fluorescence emanating from the microchannel is collected through the excitation objective lens and directed to a spectrometer for detection. The optical subsystem contains a 405 ± 10 nm bandpass (BP) filter, a 425 nm dichroic mirror, and a 420 longpass (LP) filter optimized for PB dye fluorescence. The optical assembly is mounted to a three dimensional (3D) motorized platform for precision alignment to the microchannel.

The design and fabrication process for the microdevices used in this study was described in the previous chapter. Briefly, devices were purchased from Micronit Microfluidics (Enschede, Netherlands) and fabricated according to standard isotropic (hydrofluoric acid) HF etching procedures [95, 103, 122, 145, 146]. Each device features a perpendicular 1 cm injection cross channel with an inlet/outlet hole on each end and an

8.2 cm separation channel with an inlet/outlet hole on each end, two tapered bends, and a 7.5 cm effective separation length [97, 148].

3.3.3 EOF Activation and Electrophoretic Conditions

Alternating rinses of 100 mM hydrochloric acid (HCl) (BDH Chemicals, Darmstadt, Germany) and 100 mM sodium hydroxide (NaOH) (Sigma-Aldrich Co., St. Louis, MO) were pulled through the capillary channels by vacuum 3x to clean the device. Vacuum was then applied to fill all channels with 35 mM borate running buffer, pH 9 (Sigma-Aldrich Co.). A blank run with running buffer was done between each separation using a HVS448 6000 D high voltage power supply (LabSmith, Inc., Livermore, CA). First, a potential was applied across the sample well (ground) and the waste well (-1500 Volts [V]) while keeping the anode and cathode grounded for 10 seconds (s) to induce a cross-injection. The potential was changed and applied to the anode (3000 V), cathode (-3000 V), and sample/waste wells (2400 V each) to achieve an electric field strength of 732 V/cm down the capillary.

3.3.4 Sample Preparation of Icy Moon Analogues and Geyser Sample

For the H_2CO_3, Na_2CO_3, and H_2SO_4 icy moon analogues, each dilution series was mixed 1:1, 1:2, or 1:10 with a combination of 35 mM borate buffer, pH 9, and 20 mM PB dye, totaling 330 µL. For the 1:1 mixture, 165 µL of analogue was combined with 163 µL of buffer and 2 µL of PB dye. For the 1:2 mixture, 110 µL of analogue was combined with 218 µL of buffer and 2 µL of PB dye. For the 1:10 mixture, 30 µL of analogue was combined with 298 µL of buffer and 2 µL of PB dye. For the Mg_2SO_4 analogue, each dilution series was mixed with EDTA in 35 mM borate buffer, pH 9, and reacted with 2

µL of PB dye to make 200 µL of 0, 5, or 10 mM EDTA solutions. A standard comparison for each icy moon analogue was made by mixing 1 µL of amino acid standard stock solution 1 with 18 µL of 35 mM borate buffer, pH 9, and 1 µL of PB dye, then diluted 1000x before analysis. A blank comparison for each analogue was made by mixing 1 µL of 10x d DI water with 18 µL of 35 mM borate buffer, pH 9, and 1 µL of PB dye, then diluted 1000x before analysis. All solutions were stored in the dark for 2 hours (hr) to react.

The icy moon analogue sample taken from Champagne Geyser at Chaffin Ranch in Utah was diluted 1:1 with DI water for analysis when applicable; 2 µL of diluted sample was mixed with 36 µL of 35 mM borate buffer, pH 9, and 2 µL of PB dye. For a standard comparison, 2 µL of amino acid standard stock solution 2 was mixed with 36 µL of 35 mM borate buffer, pH 9, and 2 µL of PB dye. For the internal standard, 1 µL of undiluted sample was mixed with 1 µL of amino acid standard stock solution 2, 36 µL of 35 mM borate buffer, pH 9, and 2 µL of PB dye. A blank was run by mixing 2 µL of 10x d DI water with 36 µL of 35 mM borate buffer, pH 9, and 2 µL of PB dye. The solutions were made in triplicate and stored in the dark for 2 hr to react.

3.3.5 Sample Analysis

Resulting electropherograms were baseline-subtracted and fitted using a 0.2 % Loess filter via the chromatographic analysis program PeakFit (Systat Software, Inc., San Jose, CA). Fitted electropherograms were extracted to the graphical data analysis program OriginPro (OriginLab Co., Northampton, MA) for further characterization of signal-to-noise (S/N) and resolution data extracted from the fitted files.

3.4 Results and Discussion

Using a benchtop μCE-LIF detection system, amino acids were analyzed in four separate icy moon analogue solutions: Na_2CO_3, H_2CO_3, H_2SO_4, and $MgSO_4$. The H_2CO_3 standard represented a best-case scenario where salt and acid concentrations were not significantly high enough to cause issues with experimental analysis. The Na_2CO_3 standard simulated the potential for encountering high sodium (Na^+) concentrations on Europa's surface or Enceladus's plume. The H_2SO_4 standard characterized an extremely low-pH scenario with high acid concentrations. The $MgSO_4$ standard simulated the worst-case scenario with both high SO_4^{2-} and high Mg^{2+} concentrations, affecting experimental analysis. Each solution contained a standard amino acid solution of serine, alanine, glycine, valine, aspartic acid, and glutamic acid (each 1 μM) and was diluted accordingly for each experiment.

3.4.1 H_2CO_3 Icy Moon Analogue

Ten different concentrations of H_2CO_3 (2000, 1000, 500, 200, 100, 50, 20, 10, 5, and 2 nM) were analyzed at three separate dilutions before reaction (1:1, 1:2, and 1:10). For clarity, only the 2000 nM, 200 nM, 20 nM, 10 nM, 2 nM, and standard containing no Na_2CO_3 are shown at the 1:1 dilution (Figure 3.2). The complete data set of all dilutions is shown in Supplementary Figure A.2.2. . Being a weak acid, H_2CO_3 did not require dilution to give desired separations. The borate buffer regulated the pH of each sample to allow a reaction to occur, and no extraneous salts were present, so there were no deleterious electrodispersion effects on the injection. In addition, S/N of glycine remained consistent for each dilution series (Figure 3.6 A).

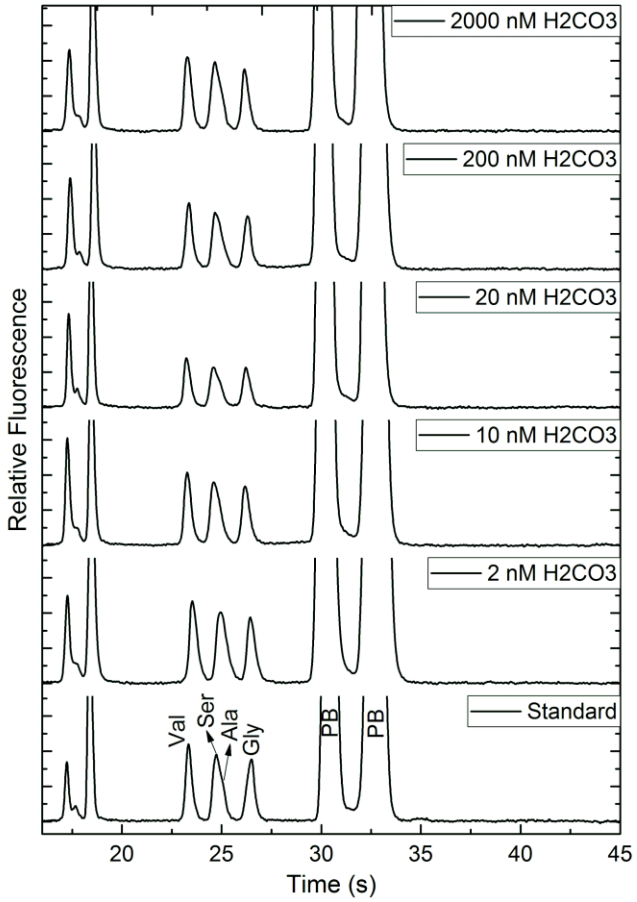

Figure 3.2. MicroCE separations of an amino acid standard (Val, Ser, Ala, Gly, Glu, and Asp - each with a 100 nM starting concentration) in varying starting concentrations of H_2CO_3 diluted 1:1 before labeling (732 V/cm separation potential).

3.4.2 Na_2CO_3 Icy Moon Analogue

Ten different concentrations of Na_2CO_3 (1000, 500, 250, 100, 50, 25, 10, 5, 2.5, and 1 mM) were analyzed at three separate dilutions before reaction (1:1, 1:2, and 1:10). For clarity, only the 1 M, 100 mM, 10 mM, 5 mM, 1 mM, and standard containing no Na_2CO_3 are shown at the 1:1 and 1:2 dilution, and each dilution series is scaled to the same relative fluorescence intensity (Figure 3.3). The complete data set at all dilutions is shown in Supplementary Figure A.2.3. As concentration of Na_2CO_3 decreases and dilution factor

increases, injection efficiency increases, enabling separation and quantitation. High ionic strength causes electrodispersion effects during injection [186, 187]; a sample dilution mitigates these effects. Separation efficiency reached a plateau below 10 mM Na_2CO_3 (Figure 3.6 B).

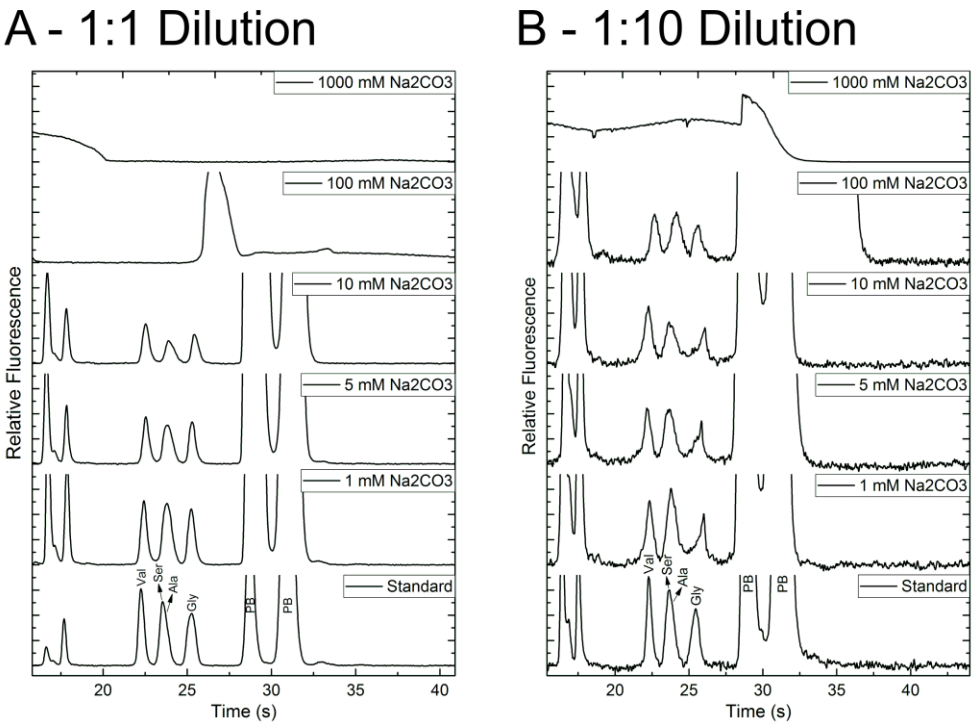

Figure 3.3. MicroCE separations of an amino acid standard (Val, Ser, Ala, Gly, Glu, and Asp - each with a 100 nM starting concentration) in varying starting concentrations of Na_2CO_3 diluted (A) 1:1 and (B) 1:10 before labeling (732 V/cm separation potential).

3.4.3 H_2SO_4 Icy Moon Analogue

Ten different concentrations of H_2SO_4 (1000, 500, 250, 100, 50, 25, 10, 5, 2.5, and 1 mM) were analyzed at three separate dilutions before reaction (1:1, 1:2, and 1:10). For clarity, only the 1 M, 100 mM, 10 mM, 5 mM, 1 mM, and standard containing no H_2SO_4 are shown, and each dilution series is scaled to the same relative fluorescence intensity

(Figure 3.4). The H_2SO_4 analogue generated a pattern of separations similar to that of the Na_2CO_3 analogue. As concentration of H_2SO_4 decreases and dilution factor increases, injection efficiency increases and the buffered solution is able regulate pH, enabling a reaction, separation, and quantitation. The 1:1, 1:2, and 1:10 dilutions give their best glycine peak resolution at 2.5 mM, 5 mM, and 10 mM H_2SO_4, respectively (Figure 3.6 C). The 1:10 dilution series appears to plateau for both peak efficiency and S/N as concentration of H_2SO_4 decreases. The 1:2 and 1:1 dilution series would likely show a similar trend at lower concentrations of H_2SO_4. Further dilution of the standard to 1:20 would enable analysis of higher H_2SO_4 concentrations but would also further drop the signal of the amino acids. However, this 1:20 dilution would likely remain within the scope of the Europa Lander Report, which requires detection of 1 picomole of organic in a 1-gram (g) sample [184]. If a 1 picomole organic is initially extracted in 1 mL of liquid and further concentrated to 10 µL, the resulting concentration would be 100 nM. This sample can be safely diluted 20x to 5 nM before approaching the 2.11 nM LOD reported for the µCE-LIF system used in this study and 1000x to 100 pM before approaching the 75 pM LOD reported for similar µCE-LIF instruments using an alternative detector [88].

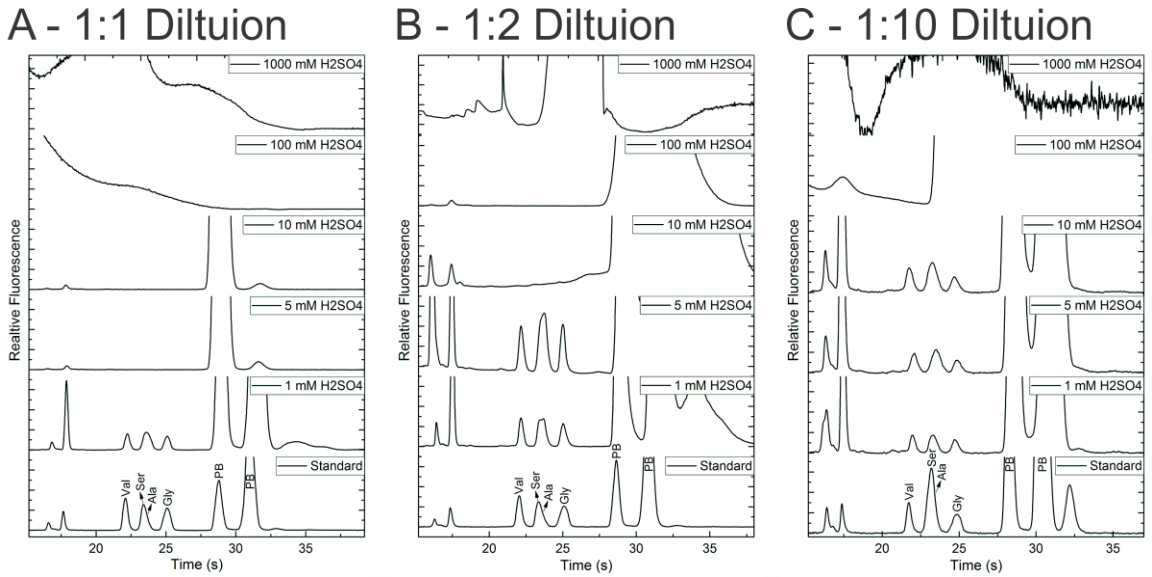

Figure 3.4. MicroCE separations of an amino acid standard (Val, Ser, Ala, Gly, Glu, and Asp – each with a 100 nM starting concentration) in varying starting concentrations of H_2SO_4 diluted (A) 1:1, (B) 1:2, and (C) 1:10 before labeling (732 V/cm separation potential).

3.4.4 $MgSO_4$ Icy Moon Analogue

For examining the $MgSO_4$ analogue, a standard amino acid solution of serine, alanine, glycine, valine, aspartic acid, and glutamic acid (each 1 µM) was made. Ten different concentrations of $MgSO_4$ (1000, 500, 250, 100, 50, 25, 10, 5, 2.5, and 1 mM) were analyzed at three separate concentrations of EDTA after reaction (0 mM, 5 mM, and 10 mM). For clarity, only the 1 M, 100 mM, 10 mM, 5 mM, 1 mM, and standard containing no $MgSO_4$ are shown at 0 and 5 mM EDTA, and each dilution series is scaled to the same relative fluorescence intensity (Figure 3.5). The complete data set is shown in Supplementary Figure A.2.4. As concentration of $MgSO_4$ decreases, injection efficiency increases (Figure 3.6 D), enabling separation and quantitation. Addition of EDTA also increases separation efficiency by chelating Mg^{2+}. Mg^{2+} suppresses electroosmotic flow (EOF) and consequentially induces poor injection and separation at high concentrations

[188]. Addition of even a small concentration of EDTA enables high-resolution separations of amino acids in a $MgSO_4$ icy moon analogue sample.

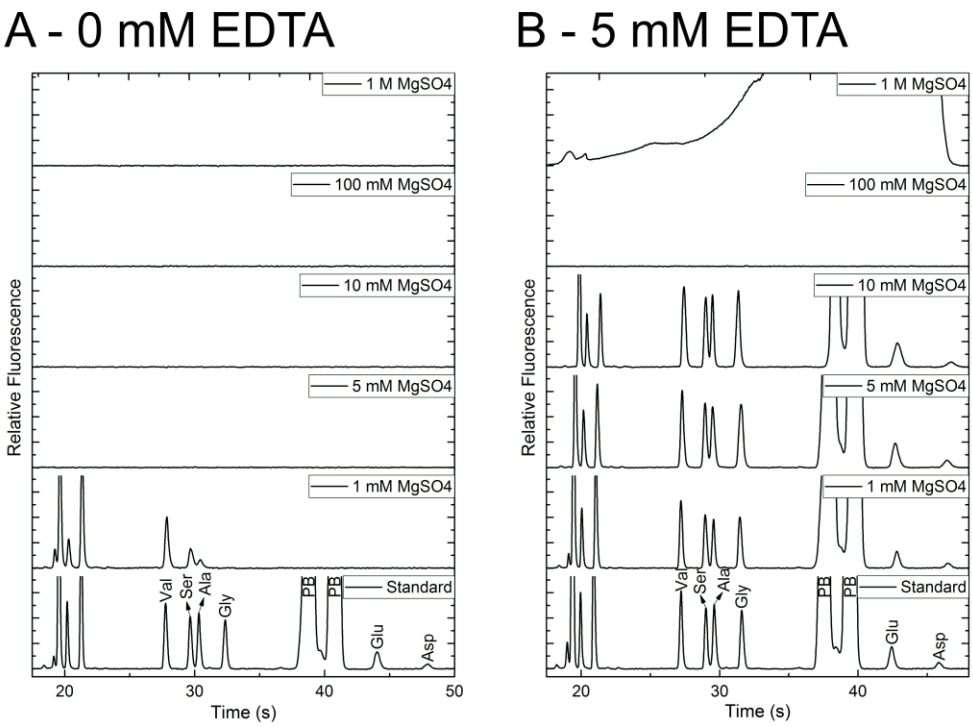

Figure 3.5. MicroCE separations of an amino acid standard (Val, Ser, Ala, Gly, Glu, and Asp - each with a 100 nM starting concentration) in varying starting concentrations of $MgSO_4$ in (A) 0 mM and (B) 5 mM EDTA (732 V/cm separation potential).

3.4.5 Summary of Icy Moon Analogue Signal-to-Noise (S/N) Trends

The unknowns contained within a sample of interest can affect the quality of a µCE separation in a variety of ways. Of those discussed here, pH is one of the more straightforward issues to resolve. As seen with the Na_2CO_3 example, a buffer with a sufficient buffering capacity can regulate lower pH samples and maintain the pH needed for PB dye labeling to occur (Figure 3.6 A) [153]. However, more concentrated buffer or dilution of the sample is required for low pH samples containing strong acids, like H_2SO_4

(Figure 3.6 C). Metal cations dissociated in solutions can require a more complex method of treatment. As demonstrated with the Na_2CO_3 example, monovalent cations, such as Na^+, can cause electrodispersion effects that disrupt EOF (Figure 3.6 B) [186, 187]. A concentration of 10 mM can be tolerated before dilution is required using this buffer system. Mg^{2+} ions can pose a more complicated challenge. The $MgSO_4$ example displays that even a 1 mM concentration of Mg^{2+} ions can completely suppress EOF by ionically binding to the capillary wall and disrupting the zeta potential (Figure 3.6 D) [188, 189]. Removal of these cations via dialysis would decrease their deleterious effects but would also greatly dilute the sample, potentially lowering the concentrations of any organics present below the LOD of the system. Therefore, addition of EDTA to chelate the free Mg^{2+} ions in solution is the preferred approach.

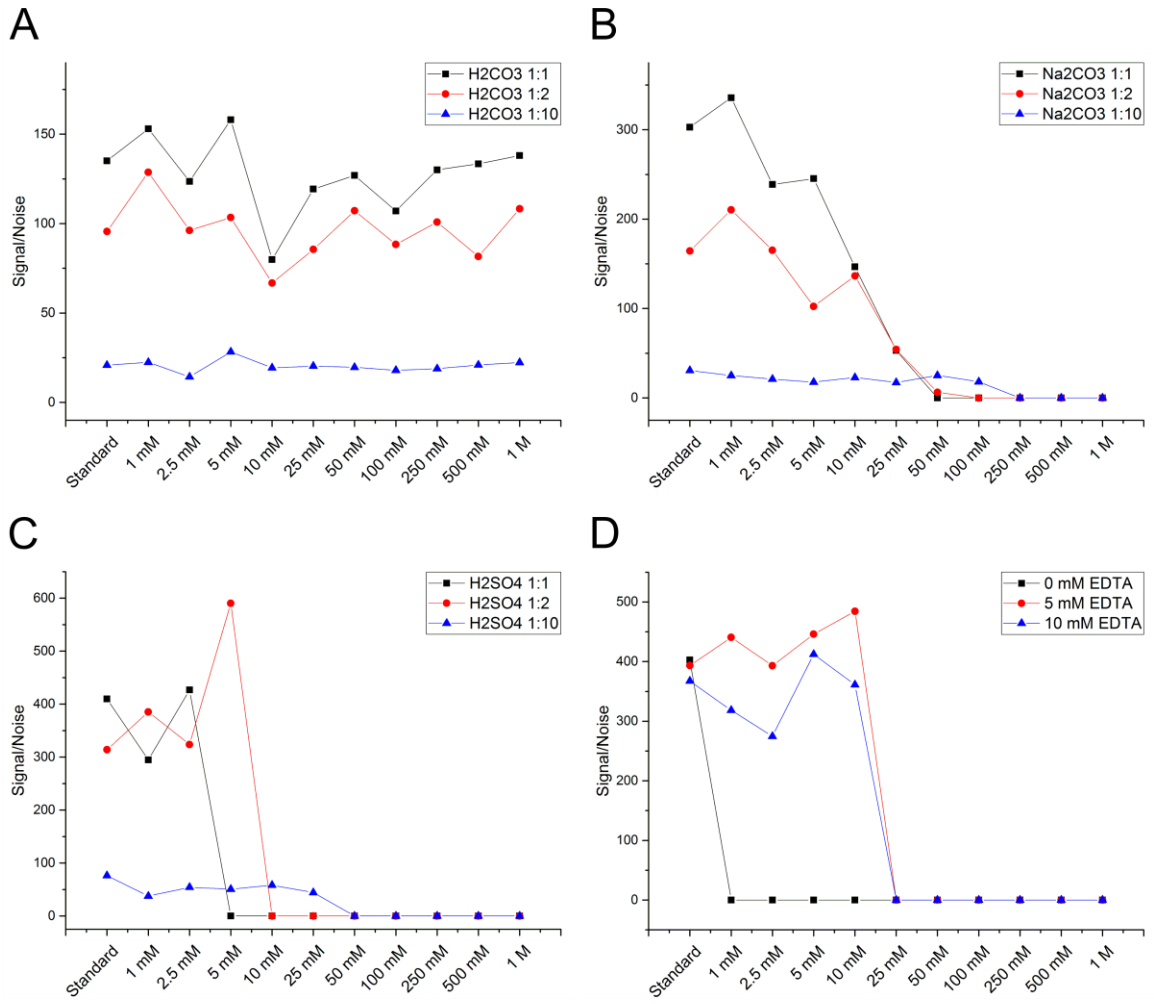

Figure 3.6. Glycine signal-to-noise (S/N) of (A) H_2CO_3, (B) Na_2CO_3, and (C) H_2SO_4 for each dilution series (1:1, 1:2, and 1:10) and of (D) $MgSO_4$ for each concentration of EDTA (0, 5, and 10 mM) at indicated starting concentrations (1000, 500, 250, 100, 50, 25, 10, 5, 2.5 and 1 mM for Na_2CO_3, H_2SO_4, and $MgSO_4$, and 2000, 1000, 500, 200, 100, 50, 20, 10, 5 and 2 nM for H_2CO_3).

3.4.6 Champagne Geyser Icy Moon Analogue Sample

A liquid sample was collected from Champagne Geyser at Chaffin Ranch in Utah. Like many of the geysers located along the Green River in Utah, the Champagne Geyser is largely sourced from underwater cold springs and aquifers [190]. CO_2 eruptions caused from the decarbonation of marine carbonites propel the cold-water brines to the surface [191-194]. The presence of carbonates and sodium salts and the high-ejection pressures are

analogous to the potential environment of an Enceladus or Europa plume or subsurface ocean. Analysis of trace organic molecules contained within these samples serves as a good Earth analogue method for future biosignature discovery missions to these icy moons.

Since the geyser sample was collected as a liquid, no organic extraction from a solid sample was necessary. Dilution of the sample 1:20 was required in order to reduce the salt concentration sufficiently to enable quality quantitation. The blank, standard, sample, and sample + standard were all prepared at the same volume (40 µL) to avoid any potential matrix effects during reaction. When compared to the amino acid standard and aligned using the characteristic PB dye peaks (37 and 38 s), the geyser sample was found to contain Leu (26 s), Val (26.5 s), Ser (28.5 s), Ala (29 s), and Gly (31 s) (Figure 3.7). Triplicate analysis of the electropherograms for the geyser sample are shown in Supplementary Figure A.2.5. A previously characterized standard curve was used to quantify alanine and glycine at 80.1 ± 0.8 µM and 900 ± 100 nM, respectively (Supplementary Table A.2.2). Using the spiked sample, leucine, valine, serine, and glycine were quantified at 4.4 ± 0.8 µM, 830 ± 80 nM, 780 ± 60 nM, and 1.0 ± 0.2 µM, respectively (Supplementary Table A.2.2). The concentration of alanine in the sample was significantly high enough to cause substantial variation in peak area and was not quantified using the spiked standard. The calculated concentration of glycine via standard curve was compared to the calculated concentration of glycine via spiked standard using a 2-tailed paired t-test with a set confidence value of 0.95. The obtained p value of 0.234 was greater than the set alpha value of 0.05 (1.00 - confidence value) (Supplementary Table A.2.3), suggesting that the calculated concentration of glycine from the spiked standard data set was statistically similar to the calculated concentration of glycine from the standard curve data set.

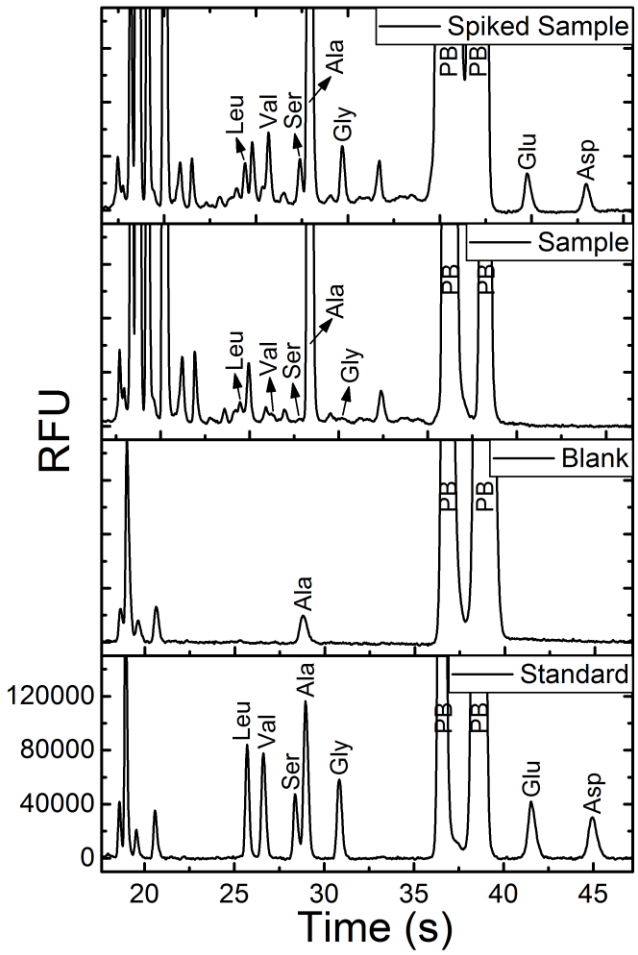

Figure 3.7. Electropherogram analysis of a sample taken from Champagne Geyser, an icy moon analogue geyser at Chaffin Ranch in Utah (732 V/cm separation potential).

Other primary amine-containing compounds were present in the sample but were not confirmed via direct spiking experiments. These organic molecules must be identified by other means, such as a more comprehensive set of internal standards, a constructed database of organic molecules, or combination with another detection technique. Combination with an orthogonal organic molecule separation and detection technique, such as mass spectrometry, could create an exceptionally powerful tool for the detection and quantification of organic molecules in planetary analogue environments. Not only

would ambiguity between overlapping organics be alleviated through direct mass identification, but any unknown organics could potentially be identified through their masses and fragmentation patterns as well.

3.5 Conclusions

High salt concentrations and low pH sample solutions affect μCE-based separations. Dilution of these salts or low pH samples can ameliorate deleterious effects by improving the reaction and injection efficiencies. Detection as well as quantification of organic molecules can be achieved using a predetermined set of standards. Here, high-resolution separations of an amino acid standard solution, including valine, serine, alanine, glycine, glutamic acid, and aspartic acid, contained within icy-moon-like solutions of sulfuric acid, carbonic acid, sodium carbonate, and magnesium sulfate were obtained using a benchtop μCE-LIF detection system. Separations were improved by diluting the salts in solution, regulating the pH, and chelating cations with EDTA. Using these methods, a sample taken from Champagne Geyser at Chaffin Ranch in Utah was analyzed for amino acids and found to contain leucine, valine, serine, alanine, and glycine by direct comparison to spiked standards. Alanine and glycine were quantified via standard curve at 80.1 ± 0.8 μM and 900 ± 100 nM, respectively, and leucine, valine, serine, and glycine were quantified via spiked standard at 4.4 ± 0.8 μM, 830 ± 80 nM, 780 ± 60 nM, and 1.0 ± 0.2 μM, respectively. Other primary amine-containing compounds were present in the sample but were not identified via direct spiking of internal standards. Identification of these molecules can be accomplished by either directly spiking in a more comprehensive set of internal standards with the unknown sample or externally generating a database of standards for external comparison.

The μCE-LIF detection system used for these analyses was designed for benchtop work. Miniaturization and automation with microfluidic devices are possible and do not impact the performance of the technique [88]. Further analyses of other classes of compounds, such as carboxylic acids, aldehydes, and ketones, is also possible but would require separate dye-labeling techniques for detection [81, 82]. Additionally, a conductivity probe for measuring salt concentrations before conducting separations could enable predetermination of dilution rates of sample or suggest if addition of a chelating reagent were necessary, greatly reducing the complexity of analysis.

While many remote sensing techniques provide invaluable information regarding the planetary processes of celestial bodies within the Solar System, direct sampling will be required for the complete analysis of future habitability studies. Biosignature discovery instruments for outer-planetary missions must possess the sensitivity and selectivity required for detection of trace organic molecules. This work outlines the successful analysis of trace amino acids contained within a Europa analogue sample and represents a significant step forward for the liquid-based μCE-LIF analysis of small organic molecules and biopolymers for future space missions to icy bodies like Enceladus and Europa. Ongoing and future work will seek to miniaturize the μCE-LIF system using flight-ready hardware and further analyze trace concentrations of other relevant classes of organic compounds, such as carboxylic acids, aldehydes, ketones, thiols, and polycyclic aromatic hydrocarbons (PAH's).

CHAPTER 4. OPERATION OF PNEUMATICALLY-ACTUATED MEMBRANE-BASED MICRODEVICES FOR *IN SITU* ANALYSIS OF EXTRATERRESTRIAL ORGANIC MOLECULES AFTER PROLONGED STORAGE AND IN MULTIPLE ORIENTATIONS WITH RESPECT TO EARTH'S GRAVITATIONAL FIELD

Adapted with permission from:

Z. Duca, G. Tan, T. Cantrell, M. Van Enige, M. Dorn, M. Cato, N. Speller, A. Pital, R. Mathies, and A. Stockton (2018). "Operation of pneumatically-actuated membrane-based microdevices for in situ analysis of extraterrestrial organic molecules after prolonged storage and in multiple orientations with respect to Earth's gravitational field," *Sensors and Actuators: B*, 272 (229-235).

https://doi.org/10.1016/j.snb.2018.05.040

4.1 Abstract

Pneumatically-actuated monolithic membrane microvalves are powerful microfluidic tools that can be integrated into programmable microfluidic architectures (PMAs) for multiple portable chemical analysis applications, including point-of-care (POC) diagnostics, environmental science, space exploration, etc…. However, these systems have not seen wide-scale deployment in industry or spaceflight due in part to (1) a concern that these systems may have a limited shelf-life and (2) a concern that performance depends specific device orientation in a gravitational field. To address these

concerns, we functionally tested a Mars Organic Analyzer microdevice fabricated in 2005 after 10 years of storage under ambient conditions. Using a square wave with a 500 millisecond (ms) actuation pulse width and a 1000 ms period and operating under vacuum at -980 millibar (mbar) from ambient pressure, all pneumatically-actuated valves opened in less than 1 hour. The vacuum required to actuate an open valve ranged from -218 to -175 mbar from ambient pressure. The microvalves were then programmed to transfer fluid through the microdevice for flow rate characterization. Fluidic transfer occurred at a flow rate of 122 ± 8 microliters/minute (μL/min) right-side up in Earth's gravitational field and 110 ± 10 μL/min upside down in Earth's gravitational field, indicating likely successful implementation in an orbital microgravity environment. This demonstration that microdevices retain full functionality after over 10 years of storage combined with successful operation in multiple orientations in Earth's gravitational field further validates the value of microdevices based on these microvalves for fluidic manipulation and sample handling in outer planetary missions.

4.2 Introduction

The search for life beyond Earth has been an ongoing endeavor since the Viking missions' initial search for organic chemical signatures in the Martian regolith in 1976 [23-27]. The onboard thermal volatilization gas chromatography mass spectrometry (TV-GS-MS) system detected chlorinated hydrocarbons and other organic chemicals used to clean the spacecraft prior to launch [23, 25, 26]. With promising but ambiguous data from the biological suites [24, 27], the results of these missions were interpreted as indicating the absence of life on Mars [23, 25, 26]. The only other organic analysis system sent to Mars was also a pyrolysis-based GC-MS system included on the Mars Science Laboratory

Sample Analysis at Mars (MSL SAM) instrument suite, which detected only chlorinated hydrocarbons and contaminants resulting from leakage in the *N*-methyl-*N*-*tert*-butyldimethylsilyl-trifluoroacetamide (MTBSTFA) derivatization system [28]. The Phoenix lander Microscopy, Electrochemistry, and Conductivity Analyzer (MECA) Wet Chemistry Laboratory (WCL) experiment measured parts-per-thousand (ppth) levels of perchlorates [29, 30], which upon heating to 300-600 °C oxidize *in situ* organic matter to chlorinated hydrocarbons and other species detected by both Viking and MSL SAM [31, 32]. The combined data from these missions indicate that an alternate method using wet chemical extraction will be necessary for quantitative, compositional characterization of native *in situ* organic molecules on Mars [23, 25, 33].

Mars is not the only location in the Solar System with the potential to host life. The icy moons of Jupiter (Europa) and Saturn (Enceladus) have also been identified as high priority targets for future exploration missions [195]. Evidence has supported the presence of global subsurface oceans on both Enceladus [69] and Europa [34], and recent data has indicated ongoing hydrothermal activity on Enceladus [67]. Data has also suggested plume activity on Europa [37], which may also be tied to ongoing hydrothermal activity [35, 36]. The Cassini Ion Neutral Mass Spectrometer (INMS) detected small organic molecules in a plume emitting from the South pole of Enceladus [66, 68, 196] but had neither the mass range nor sensitivity required to address the low level complex organics expected in outer planetary samples. Therefore, a more sensitive and higher resolution technique is required for future analysis of complex real samples. *In situ* quantitative and compositional analysis of organic molecules on the Martian surface or in the plumes or subsurface oceans of Enceladus or Europa would provide relevant, detailed information on formation,

habitability, and on-going planetary processes of these celestial bodies and could provide the first evidence of the potential for extant life beyond Earth [70].

Microcapillary electrophoresis with laser-induced fluorescence (μCE-LIF) is a liquid-based technique capable of highly sensitive (sub-parts-per-trillion, pptr), automated, and quantitative compositional analysis of multiple organic compound classes, including amines, amino acids, aldehydes, ketones, carboxylic acids, thiols, and polycyclic aromatic hydrocarbons [81, 82, 88, 98, 117, 144, 160]. This lower temperature and liquid-based analysis avoids undesirable decomposition of organics in the presence of high salt and perchlorates [80]. Mars Organic Analyzer (MOA) portable μCE-LIF prototypes have been field tested in the Panoche Valley, CA [96], and in the Atacama Desert, Chile [116], and have conducted high resolution analyses of trace species in multiple relevant planetary analogue samples, including those from the Murchison meteorite [88], hydrothermal sites [82, 117], the Saline Valley, and the Rio Tinto [80]. MicroCE-LIF systems based on these prototypes have been proposed for missions to Mars, Enceladus, and Europa [110, 118-121].

The microdevices at the heart of μCE-LIF and MOA technology integrate a μCE separation channel with an automated microfluidic sample processor that uses pneumatically-actuated normally-closed microfabricated monolithic membrane microvalves first developed in 2003 (Figure 4.1 a) [113]. In order to minimize contamination between mixing cycles, the microdevice utilizes specially designed bus valves in addition to standard (stop) valves [96]. Bus valves, as opposed to standard valves, allow fluid flow through the primary input/output bus channel without actuation, an enabling feature for this application-specific device (Figure 4.1 b-c). Multiple valves in

series operated sequentially form a peristaltic pump, and digital arrays of these microvalves form programmable microfluidic architectures (PMAs) for complex microfluidic processing, including metering, mixing, dilution, reaction, etc… [110].

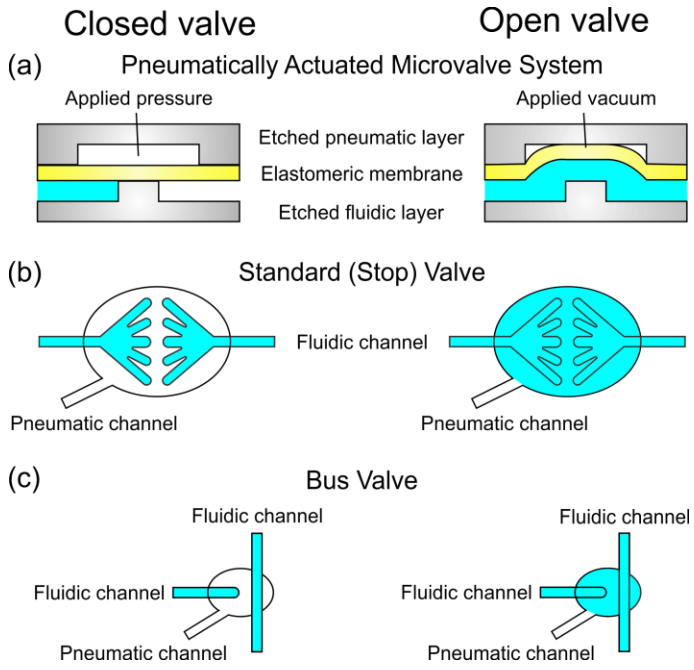

Figure 4.1. (a) Cross-section of a pneumatically-actuated, normally closed monolithic membrane microvalve and depiction of (b) a standard (stop) valve and (c) bus valve. Application of a vacuum to the displacement chamber deflects the PDMS membrane layer, opening the valve and allowing fluid flow along the discontinuity. A mild pressure to the chamber deflects the membrane back, forcing the fluid out and to the nearest open fluidic connection.

Miniaturization of microfluidic processing architectures based on normally-closed monolithic membrane-based microvalves has made this technology useful in fields where portability and speed of analysis are imperative [110, 160]. Membrane-microvalve processing architectures have been integrated with many chemical analysis techniques, including PCR (polymerase chain reaction) [197], ELISAs (enzyme-linked immunosorbent assays) [198], DNA (deoxyribonucleic acid) sequencing [76, 199], and μCE [96, 110, 116, 160]. These multipurpose architectures grew out of developments in

single-purpose devices, like that shown in Figure 4.2 a. This single-purpose device was fabricated in 2005 for μCE-LIF detection of organic molecules in Mars-relevant environments using a portable MOA prototype. While the layout of this device is now outdated [160], the valve technology has not changed significantly, and the device itself presents a unique opportunity to study the longevity of the microvalve technology.

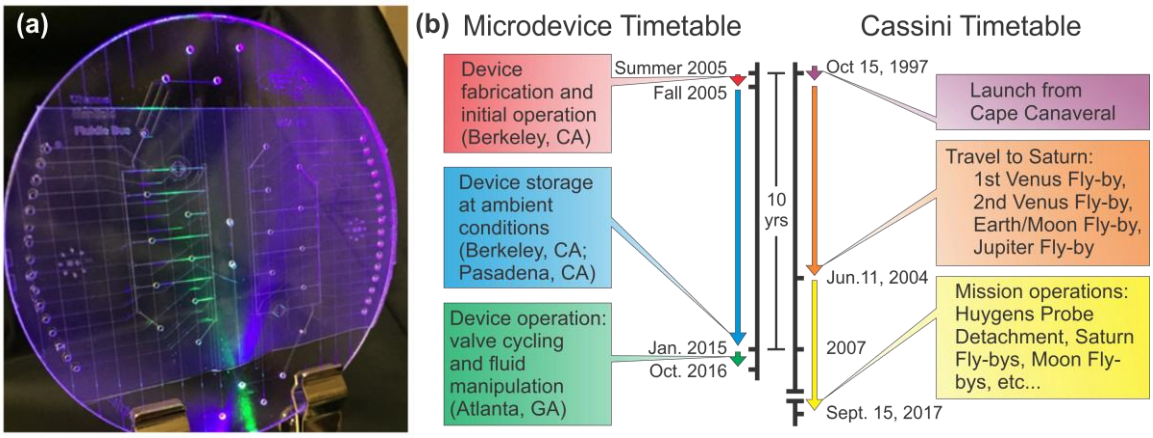

Figure 4.2. (a) Photograph of a microdevice designed for μCE-LIF analysis on Mars and fabricated in 2005. The device diameter is 100 mm. (b) Timeline of significant events from device fabrication to device operation and a timeline of significant events in the Cassini mission, a model Saturnian system mission.

Despite the power of microfluidic systems and the extensive studies done on the bonding behavior of PDMS to glass [200-202], the deployment of these systems for spaceflight has been limited by misconceptions that (1) microdevices have a limited shelf-life due to irreversible bonding of the PDMS (polydimethylsiloxane) elastomer to the glass substrate after an extended duration of non-operation and (2) fluidic manipulation within the device cannot occur in microgravity environments. These misconceptions persist despite no evidence in the literature to support them. Here, we are the first to assess PDMS microdevice extended shelf life by showing that microvalves in a Mars Organic Analyzer prototype microdevice function after 10 years of storage in ambient conditions. We open

all valves on the prototype device after storage and determine the vacuum required to actuate valves. We functionally test the device by using the valves to transfer dye through the microdevice in multiple orientations relative to Earth's gravitational field (G). We define the microdevice orientations to be +G when right-side up and -G when upside down with respect to Earth's gravitational field. We then characterize flow rate at both +G and -G orientations to demonstrate the robustness of PMA-based microdevices for fluidic manipulation in outer planetary missions.

4.3 Materials and Methods

4.3.1 Microfluidic Device Fabrication and Treatment

The microfluidic device was fabricated in 2005 for automated on-chip fluidic manipulation and electrophoretic separations with the MOA prototype instrument; the fabrication process was previously described in detail [96]. Briefly, amorphous polysilicon (aSi, 1000 Å) was deposited on a 100 millimeter (mm) diameter, 700 micrometer (μm) thick D263 borofloat glass wafer (Precision Glass and Optics, Santa Ana, CA). Photoresist (S1818) was spin-coated and patterned using a chrome mask and MA-6 aligner. The photoresist was developed and the exposed aSi was removed via SF_6 plasma reactive-ion etching (RIE). After patterns were wet etched with 49% HF, the photoresist was stripped and the backing aSi was removed with SF_6 RIE. Using diamond-tipped bits (Abrasive Technology, Lewis Center, OH), holes for both fluidic and pneumatic access were drilled to a 1.1 mm diameter. The remaining aSi was removed by RIE and a 254 μm Sylgard 184 PDMS layer (Dow Corning, Midland, MI) was used to bond the fluidic and pneumatic

wafers, forming a glass-PDMS-glass stack. The microdevice was then stored unused for 10 years at ambient temperature and pressure.

4.3.2 Microdevice Operation

For testing, the microdevices were housed in a custom-built manifold (Protolabs, Maple Plain, MN) (Supplementary Figure A.3.6) and monitored using an Amoeba Digital Microscope (Celestron, Torrance, CA). The manifold, with a custom PDMS gasket, enabled airtight connection between the microdevice and the off-chip pneumatic control system. The manifold was designed to allow visualization during operation.

The microvalves used in this microdevice have been previously described [113, 116]. Each of the 32 valves in this design consists of a discontinuous fluidic channel etched in a glass substrate with a displacement chamber etched in the pneumatic layer opposite the fluidic layer across the elastomeric PDMS membrane. Application of a vacuum to the displacement chamber deflects the PDMS membrane, enables fluid flow across the discontinuity, and draws fluid into the chamber [110].

The microvalves were actuated by LHD (Lee's High Density Interface) Series 3-way Face-Mount Style solenoid valves (The Lee Company, Essex, CT) that were switched between vacuum and ambient atmospheric pressure. Automated control of the solenoid valves was accomplished via code programmed into an Arduino Uno connected to a custom-built electronic circuit for valve opening experiments and via a custom LabVIEW (Laboratory Virtual Instrument Engineering Workbench) program controlling a 9472 Sourcing DO (digital output) C Series Module (National Instruments, Austin, TX) connected to a Compact Data Acquisition (cDAQ-9178) chassis (National Instruments,

Austin, TX) for fluid transfer experiments. Closed solenoid valves were given a constant pressure input. Fluidic manipulation was accomplished via a series of "open-close-wait" string commands that were sent via LabVIEW as binary control signals to the cDAQ controller. Wait steps after each open/close step were varied and optimized as described in detail in "Experimental".

4.3.3 Reagents

Blue food coloring was prepared at a 1:10 dilution in Millipore water (18 MΩ, megaohms) and used to visualize fluidic transfer rates at both +G and -G orientations.

4.3.4 Experimental

Valves were opened by following a square wave cycling protocol: apply a -750 millibar (mbar) pulse for 500 millisecond (ms), return to standard pressure for 500 ms. Valves that did not open in less than 5 hours were cycled at -980 mbar. All valves opened within 1 hour when cycling at -980 mbar.

Fluid transfer was accomplished by actuating valves in series to form a peristaltic pump using a two-stroke program [203]. Each actuation series of valves along the device was considered one pumping cycle. Wait times between valve actuation steps were kept equivalent. The total volumetric pumping rate was determined by measuring the amount of time required for complete transfer of 50 microliters (µL) of fluid. Fluidic transfer was characterized for wait times ranging from 200 to 20 ms. This process was performed both with gravity (+G orientation, or droplet applied to a wafer right-side up) and against gravity (-G orientation, or droplet suspended from a wafer turned upside down).

For determination of fluid transfer rates at both +G and -G orientations, valves were primed by dispensing 50 µL of Millipore water into the fluidic reservoir inlet and filling the channels of the microdevice by executing 10-20 pumping cycles. Once primed, 50 µL of blue food coloring was dispensed into the empty inlet. Fluidic transfer was accomplished by running between 30-50 pumping cycles until completion of dye transfer. The pumping process was filmed and timed using an AD-413MT-FVW Series Digital Microscope (DinoLite, Torrance, CA).

4.4 Results and Discussion

4.4.1 Microdevice Design and Longevity

The microdevice, fabricated in 2005 at the UC Berkeley Microfabrication Laboratory as part of MOA prototype µCE-LIF system, is a 100-mm diameter wafer with two identical halves. Each half consists of a series of 16 pneumatic valves for fluidic manipulation and a separation cross channel for µCE-LIF analysis (Figure 4.2 a). To investigate the effect of extended storage time, like that experienced during an outer planetary mission flight, the device was stored unused for 10 years in ambient conditions (Figure 4.2 b). After this time, the microdevice was housed in a custom-built breadboard system for pneumatic control and video capture, as described in the Materials and Methods.

Initially, the valves were opened by cycling a square wave signal with a 500 ms pulse width and 1000 ms period between -750 mbar and standard pressure. Figure 4.3 shows the opening of a valve after repeated cycles. When open, the shadow of the valve appeared more bubble-like with a strong reflection. When filled with a food coloring sample, no bleeding of fluid into the pneumatic control line was observed, even after

continuous and prolonged actuation, indicating that the elastomeric membrane remained intact without perforation, fracture, or major pinholes during both prolonged storage and throughout the opening protocol. Multiple valves were opened in less than 5 hours of cycling at -750 mbar from atmospheric pressure. All valves opened in less than 1 hour when cycled at -980 mbar. In addition to using the LHD solenoid valves, a 10-year-old LHLX0500200BB (Lee's High Density Interface Magnetically Latching) L Series 3-way Face-Mount Style solenoid valve was used to open a 10-year-old microvalve and shown to operate well within the factory pressure ratings (Supplementary Table A.3.4). The ease of opening of these microvalves demonstrates that microdevices based on normally-closed membrane-based microvalves retain functionality after 10 years of storage time, a storage time commensurate with that required by outer planetary missions [52, 204].

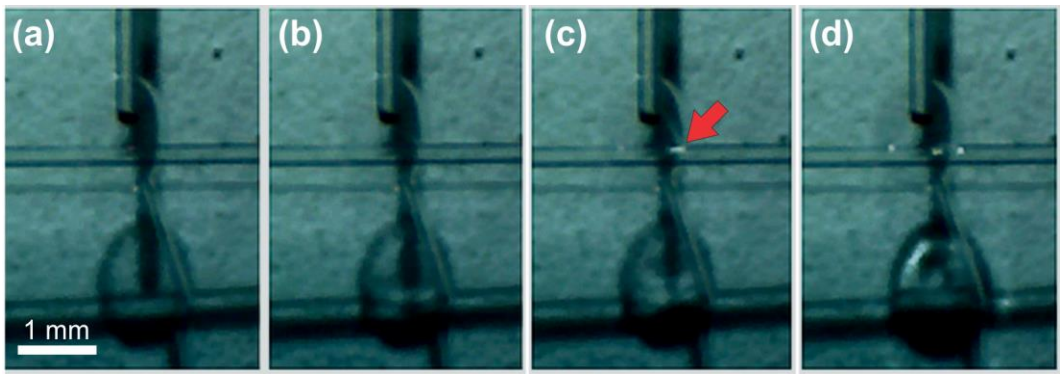

Figure 4.3. Still frames of a video capturing a microvalve opening after 5 hours of vacuum cycling at 750 mbar from ambient atmospheric pressure. (a) Closed valve under no vacuum (t, time = 0). (b) Closed valve under vacuum (t = 4:00:00). (c) Valve beginning to open under vacuum (t = 4:54:03). Arrow shows change in reflection, indicating an opening valve (d) Opened valve under vacuum (t = 5:00:00).

4.4.2 Fluid Manipulation at +G (right-side up)

Figure 4.4 displays still frames from a video of three valves in series operating sequentially to form a peristaltic pump pushing fluid left to right from valve 1 to valve 3.

The pumping rate was optimized by keeping wait times between steps equivalent and varying them together. Pumping rates for each wait time were determined by measuring the amount of time required for complete transfer of 50 μL of fluid (Figure 4.5). While not required for functionality, priming the system to remove bubbles in the microchannels was done by repeatedly pumping water through the valve system by sequential actuation of valves. Bubbles impact the pumping rate reproducibly (data not shown) but do not significantly impact performance otherwise. Therefore, any concern about bubbles is unfounded. The maximum rate of fluidic transfer (122 ± 8 microliters/minute, μL/min) was found when the wait time between valve actuation steps was 50 ms. This rate is comparable with other μCE-LIF devices from 2005 and of this design [203], providing further evidence of retained microfluidic manipulation performance after prolonged storage.

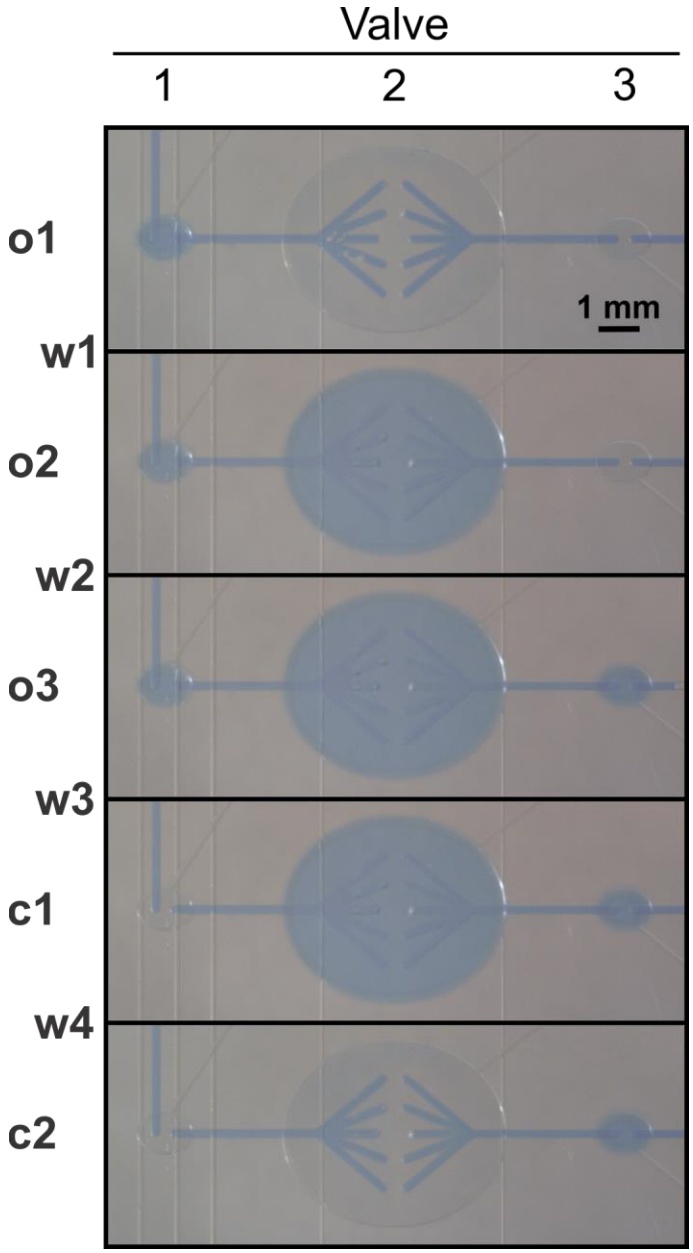

Figure 4.4. Demonstration of microfluidic transfer by the 2005 microdevice. Valves were actuated in series from valve 1 to 3 to form a peristaltic pump. Blue food coloring was used for visualization with a flow rate of 122 ± 8 µL/min.

4.4.3 Fluid Manipulation at -G (upside down)

Fluidic manipulation was also performed at -G orientation (upside down) using the same pumping sequences as used at +G (right-side up) (Figure 4.6). Loading the device

was typically conducted at +G for ease of manually dispensing liquid to the main fluidic input but was done at -G as well. The device was then turned over before operating the pumping sequence. Results showed a maximum fluidic transfer of 110 ± 10 µL/min, a rate statistically equivalent to that of the device operating at +G. When the wait times were varied from 10 to 200 ms, no statistically significant difference was observed in microfluidic performance (Figure 4.5).

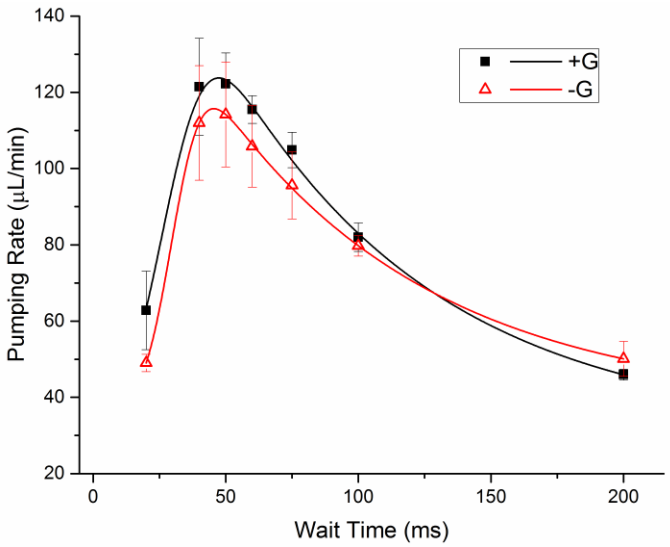

Figure 4.5. Characterization of the pumping rate dependence on valve actuation wait times.

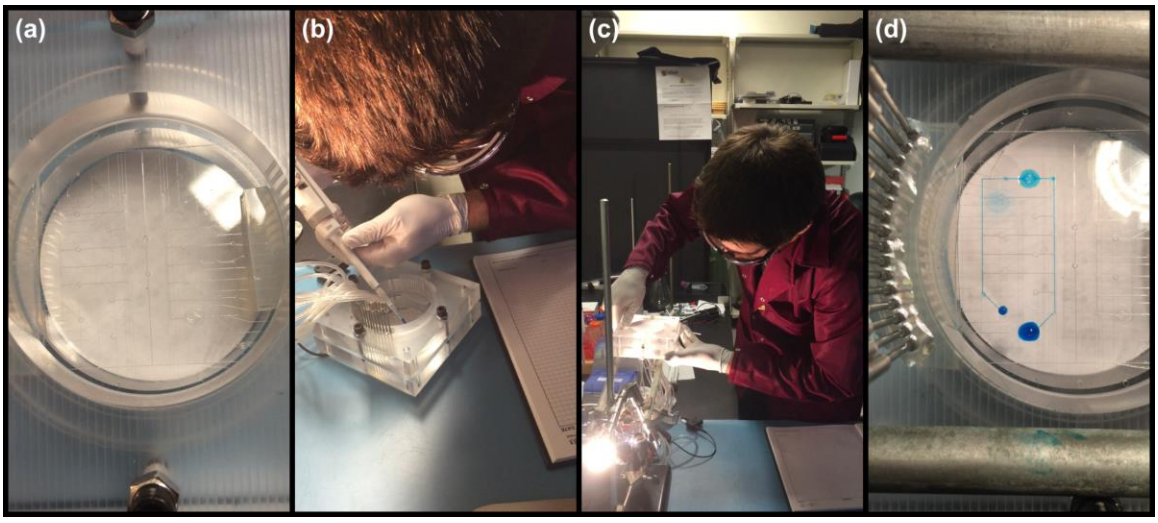

Figure 4.6. Operation of the microdevice at -G. (a) Microdevice primed for fluid transfer. (b) Fluid loading on a microdevice at +G. (d) Rotation and positioning of the microdevice from +G to -G. (e) Fluid transfer at -G.

4.4.4 Dominant Forces Experienced and Extension to Microgravity

When the device is flipped over, the droplet remains stationary because of the combinatory effects of cohesion due to the surface tension of water and adhesion of the droplet to the glass surface. Assuming no adhesion force and an ideal droplet with surface tension 72 millinewtons/meter (mN/m) [205] extending from a 1.1 mm capillary hole, the maximum droplet size at -G orientation on Earth is calculated to be 25.36 µL using the pendant drop experiment Equation (4.4.4.8):

$$mg = \pi d\gamma \qquad (4.4.4.8),$$

where m is the mass of the droplet, g is the acceleration due to gravity, d is the diameter, and γ is the surface tension. As distance from Earth increases, the gravitational field decreases, increasing the allowable droplet size. At reduced gravitational force (0.1 -G) the maximum droplet size scales to 253.6 µL. At zero gravitational force, the theoretical

droplet size goes to infinity without any external forces, enabling very large droplets to remain on the glass surface and available for microfluidic-based analyses in a micro-gravity environment.

4.5 Conclusions

Automated microfluidic systems are ideal for point-of-analysis assays requiring high speed and low mass, power, and volume. These devices must be robust to prolonged storage for both terrestrial and extraterrestrial applications, and this work shows that Mathies/Grover-style normally-closed monolithic membrane microvalves have this capability. A further requirement for space flight, especially for microgravity applications, is that microfluidic manipulation must be independent of device orientation within a gravitational field. These microvalves transfer fluid equivalently whether right-side up or upside down in Earth's gravitational field, which demonstrates fluidic manipulation independent of orientation within a gravitational field. PDMS appears to experience limited deleterious effects in radiation environments similar to those anticipated in orbit about Saturn or Jupiter [184, 206-208], and it is available in low-outgassing formulations that meet spaceflight requirements (eg. NuSil). Future work to ready the system for space flight will demonstrate microdevice functionality after extreme thermocycling and exposure to hard vacuum, radiation, and launch-simulated vibrational conditions. Combined with their effective widespread use in terrestrial applications, a complete demonstration of survivability and functionality in space environments will enhance the value of microvalve-based systems for fluidic manipulation in all terrestrial and extraterrestrial applications.

CHAPTER 5. EXAMINATION OF MICRODEVICE THERMAL STABILITY AND REACTIVITY OF PACIFIC BLUE DYE AFTER DRYING VIA SPIN VACUUM

Current work in progress:

5.1 Abstract

Missions to outer-planetary bodies such as Europa or Enceladus necessitate the use of specialized equipment and reagents. Chosen analytical techniques must prove capable of functioning after lengthy transit times, abnormal temperature swings, extreme vibrational anomalies, etc…. Microcapillary electrophoresis (μCE) with laser-induced fluorescence (LIF) is an organic molecule detection technique under development as an outer-planetary analytical method. Microdevices designed for automated mixing procedures and μCE-LIF analyses have been shown to fully retain functionality after remaining in storage for 10+ years and portable μCE-LIF detection instruments have been field tested in locations such as the Panoche Valley, CA, and the Atacama Desert, Chile. Here, 10-year-old microdevices were studied through a series of thermocycling tests from -196 °C to 100 °C. No deleterious effects were noted until 4 rounds of temperature cycling. The effect of drying 10+-year-old Pacific Blue (PB) dye with amino acids was examined by performing a set of three experiments: a liquid control where every solution was mixed normally in its liquid form, a partial-liquid control where each amino acid solution was dried using a spin vacuum and resuspended to mix before adding liquid PB, and a dry test where each amino acid solution was dried using a spin vacuum and resuspended to mix

after adding dry PB. The liquid and partial-liquid controls exhibited similar reactivities and thus signal-to-noise (S/N), while a slightly S/N intensity was noticed for the aspartic acid dry test. A likely cause of this decreased signal was the hydrolysis of PB. A 2x excess of PB when stored with amino acids would alleviate any potential loss in S/N. These results indicate that dry storage of PB with amino acid standards an acceptable method for future automated μCE-LIF analyses after extended storage of the microdevice in dry conditions.

5.2 Introduction

Designing an instrument for an outer planetary mission is a challenging task. The transit may last years, and one or more gravity assists may be required to reach the desired destination. For example, the Cassini-Huygens mission underwent two gravity assists at Venus and Earth to reach the Saturnian system [63]. During these gravity assists, the spacecraft may pass through the shadow of the planet, dropping the onboard temperature, or close to the Sun, raising the temperature. Therefore, to simulate these conditions, instruments and their individual components are often subjected to similar temperature conditions to assess their thermal ruggedness. These temperature changes are generally repeated multiple times to fully characterize an instrument and demonstrate optimal performance.

In addition to surviving possible extreme high and low temperature conditions, on-board instruments for missions to outer-planetary bodies necessitate the use of specialized equipment and reagents. Chosen analytical techniques must prove capable of functioning after lengthy transit times in vacuo [52, 204]. Microcapillary electrophoresis (μCE) with laser-induced fluorescence (LIF) is an organic molecule detection technique under

development as an outer-planetary analytical method. Microdevices designed for automated mixing procedures and μCE-LIF analyses have been shown to fully retain functionality after remaining in storage for 10+ years [209] and miniaturized μCE-LIF detection systems have been field tested in locations such as the Panoche Valley, CA, and the Atacama Desert, Chile [96, 116].

Microdevices contained within automated μCE-LIF instruments utilize programmable microfluidic arrays (PMAs) for precise routing of fluids, such as mixing, metering, diluting, etc… [110]. These structures can eliminate the need for bulky vacuum pumps and have proven to be valuable components for creating more compact, modular, and energy efficient instruments [97]. While these microdevices have been developed extensively for outer-planetary organic molecule detection methods, further characterization of the thermal survivability of the devices, as well as the stored reagents, should be examined.

Here, 10-year-old microdevices were subjected to thermocycles from -196 °C to 100 °C and examined for defects. The effect of drying 10+-year-old Pacific Blue succinimidyl ester (PB or PBSE) dye and an amino acid standard was also examined by performing a set of three experiments: a liquid control simulating a normal lab protocol, a partial-liquid control to eliminate reactivity concerns, and a dry test simulating a mission protocol. Signal-to-noise (S/N) of organics for the liquid control, dry control, and dry test were compared for statistical similarities. Practical solutions for any loss of S/N noticed for the dry test were presented.

5.3 Materials and Methods

5.3.1 Reagent Preparation

Reagents were used as received except where noted. Millipore deionized (DI) water (18 MΩ, megaohms) was distilled (d) 10x in a high efficiency particulate air (HEPA)-filtered environment and used to make all aqueous solutions. Borate running buffer (Sigma-Aldrich Co.), pH 9, was recrystallized 10x using d DI water and prepared as a 200 mM stock aqueous solution. NaOH (Sigma-Aldrich Co., St. Louis, MO) and HCl (BDH Chemicals, Darmstadt, Germany) were prepared as 1 M stock aqueous solutions and diluted where necessary. All aqueous solutions were stored at 4 °C when not in use, and all DMF solutions were stored at -20 °C when not in use.

For the liquid controls, five separate liquid control stock solutions were made (Figure 5.1): blank, standard 1, standard 2, sample 1, and PB. The blank was a solution of 10X distilled (d), deionized (DI) water. The standard 1 solution contained amino acids valine, alanine, glycine, glutamic acid, and aspartic acids each at 900 nM in 35 mM borate buffer. The standard 2 solution contained the same amino acids each at 1.8 µM in 70 mM borate buffer. The sample 1 solution contained amino acids leucine, serine, and glycine each at 1.8 µM in 10x d DI water. The PB solution contained PB at 2 mM in 10% dimethylformamide (DMF)/90% ethanol.

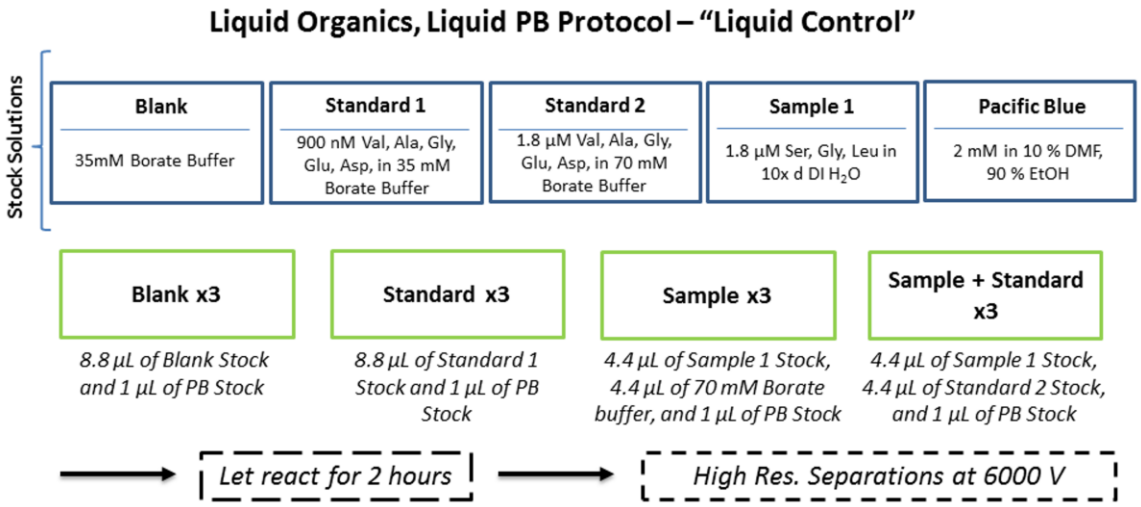

Figure 5.1. Outline for the liquid control experimental protocol.

For the partial-liquid control, four separate stock solutions were made (Figure 5.2): blank, standard 1, sample 1, and PB. Each solution was made the same as the ones from the dry test. The blank was a solution of 35 mM borate buffer made from the 10x d DI water. The standard 1 solution contained amino acids valine, alanine, glycine, glutamic acid, and aspartic acids each at 900 nM in 35 mM borate buffer. The sample 1 solution contained amino acids leucine, serine, and glycine each at 900 nM in 10x d DI water.

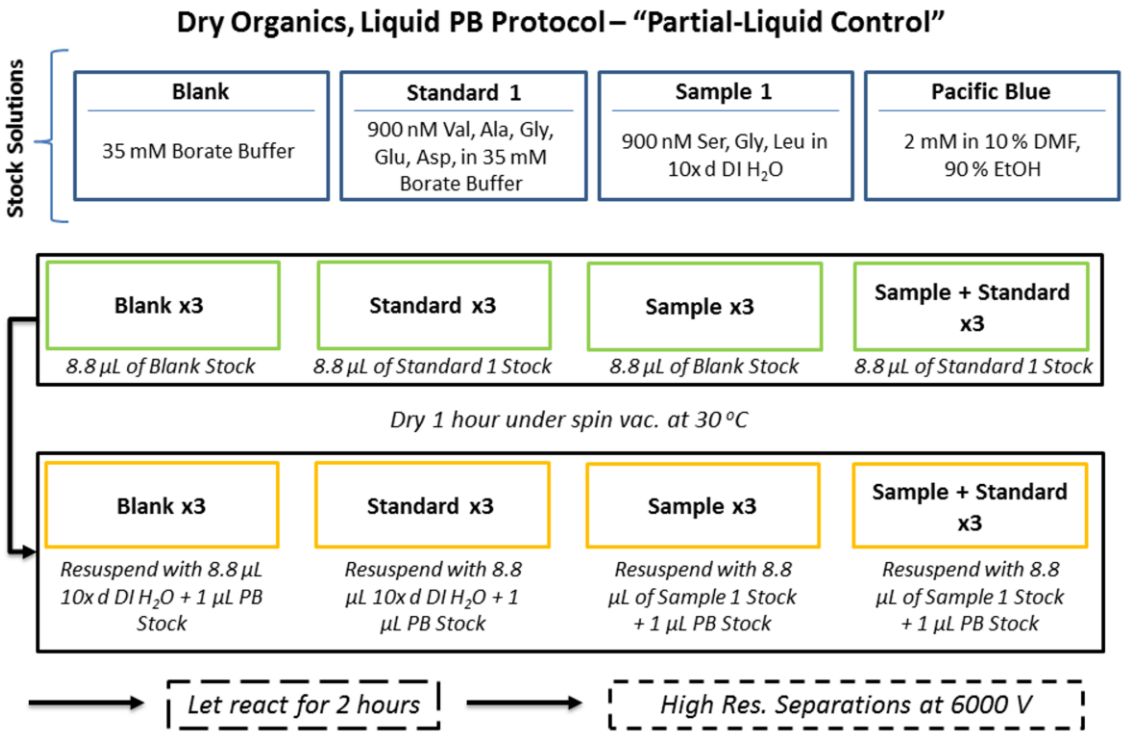

Figure 5.2. Outline for the partial-liquid control experimental protocol.

For the dry test, four separate stock solutions were made (Figure 5.3): blank, standard 1, sample 1, and PB. The blank was a solution of 35 mM borate buffer made from the 10x d DI water. The standard 1 solution contained amino acids valine, alanine, glycine, glutamic acid, and aspartic acids each at 900 nM in 35 mM borate buffer. The sample 1 solution contained amino acids leucine, serine, and glycine each at 900 nM in 10x d DI water. The PB solution contained PB at 2 mM in 10% DMF/90% ethanol.

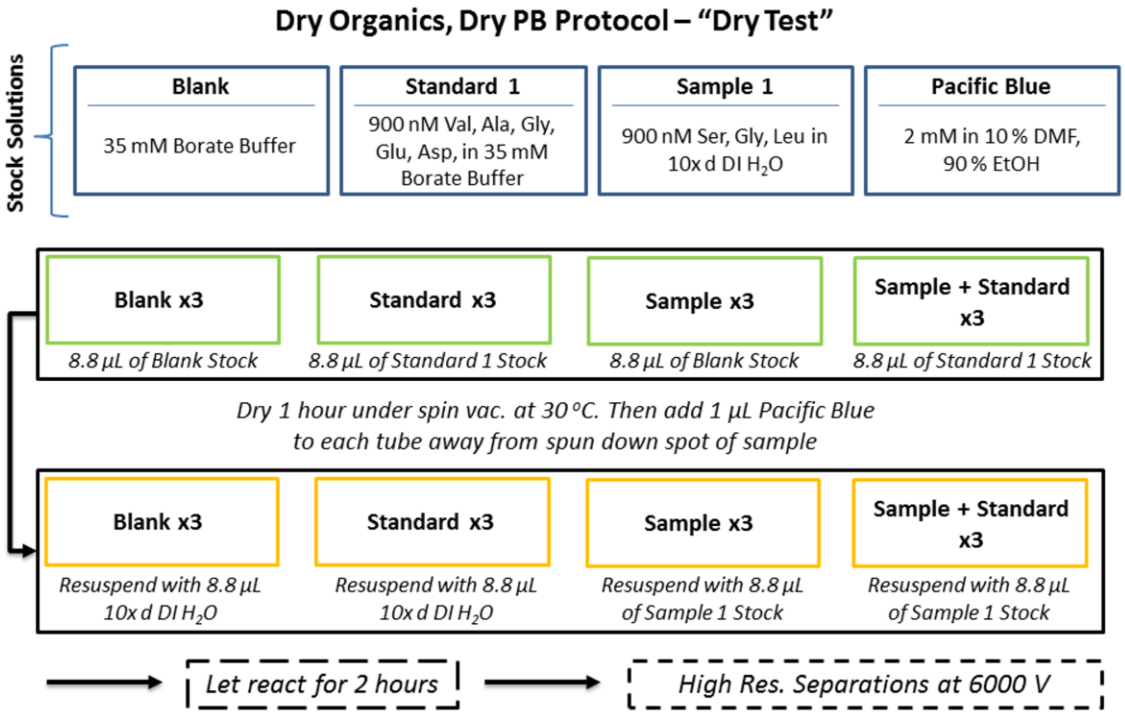

Figure 5.3. Outline for the dry test experimental protocol.

5.3.2 Thermocycling Tests

Thermocycling experiments were done using a blank glass wafer, a digital fluidic processing microdevice, and a 10-year-old microdevice for analyses via microcapillary electrophoresis with laser-induced fluorescence (µCE-LIF). Each device was subjected to the same freeze/thaw/heat cycle. Initially, the device was placed into liquid nitrogen (-196 °C) for 2 hr. After this time, the device was warmed to room temperature (RT) for 1 hour (hr) and heated to 100 °C for 2 hr. This process was repeated 3x for the blank wafer and microfluidic processing device and 4x for the 10-year-old µCE-LIF microdevice. Images were captured at each interval to assess abnormalities.

5.3.3 PB Dry Storage Tests: Liquid Control

Reaction mixtures of the stock solutions were made in triplicate. The blank consisted of 8.8 µL of the blank stock and 1 µL of the PB stock. The standard consisted of 8.8 µL of the standard 1 stock and 1 µL of the PB stock. The sample consisted of 4.4 µL of the sample 1 stock, 4.4 µL of 70 mM borate buffer, and 1 µL of the PB stock. The sample + standard consisted of 4.4 µL of the sample 1 stock, 4.4 µL of the standard 2 stock, and 1 µL of the PB stock. Each tube was left to react for 2 hr and analyzed for high resolution separations at 732 V/cm using the benchtop µCE-LIF system.

5.3.4 PB Dry Storage Tests: Dry Control

Reaction mixtures of the stock solutions were made in triplicate as they were made in the dry test. After drying under vacuum at 30 °C, the blank and standard tubes were resuspended with 8.8 µL of 10x d DI water and the sample and sample + standard tubes were resuspended with 8.8 µL of the sample 1 stock. Each tube was then mixed with 1 µL of the PB stock, left to react for 2 hr, and analyzed for high resolution separations at 732 V/cm using the benchtop µCE-LIF system.

5.3.5 PB Dry Storage Tests: Dry Test

Reaction mixtures of the stock solutions were made in triplicate. The blank consisted of 8.8 µL of the blank stock. The standard consisted of 8.8 µL of the standard stock. The sample consisted of 8.8 µL of the blank stock. The sample + standard consisted of 8.8 µL of the standard 1 stock. Each tube was spin under vacuum at 30 °C for 1 hr, and 1 µL of the PB stock was added to each tube slowly near the dried material, allowing

evaporation of the DMF and ethanol. The blank and standard tubes were resuspended with 8.8 µL of 10x d DI water and the sample and sample + standard tubes were resuspended with 8.8 µL of the sample 1 stock. Each tube was left to react for 2 hr and analyzed for high resolution separations at 732 V/cm using the benchtop µCE-LIF system.

5.3.6 Contamination Test

Three empty microcentrifuge tubes were spun under vacuum for 1 hr at 30 °C as done in previous tests. Three control microcentrifuge tubes were taken directly from packaging and not spun. Borate buffer (8.8 µL, 35 mM) and 2 mM PB in 10% DMF/90% ethanol (0.5 µL) were added to react for 2 hr and analyzed for high resolution separations at 732 V/cm using the benchtop µCE-LIF system.

5.4 Results and Discussion

5.4.1 Microdevice Thermal Stability Examination

5.4.1.1 Blank Glass Wafer

A blank glass wafer was tested first to optimize cycling conditions and avoid the possibility of shattering the glass upon thermal shock (Figure 5.4. Blank wafer (A) before thermocycling, (B) at -196 °C, (C) at 100 °C, and (D) after thermocycling.Figure 5.4). For each test, the device showed no structural damage. Upon thermal shock with liquid nitrogen for each test, no fracturing or shattering occurred. In addition, no structural damage was observed after warming back to room temperature. These results suggest that the glass section of the microdevice can safely be subjected to liquid nitrogen temperatures without shattering.

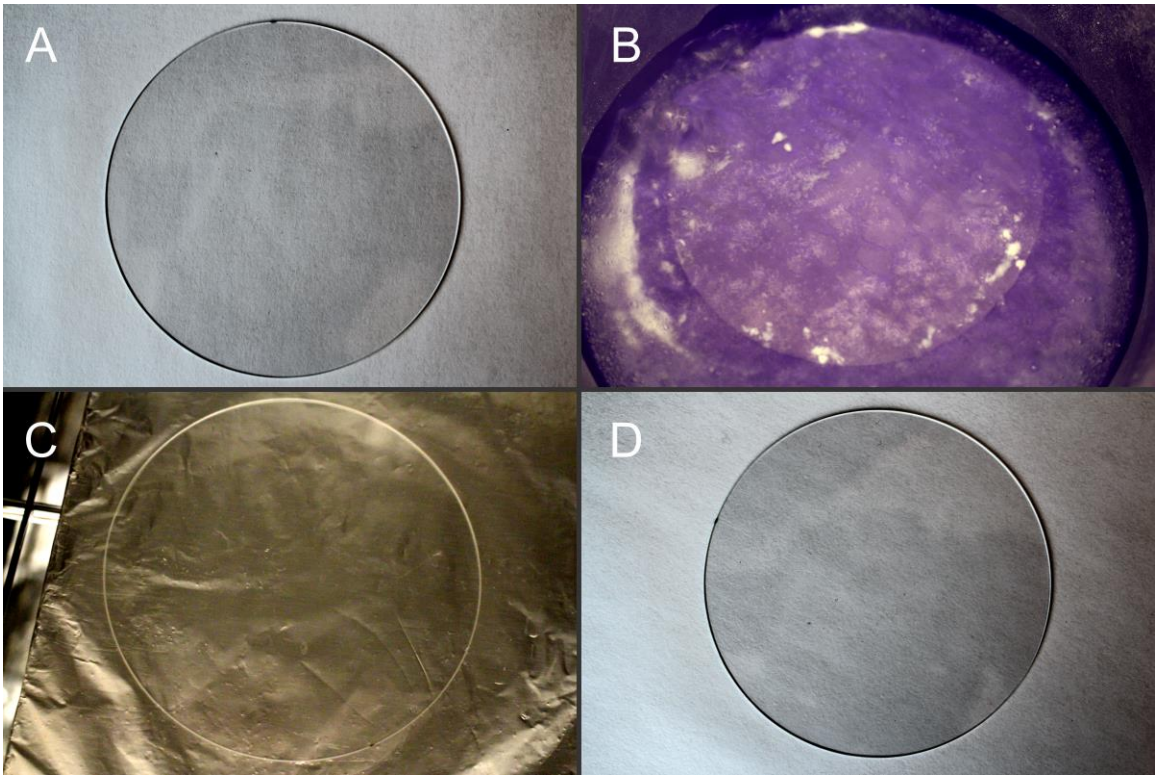

Figure 5.4. Blank wafer (A) before thermocycling, (B) at -196 °C, (C) at 100 °C, and (D) after thermocycling.

5.4.1.2 Microfluidic Processing Device

With the blank wafer tests completed, the next step was examining the thermal stability of a more recently constructed microdevice. Figure 5.5 shows a representative segment of the digital fluidic processing microdevice after each cycle during the thermocycling process. For each test, including thermal shock with liquid nitrogen and heating to 100 °C, no fracturing or shattering occurred. The device did contain a preexisting crack on the top glass layer marked by the red arrow in Figure 5.5 A. This crack did not appear to worsen after thermal shock with liquid nitrogen of heating to 100 °C as well. These results suggest that the 10-year-old microdevice can safely be subjected to liquid nitrogen temperatures without shattering.

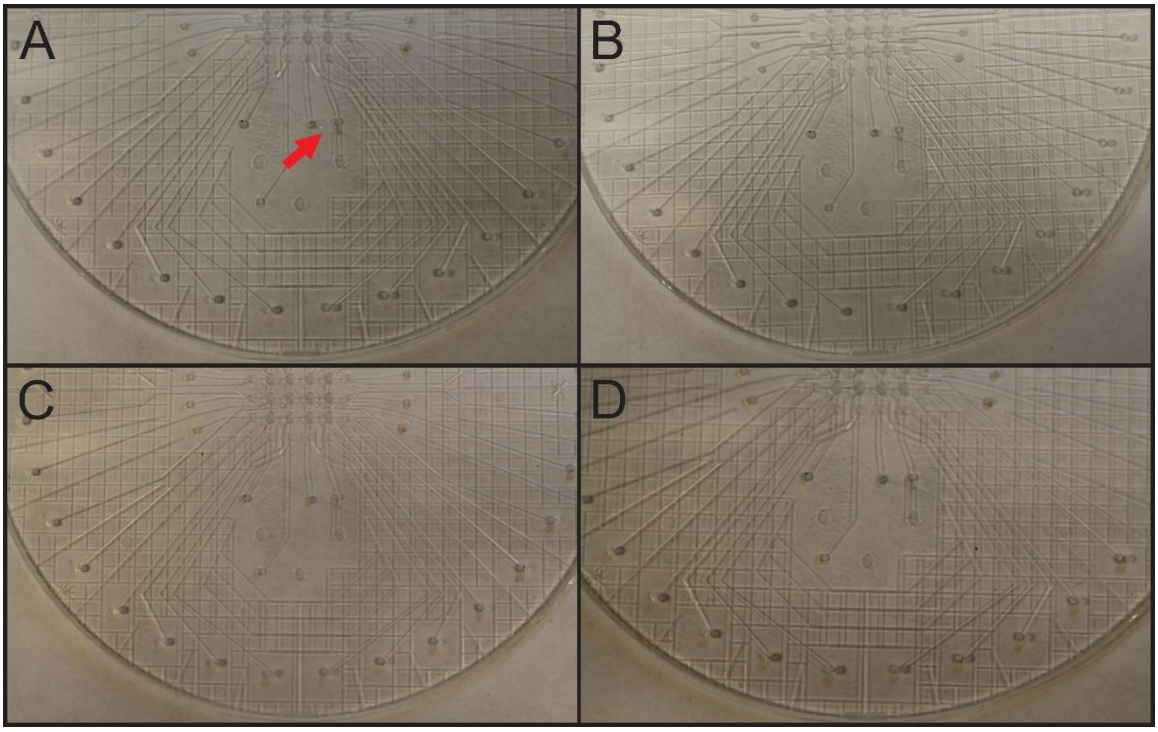

Figure 5.5. Digital fluidic processing microdevice (A) before thermocycle 1x, (B) after thermocycle 1x, (C) after thermocycle 2x, and (D) after thermocycle 3x. The red arrow indicates the location of the preexisting crack.

5.4.1.3 Ten-Year-Old μCE-LIF Microdevice

A 10-year-old microdevice was subjected to the same thermocycling conditions to those of the digital fluidic processing microdevice, except the thermocycling process was repeated 4x. Figure 5.6 shows the device during selected steps of the thermocycling process. No major structural anomalies were seen until the fourth cycle, when minor fracturing began to occur along the edges of the top layer of the glass-PDMS-glass stack. The 10-year-old microdevice also contained small bonding defects in glass-glass bonding below the glass-PDMS-glass stack. Likely created during the microdevice manufacturing process, these defects did not appear to worsen over time and did not have any effect on microvalve fluid transfer capability. These data demonstrate that microdevices containing

PDMS membranes can survive at least 3 extreme thermocycles from -196 °C to 100 °C and would likely survive significantly more thermocycles using less extreme temperatures.

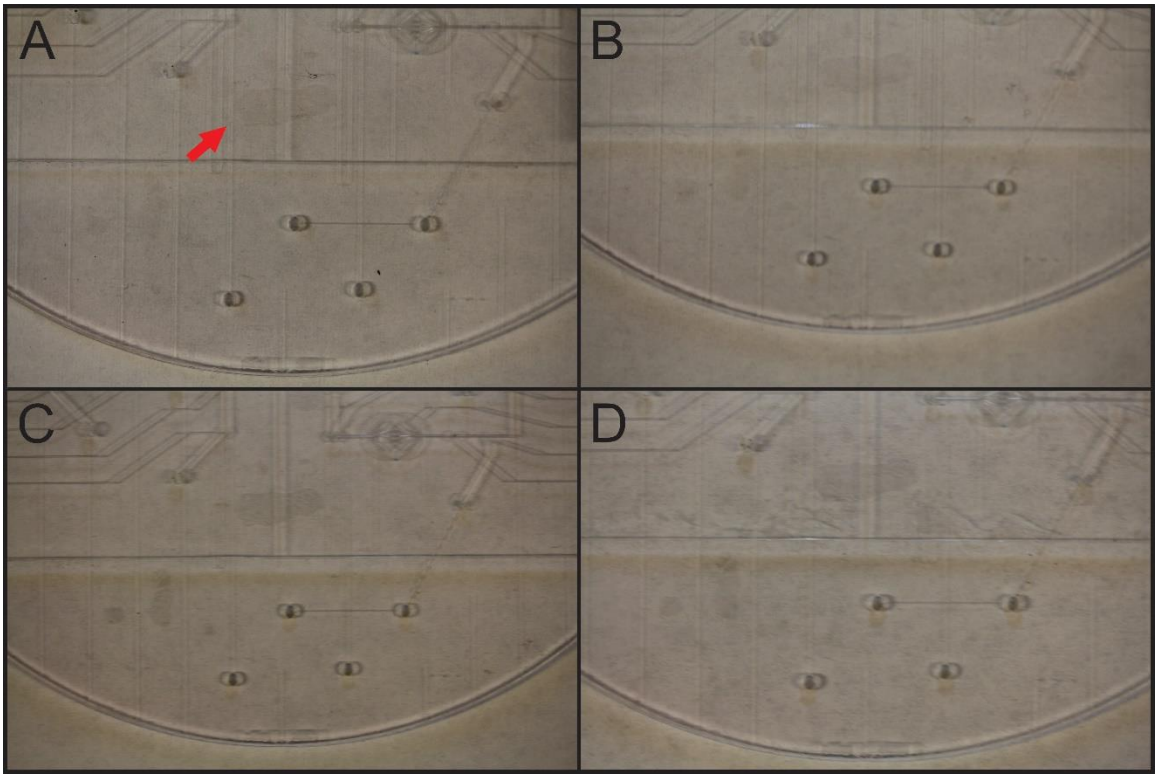

Figure 5.6. 10-year-old microdevice (A) before cycle 1 of the 1x thermocycle, (B) after cycle 1 of the 1x thermocycle, (C) before cycle 1 of the 5x thermocycle, and (D) after cycle 5 of the 5x thermocycle. The red arrow indicates the location of a preexisting delamination.

5.4.2 PB Reactivity after Drying via Spin Vacuum

The effect of drying 10+-year-old PB dye with amino acids was examined by performing a set of three experiments: a liquid control where every solution was mixed normally in its liquid form, a partial-liquid control where each solution was dried using a spin vacuum and resuspended to mix before adding liquid PB, and a dry test where each solution was dried using a spin vacuum and resuspended to mix after adding dry PB (Figure 5.7). The liquid control represented a typical in-lab protocol done on Earth. The partial-

liquid control was meant to examine loss of organics during the spin vacuum process for an in-lab protocol done on Earth. The dry test simulated a planned mission procedure done in space.

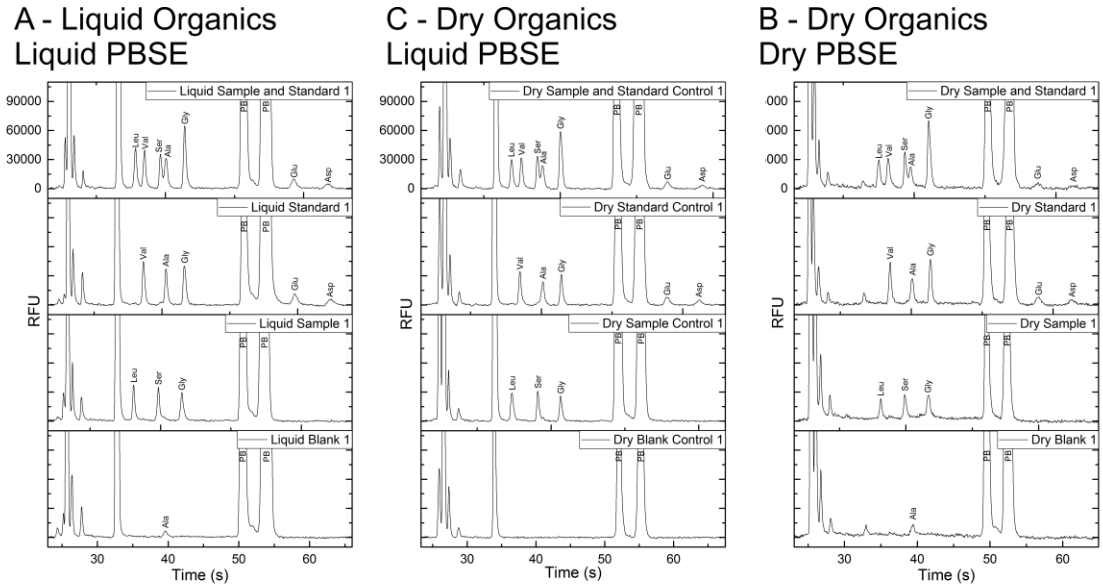

Figure 5.7. Dry reagent and PB in 10% DMF/90% ethanol test. (A) Liquid control; (B) partial-liquid control; (C) dry test. Electropherograms are scaled to the same relative fluorescence intensity. (Separation potential at 732 V/cm).

No noticeable decrease in S/N was noticed between the liquid control and the partial-liquid control for the sample and standard, signifying there was no significant loss of organic material during the spin vacuum process (Figure 5.8). This visual similarity was confirmed via a 2-tailed paired t-test with a set confidence value of 0.95, where all obtained p values for comparing the liquid control to the partial-liquid control were significantly greater than the set alpha value of 0.05 (1.00 - confidence value) (Supplementary Table A.4.5). A decrease in signal intensity was noticed in the dry test. However, when individually comparing the liquid control and the partial-liquid control to the dry test using a 2-tailed paired t-test with a set confidence value of 0.95, all p values were above the set

alpha value of 0.05, excluding the aspartic acid comparison between the liquid control and the dry test and the partial-liquid control and the dry test. Any loss in reactivity was likely due to hydrolysis of PB, but this reduced reactivity was not significantly pronounced except for the case of aspartic acid. Addition of a more concentrated PB solution would likely generate organic peaks with intensities closer to the liquid and partial-liquid control experiments but would not be explicitly required for the dry test.

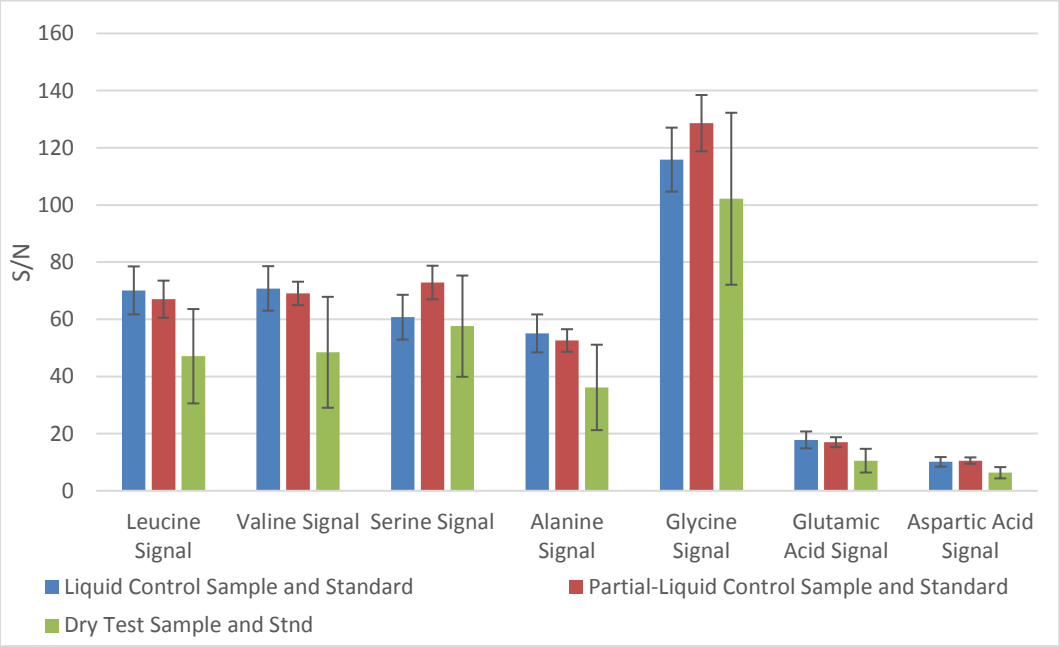

Figure 5.8. Analysis of dry reagents stored with PB in 10% DMF/90% ethanol: (Blue, Left) liquid control, (Red, Center) partial-liquid control, (Green, Right) dry test. Error bars represent the standard deviation of triplicate measurements of the S/N of each amino acid.

A test was done to determine if the drying step using the spin vacuum was introducing contamination. Three empty microcentrifuge tubes were spun under vacuum for 1 hr at 30 °C as done in previous tests, and three control microcentrifuge tubes were taken directly from packaging and not spun. Figure 5.9 illustrates that no significant difference in contamination was noticed between the sets of spun and unspun tubes,

suggesting that loss in reactivity is most likely due to PB hydrolysis and not aerosolization of organics during the spin vacuum process.

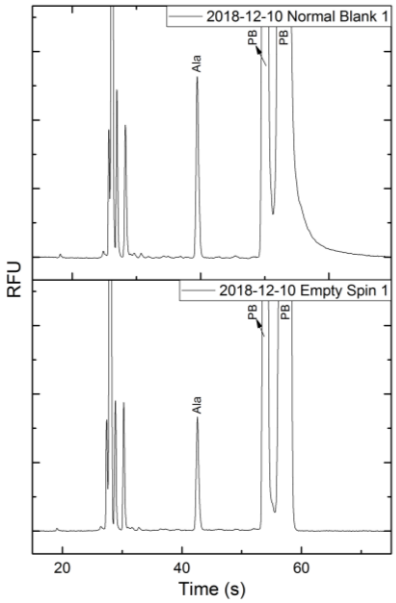

Figure 5.9. Dry reagent and PB in 10% DMF/90% ethanol contamination test. Electropherograms are scaled to the same relative fluorescence intensity. (Separation potential at 732 V/cm).

5.5 Conclusions

Ten-year-old microdevices were studied through a series of thermocycling tests from -196 °C to 100 °C. No deleterious effects were noted until 4 rounds of temperature cycling, indicating that these PDMS membrane-based microdevices could survive 3 unlikely critical temperature failures during a space mission and could likely survive many cycles at less extreme high and low temperatures. The effect of drying 10+-year-old PB dye with amino acids was examined by performing a set of three experiments: a liquid control, a partial-liquid control, and a dry test. The liquid and partial-liquid controls exhibited similar reactivities, while a slightly lower S/N intensity was noticed for the dry

test. However, statistical analysis revealed that only the aspartic acid dry test was significantly different than the liquid and partial-liquid controls. A likely cause of this decreased signal for aspartic acid was the hydrolysis of PB. A 2x excess of PB when stored with amino acids would alleviate any potential loss in S/N. These results indicate that PB dye can retain sufficient reactivity when stored dry with amino acid standards.

Microdevice stability during and after thermocycling can be examined further. Less extreme temperatures, such as -20 °C to 80 °C, are more likely to be expected during transit to the outer Solar System due to the on-board heat management instruments for spacecraft and equipment survival. On-board instruments would only experience exceptionally extreme temperatures only during a critical mission failure. Microdevice functionality through a series of flow rate experiments can be examined before and after thermocycling at these more reasonable temperatures. Further PB dry storage experiments can be done using a fast-prototyped microfluidic processor to compare on-chip reactivity to off-chip reactivity. Each reaction protocol done for the microcentrifuge tube experiments, including the liquid control, the partial-liquid control, and the dry test, can be redone using the fast-prototyped microfluidic processor to mix the solutions. Amino acids contained in the processed solutions can be identified and quantified using high resolution separations as done previously. Amino acid content for the on-chip samples should be examined and compared to the off-chip experiments. Statistically similar data sets will support the conclusion that labeling using dried PB on-chip is an acceptable method for future automated μCE-LIF analyses after extended storage of the microdevice in dry conditions.

CHAPTER 6. A COMPACT LENS TUBE LASER-INDUCED FLUORESCENCE DETECTION SYSTEM FOR BULK AMINE ANALYSIS

Current work in progress:

6.1 Abstract

The icy moons Enceladus and Europa have become high-priority targets for future habitability studies within the Solar System. Much of our information regarding these icy bodies originates from the Cassini and Galileo fly-by missions. The data from these flagship operations have contributed considerably to understanding their surface compositions and have even evidenced the presence of subsurface oceans beneath their icy crusts. However, our knowledge of the potential biosignatures contained on the surfaces or within the oceans of these moons is limited. Therefore, a more definitive biosignature detection technique is necessary to begin ascertaining the habitability of Enceladus and Europa. A technique that provides the sensitivity and miniaturization needed to successfully detect trace organics in the outer Solar System is laser-induced fluorescence (LIF) detection. Here, we designed, assembled, and tested a low-cost, portable lens tube LIF detection prototype to quantify bulk organics in a liquid sample. A limit of detection (LOD) analysis was performed by reacting serial dilutions of leucine with fluorescamine dye in 35 mM borate buffer, pH 8.5. The LOD was found to be 11.8 µM, an excellent benchmark for a prototype LIF detection system of its unique design. Automated analyses were performed using a rapid-prototyped microfluidic processor and showed no

statistically-significant differences when compared to the manual analyses. A sample (Y31B) collected from the Atacama Desert in Yungay, Chile, was analyzed manually and found to contain 300 ± 50 μM of bulk primary and tertiary amine organics. When analyzed using the automated microfluidic processor, the sample was found to contain 289 ± 4 μM. These results have shown promising usability of automated microdevices and portable lens tube LIF detection systems in more restricting environments, like those on Enceladus and Europa.

6.2 Introduction

Scientists and other intellectuals have always held an interest in the mystery of life in the Solar System. However, a definitive search for evidence of extraterrestrial beings did not occur until the Viking missions to Mars in 1976. The on-board payload featured a thermal volatilization gas chromatography mass spectrometer (TV-GS-MS) to detect traces of organic matter [26]. Unfortunately, the bulk of the organics detected were the chemicals used to clean the spacecraft before launch and chlorinated hydrocarbons as a result of the reaction of Martian perchlorates with organic material [24, 27-29, 32]. As a result, decades passed before the next attempt at detecting organics on another body within the Solar System with the Mars Science Laboratory Sample Analysis at Mars (MSL SAM) pyrolysis-based GC-MS. Similar to the Viking mission, the only organic molecules identified were chlorinated hydrocarbons and contaminants resulting from leakage in the N-methyl-N-tert-butyldimethylsilyl-trifluoroacetamide (MTBSTFA) derivatization system [28]. While no unique organic molecules were identified on the surface of Mars, the results from these missions were too ambiguous to claim the absence of organic molecules.

While Mars' proximity to Earth makes it an enticing target for planetary studies, other potentially more habitable locations exist within the Solar System. Specifically, the icy moons Enceladus and Europa have substantially grown in interest over the past few decades and were each identified as important targets in NASA's Decadal Survey Visions and Voyages for Planetary Science [195]. The Cassini fly-by mission provided most of our knowledge of Enceladus, Jupiter's main E-Ring contributor [52, 163-165, 167]. Remote imaging displayed ongoing hydrothermal activity at the south pole, and evidence has suggested the presence of a global subsurface ocean [66, 68, 69, 166]. Galileo, another fly-by mission, gathered most of our chemical information of the surface of Jupiter's Galilean moon Europa [176]. Remote imaging has even captured tenuous plume activity suggestive of a liquid ocean below the ice crust [34, 35]. While these fly-by missions and remote sensing instruments have provided useful information regarding the chemical processes of these icy bodies, more direct measurements are needed to fully characterize the potential past or present habitability of these environments.

Laser-induced fluorescence (LIF) is a powerful automation-ready detection technique capable of providing the analytical sensitivity needed to successfully detect and quantify trace organic molecules contained within the plumes or subsurface material of Enceladus or Europa [88]. LIF has enabled detection of multiple organic molecule classes, including polycyclic aromatic hydrocarbons (PAHs), amines, aldehydes, ketones, carboxylic acids, and thiols [80-82, 88, 103, 116, 117]. Due to their ubiquitous presence in the Solar System, PAHs and amino acids are well-accepted targets for habitability studies [210, 211]. Quantification of their relative abundances on an icy world can significantly enhance our knowledge of chemical and physical processes that shape the environments of

these celestial bodies. However, the surface environments of these locations are generally inhospitable, and samples from below the surface are likely needed to permit investigation of pristine materials unaffected by multiple surface processes, including ionizing radiation and weathering that degrade organics [184]. Drilling for these subsurface samples is possible, but mission architectures that include a soft lander system are often expensive and complex [212, 213]. An alternative approach for contacting the surfaces of these difficult-to-reach locations is to utilize a kinetic impactor [214]. Penetrating the surface at high speeds would not only eliminate the need for intricate lander technology but would also bury the instruments below the likely degraded surface material to access the desired subsurface samples. While impacting a hard surface at high speeds would certainly place a significant amount of stress on the internal components, models and tests have shown that LIF-based hardware can survive these strains and function normally afterwards, especially if deployed from an orbiting or flyby spacecraft to reduce impact velocity [119, 120, 215].

In addition to reducing impact velocity, one directly controllable requirement for the development of a LIF device contained within a kinetic impactor is mass limitation. Since kinetic energy is directly proportional to mass, reducing the overall mass of the impactor and its components is critical. Traditional optical detection systems for LIF have benefited greatly from miniaturization [76, 102, 107]. Miniaturized 405-nm gallium nitride (GaN) lasers are incorporated into detection optics in multiple portable systems, including Blu-Ray players, and GaN arrays are used for light-emitting diode (LED) displays [216]. However, even these systems can be somewhat expensive in terms of mass and size and are susceptible to mis-alignment due to vibrations or impact. In 2003, a LIF detection

format was introduced that utilizes microfabrication processes to perfectly align optical components into a miniaturized optical stack [106], but this system was still somewhat difficult to permanently lock in place. Coincidentally, an Indium "bump" bonding technique was developed as a method to take advantage of Indium's unique ability to self-bond under ambient conditions using standard microfabrication protocols, permanently welding components [217, 218]. However, this process typically requires a cleanroom facility with proper equipment and resources, which can significantly increase fabrication cost and time.

The development of a miniaturized LIF detection system for a kinetic impactor mission is largely an exploratory study. Therefore, the early maturation phase can take advantage of fast-prototyping methods to reduce the lengthy fabrication times and high costs associated with cleanroom development. Specifically, a recent study have outlined low-cost processes for the design, assembly, and testing of microfluidic devices for fluidic manipulation [219]. The devices examined in this study were shown to perform as effectively as their cleanroom-fabricated counterparts despite costing a fraction of the price to manufacture. In addition, miniaturized commercial optical components are now widely accessible due to an increased interest in developing portable instrumentation [111, 112]. Access to these components and techniques enables a straightforward approach to prototype an automated, rigid, and field-portable LIF module for the detection of trace organic molecules.

Not many instruments, particularly those designed to conduct organic analysis, are robust to the high g-loads of a kinetic penetrator mission. Here, we show the early development of a lens tube LIF subsystem prototype for a kinetic impactor mission.

Components for the optical assembly were purchased commercially and minimally modified to retain facile substitution. An automated fast-prototyped microfluidic processor was fabricated and used to characterize the lens tube LIF device. Limits of detection (LODs) using Pacific Blue (PB) dye were determined using a silicon photodiode and a silicon photomultiplier, and the silicon photomultiplier was chosen for the final characterization of the lens tube LIF detection module. A manual method LOD was performed by reacting leucine with fluorescamine dye in microcentrifuge tubes and transferring the solution to the automated processor for fluorescent signal quantification. A sample (Y31B) collected from the Atacama Desert in Yungay, Chile, was also reacted with fluorescamine in microcentrifuge tubes and transferred to the automated processor for fluorescent signal quantification. A 100 μM solution of leucine as a control and the Y31B sample were reacted with fluorescamine dye using the automated microfluidic processor for comparison to the manually-reacted leucine standards and Y31B sample. Our results demonstrate the promising usability of automated microdevices and portable lens tube LIF detection systems in more restricting environments, like those on Enceladus and Europa.

6.3 Materials and Methods

6.3.1 Reagents

Reagents were used as received except where noted. Deionized (DI) Millipore water (18 MΩ, megaohms) was distilled (d) 10x in a high efficiency particulate air (HEPA)-filtered environment and used to make all aqueous solutions. Borate buffer (Sigma-Aldrich Co., St. Louis, MO) was recrystallized 10x, prepared as a 100 mM aqueous stock solution at pH 8.5, and diluted appropriately where needed. A 20 mM stock solution

of 3-carboxy-6,8-difluoro-7-hydroxycoumarin PB dye (Invitrogen, Carlsbad, CA) was dissolved in dimethylformamide (DMF) (EMD Millipore Co., Billerica, MA) and diluted where needed. A 10 mM aqueous stock solution of leucine (Sigma-Aldrich Co.) was made and diluted appropriately where needed. A 100 mM stock solution of fluorescamine dye (Sigma-Aldrich Co.) was dissolved in acetone (BDH Chemicals, Darmstadt, Germany). All aqueous solutions were stored at 4 °C when not in use, and all acetone and DMF solutions were stored at -20 °C when not in use.

6.3.2 Lens Tube Detection System Fabrication

The miniaturized lens tube LIF detection module in this study uses an on-axis profile for fluorescence excitation and capture. Custom components were designed using SolidWorks, and commercial components were modified only when necessary. Component placement and alignment was modeled prior to fabrication (Figure 6.1 A-B), and optical path guides were created using the open-source Ray Optics Simulation on GitHub (Figure 6.1 C).

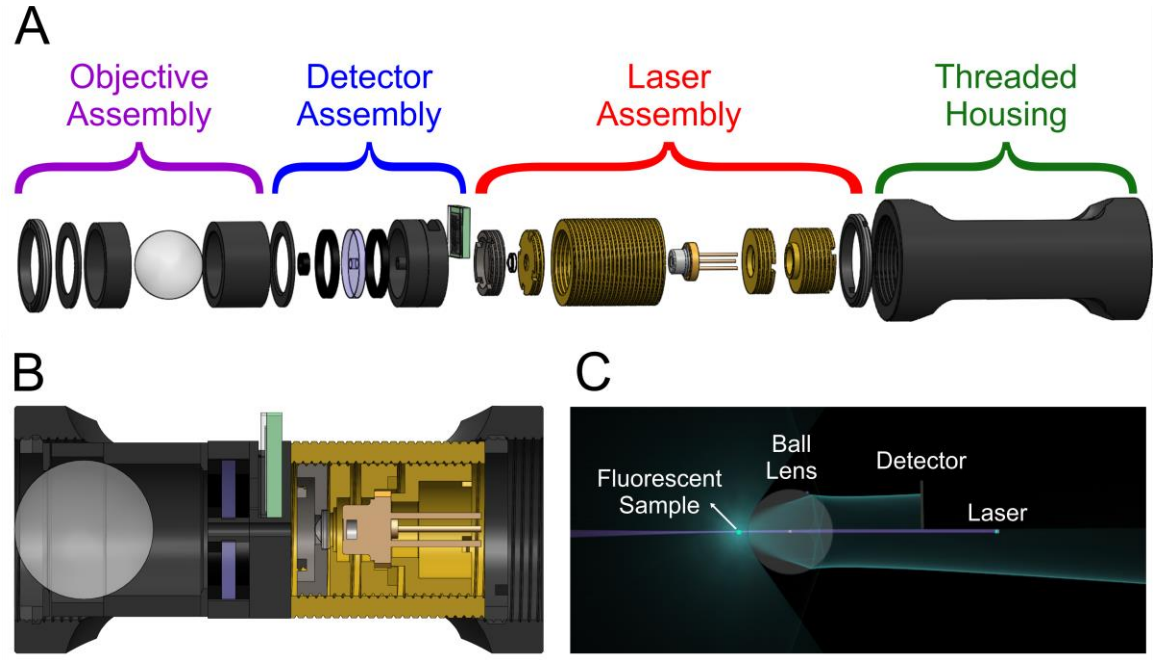

Figure 6.1. Computer-Aided Design (CAD) of the lens tube LIF detection module in (A) exploded view and (B) as a compact assembly. (C) Optical path diagram of the laser and fluorescent light sources. Light displayed is intended to guide the eye and does not represent exact scaled, calculated beam diameters.

A laser diode (Thorlabs Newton, NJ) was threaded into a custom mount containing a collimating aspheric lens (Thorlabs). The laser diode assembly was threaded into a lens tube housing (Thorlabs) and affixed using a retaining ring. The collimated laser beam was directed through a custom assembly that housed both the longpass (LP) filter (Thorlabs) and detector. An open port was designed into the side of the assembly to facilitate simple detector replacement. Both a silicon photodiode (Thorlabs) and a silicon photomultiplier (Thorlabs) were examined. A 1 mm hole was drilled through the longpass filer to allow the collimated laser beam to pass through unobstructed. The collimated laser beam was focused to the microdevice detection channel by a 10 mm fused silica ball lens (Thorlabs) that was placed in a custom housing to remain on centerline. Fluorescence was captured by the ball lens and collimated through the longpass filter to the detector for quantification.

6.3.3 Microdevice Fabrication

A 14-valve microfluidic device containing a core 2 x 2 processor was designed in AutoCAD (Figure 6.2) and fabricated using the previously reported Green Low-cost User-friendly Expedient (GLUE) microfluidics method [219]. The device is comprised of four layers in total, specifically: (1) Pneumatic layer (2) Fluidic Membrane Layer (3) Detection Layer and (4) Glass sealing layer. To fabricate the three patterned layers, three glue thin-films were freshly prepared on glass substrates. First, the fluidic membrane layer mold was vector cut (20% power [PWR] 85% speed [SPD]) from a glue thin film (White outline Figure 6.2 B) and lifting gate feature molds (Blue outlines Figure 6.2 B) were raster etched (12.5% PWR 40% SPD) into the valve regions, in the same laser cutting step. Subsequently a ~300 μm thin film of PDMS was casted over the mold using the blade coating approach to create the fluidic membrane layer. The Pneumatic layer (Figure 6.2 A) and detection layer (Figure 6.2 C) were vector cut from the two remaining glue thin films and PDMS was casted over each of these layers at a thickness of approximately 3 mm. Pneumatic accesses were punched into the pneumatic layer using a 2 mm Biopsy punch, and then this layer was aligned by eye and plasma bonded to the fluidic membrane layer. After bonding, fluidic inlet/outlet (I/O) wells were punched into the bonded pneumatic-fluidic membrane layer monolith and the detection layer using 2 mm and 4 mm biopsy punches were appropriate. These layers were again aligned by eye and plasma bonded together with the respective patterned sides oriented down. Finally, the device was sealed by plasma bonding a 75 x 50 mm glass microscope slide to the bottom side of the detection layer. The final device AutoCAD design and completed assembly are depicted in Figure 6.2 D and Figure 6.2 E, respectively.

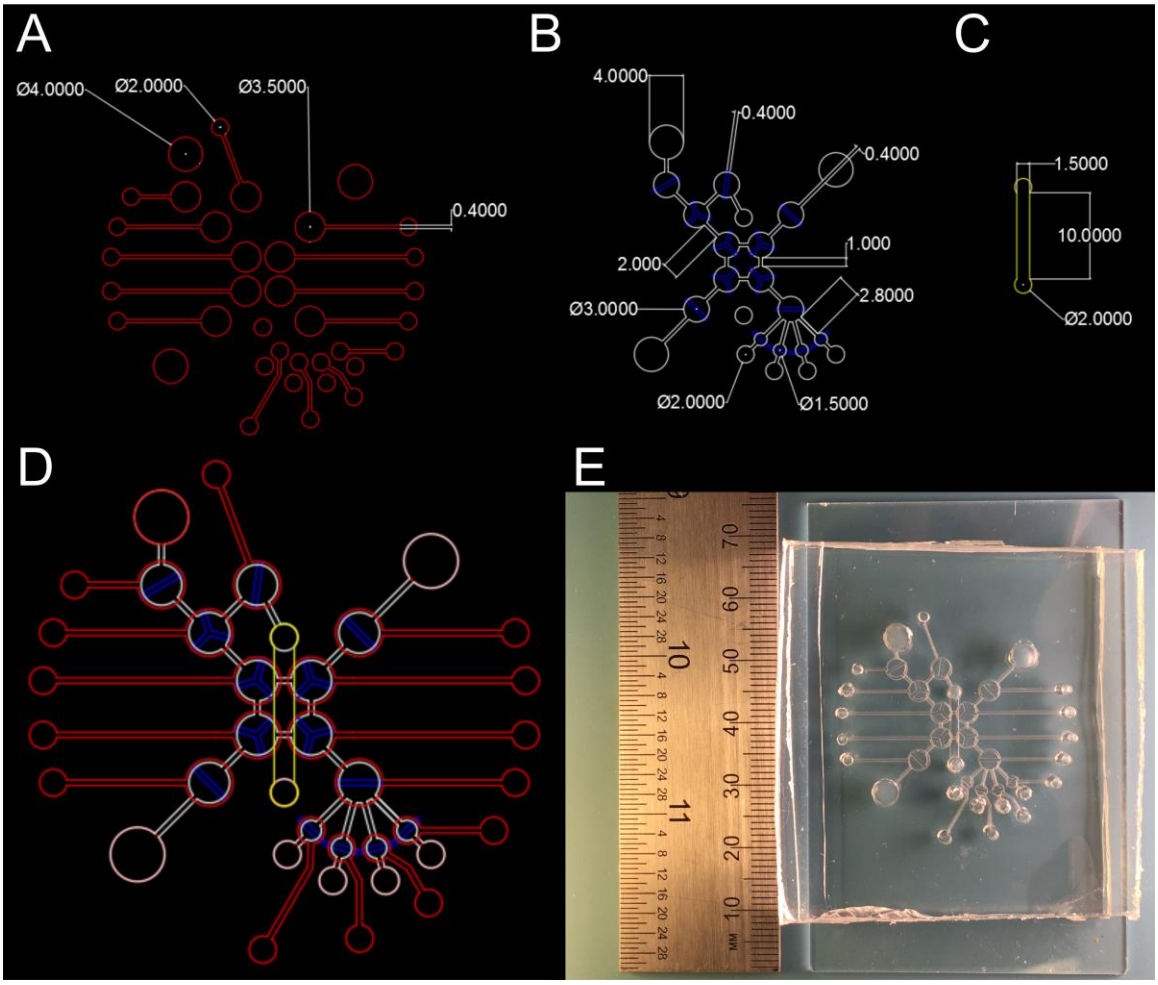

Figure 6.2. Design of a 4-layered 2x2 microfluidic processor utilizing pneumatically-actuated, normally-closed lifting gate microvalves. (A) Pneumatic layer design and dimensions. (B) Fluidic layer design and dimensions. (C) Detection channel design with dimensions. (D) Layers aligned. (E) Image of the completed microfluidic processor. All dimensions are in mm.

6.3.4 Power Supply and Digital Read-out Set-up

The laser diode and detector were powered by individual power supplies (Figure 6.3 A). Signal generated by the detector was monitored and recorded using a digital multimeter. The detection module was rigidly housed directly under the microfluidic processor (Figure 6.3 B). Micrometer-controlled optical stages were used for precise X, Y, Z alignment of the focused laser light from the lens tube assembly to the detection channel.

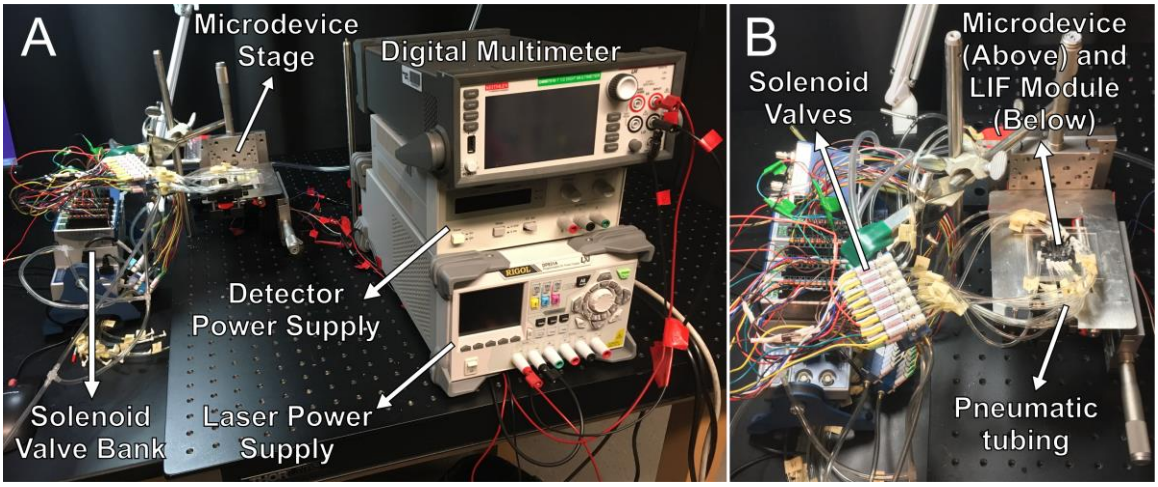

Figure 6.3. (A) Set-up for the characterization of the fast-prototyped microfluidic processor and the lens tube LIF detection module with key hardware labeled. (B) Close-up image of the solenoid valve bank and microdevice stage.

6.3.5 Microdevice Operation

The microprocessor valves were actuated by LHD (Lee's High Density Interface) Series 3-way Face-Mount Style solenoid valves (The Lee Company, Essex, CT) that were switched between vacuum and ambient atmospheric pressure. Automated control of the solenoid valves was accomplished via a custom LabVIEW (Laboratory Virtual Instrument Engineering Workbench) program controlling multiple 9472 Sourcing DO (digital output) C Series Modules (National Instruments, Austin, TX) connected to a Compact Data Acquisition (cDAQ-9178) chassis (National Instruments, Austin, TX). Closed solenoid valves were subjected to a constant pressure input of 10 psi above ambient pressure, while open valves were provided a constant vacuum pressure of 10 psi below ambient pressure. Fluidic manipulation was accomplished via a series of "open-close-wait" string commands that were sent via LabVIEW as binary control signals to the cDAQ controller.

6.3.6 Pacific Blue (PB) Dye LOD Analyses

A dilution series of PB dye was made from 1 µM to 333 µM in 35 mM borate buffer. PB dye was pulled through the microdevice detection channel using a weak vacuum to generate a constant flow of material. The dye was excited with a focused 405 nm laser, and fluorescent signal was captured by the lens tube LIF detection module for the LOD analyses. Triplicate technical replicates were done for each concentration. This process was performed for both the silicon photodiode and the silicon photomultiplier.

6.3.7 Extraction Protocol

Sample (Y31B) collected from the Atacama Desert in Yungay, Chile, was weighed and mixed with 5x distilled water at a ratio of 0.5 mg/µL microcentrifuge tube. The mixture was vortexed for 10 sec and boiled at 100 °C for 24 h. The sample was cooled at room temperature for 10 min and was centrifuged for 5 min. The liquid extract was saved and used for analysis.

6.3.8 Manual 2 x 2 Processor Analysis

The leucine stock solution was diluted to create 1000 µM, 500 µM, 200 µM, 100 µM, and 50 µM solutions in triplicate. For each concentration, 40 µL of leucine solution was pipetted into a microcentrifuge tube and mixed with 20 µL of 35 mM borate buffer and 20 µL of fluorescamine stock solution. Y31B sample extract (40 µL) was pipetted into a microcentrifuge tube and mixed with 20 µL of 35 mM borate buffer and 20 µL of fluorescamine stock solution in triplicate. Water stock solution (40 µL) was pipetted into a microcentrifuge tube and mixed with 20 µL of 35 mM borate buffer and 20 µL of

fluorescamine stock solution in triplicate to serve as a blank to show minimal external contamination. The solutions were stored in the dark for 10 min to react and pipetted into the 2 x 2 processor for analysis. Analyte solutions were pumped to the outlet valve through the detection channel using a discrete 3-valve pumping sequence [203] and excited using a 20 mW, 405 nm laser. Fluorescent signal was detected using a silicon photomultiplier. The final diluted concentrations of leucine were used for the LOD analysis.

6.3.9 Automated 2 x 2 Processor Analysis

The 200 µM leucine solution, Y31B sample extract, and blank were each mixed individually with 35 mM borate buffer and fluorescamine stock solution at a 2:1:1 (blank/standard/sample:buffer:dye) ratio, respectively, in triplicate using the 2 x 2 processor (Supplementary Figure A.5.7, Supplementary Figure A.5.8). The solutions were stored in the dark for 10 min to react and pumped to the outlet valve through the detection channel using a discrete 3-valve pumping sequence (Supplementary Figure A.5.9). Analytes were excited using a 20 mW, 405 nm laser, and fluorescent signal was detected using a silicon photomultiplier. Water was pumped through the processor to clean the device for further analyses (Supplementary Figure A.5.10). Supplementary Figure A.5.11, Supplementary Figure A.5.12, Supplementary Figure A.5.13, and Supplementary Figure A.5.14 provide schematics of the pumping routines for clear representation of fluid flow.

6.3.10 Data Manipulation and Analysis

Resulting signal profiles of the manual and automated microfluidic processor analyses were baseline-corrected and fitted using a 0.2 % Loess filter via the chromatographic analysis program PeakFit (Systat Software, Inc., San Jose, CA). Fitted

fluidic movement oscillations were imported to the graphical data analysis program OriginPro (OriginLab Co., Northampton, MA) for further characterization of signal-to-noise (S/N) data extracted from the fitted files. Noise for each signal plot was calculated as the standard deviation of the baseline in a region without expected signal.

6.4 Results and Discussion

6.4.1 Lens Tube Detection System Fabrication

Miniaturization of optical systems is now commonplace in many scientific fields. Multiple existing field-deployable devices incorporate miniaturized optical components, such as Horiba's portable Raman spectrometer for molecular identification [220, 221], compact spectroradiometers from Analytical Spectral Devices (ASD, now Malvern Panalytical) for remote sensing measurements [222], and the Qubit fluorometer from Invitrogen (now ThermoFisher) for DNA quantification [223]. These instruments were developed reduce mass, size, and power consumption, while maintaining quality and sensitivity. Careful consideration was placed into every selected component to ensure peak performance. This approach was taken when designing, building, and characterizing the lens tube LIF detection module used in this study.

Individual components were meticulously selected and modeled before assembling the final device. Significant consideration was placed into reduction of overall size. However, select parts were used to better facilitate the assembly process. Custom modifications of parts were kept to a minimum whenever possible. For the laser assembly, a collimation package was required to direct the laser diode through the lens tube assembly towards the sample for detection. A hole was drilled in the center of the longpass filter to

allow the laser light to pass through without generating a high background signal. A fused silica ball lens was chosen to focus the collimated laser light to the sample channel and collimated the captured fluorescent light back to the detector for quantification. Both a silicon photodiode and a silicon photomultiplier were tested to optimize the LOD of the instrument. Mounting the components on centerline in a lens tube housing greatly simplified alignment. Figure 6.4 A displays the individual components of the module. When assembled, the overall size of the optical set up is 4 cm in length and 1.5 cm in diameter (Figure 6.4 B).

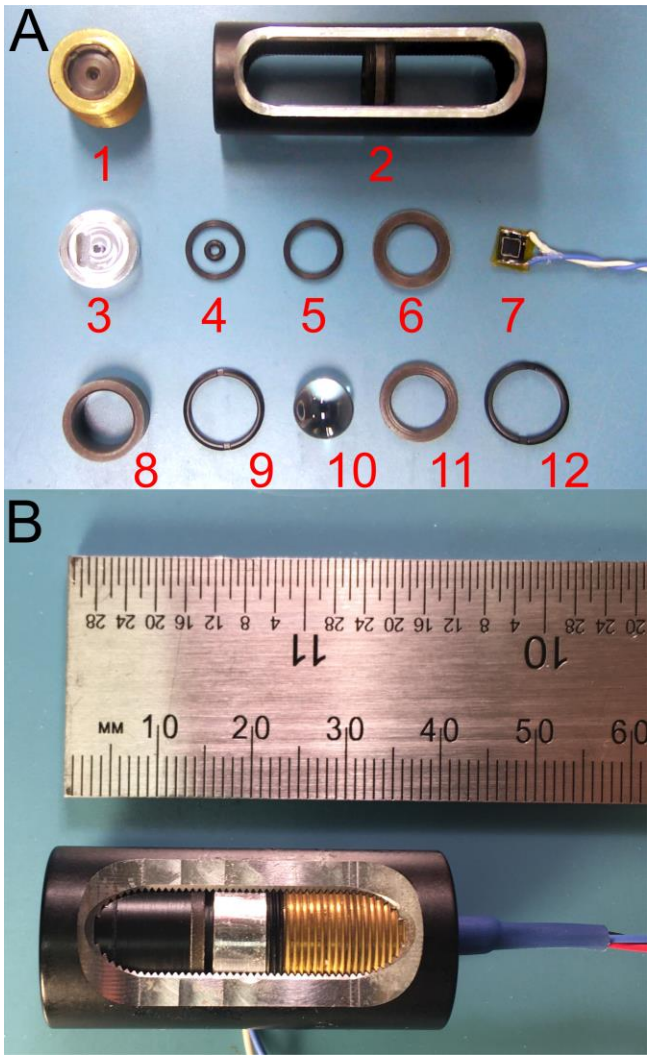

Figure 6.4. (A) Individual components of the lens tube LIF detection module. 1 – laser diode and housing, 2 – threaded housing, 3 – detector housing, 4 – detector O-ring seal, 5 – retaining ring, 6 – spacer, 7 – photodiode detector, 8 – spacer, 9 – threaded retaining ring, 10 – fused silica ball lens, 11 – ball lens alignment ring, 12 – threaded retaining ring. (B) Final assembled device. Note: the filter is not pictured in the component list but is included in the final assembly.

6.4.2 Microdevice Fabrication

To enable automated analysis of total amine content, a pneumatic microfluidic processor was fabricated, and automated analysis was demonstrated. Pneumatic processors are powerful fluidic routing tools capable of performing the complex metering and mixing

operations needed to perform automated analyses on-chip [110]. This purpose-built device comprised a core a 2 x 2 processor configuration, with 14 total lifting gate valves, and 8 I/O wells, specifically designed to facilitate automated total amine content analysis, in the same fashion that would be performed on a remote sampling mission. In this regard, 4 sample I/O wells were designed to hold the amino acid standard sample, wash water, a clean water blank, and a real sample, respectively. This is the minimum level of input samples required to get a calibrated result, and this is the most optimal operating procedure for performing analysis in a resource limited environment where calibration would occur onsite before deployment (manually) and sample analysis would occur remotely (automated). Two I/O wells were allocated to fluorescamine dye and buffer respectively, while the last I/O well was allocated as a reaction reservoir. The design incorporated two valves located between the reaction reservoir and the detection channel via to enable quick processor independent pumping of the reacted sample to the detection channel. A multilayer design was chosen to keep the detection channel centrally located on the device and reduce lateral footprint, while a glass bottom was chosen to seal the detection channel in order to avoid auto fluorescence of polydimethylsiloxane (PDMS) to enable optimal fluorescence collection.

6.4.3 Pacific Blue (PB) Dye LOD Analyses

Pacific Blue dye has been used to characterize other optical systems for organic molecule detection due to its high quantum yield and commercial availability [88, 105, 153, 154]. When characterizing the method LOD for those systems, the dye was bound to primary amines in a solution, and these tagged molecules were separated before being fluorescently detected and quantified. However, bulk flow of PB in organic-free solutions

also can be used to determine the LOD of a laser-induced fluorescence detection instrument. To characterize the lens tube LIF detection module, fluorescently excited PB dye was pulled through the focused laser beam in the detection channel and quantified. By calculating the S/N ratio of each concentration of PB from three independent dilution series and plotting the log of the results versus the log of their respective concentrations, linear regressions for both the silicon photodiode and the silicon photomultiplier were modeled (Figure 6.5). LODs of both the silicon photodiode and the silicon photomultiplier were calculated to be 433 nM and 177 nM at a S/N of 3, respectively. Due to its lower achievable LOD, the silicon photomultiplier was used for the remaining characterization studies.

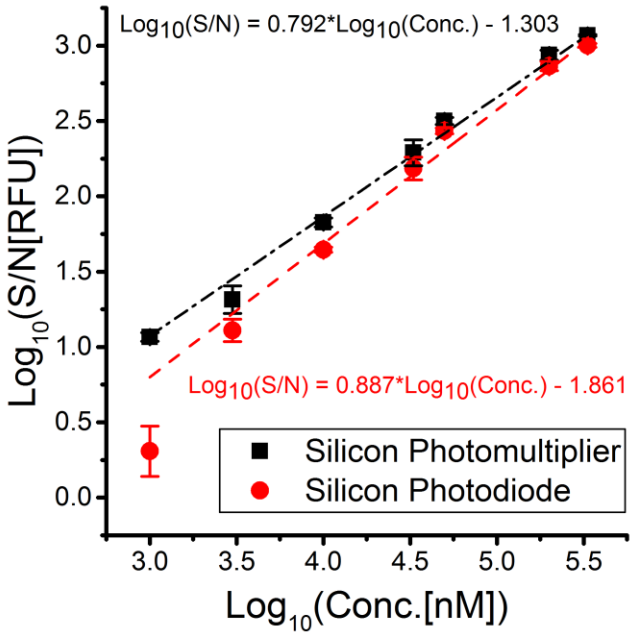

Figure 6.5. Limits of detection (LODs) of the lens tube LIF module using a silicon photomultiplier (nm) and a silicon photodiode (nm). Pacific Blue (PB) succinimidyl ester dye was excited at 405 nm, and fluorescent light was captured by the detectors. Signal was calculated as a 10 second average of captured PB dye fluorescent light, while noise was calculated as the standard deviation of the baseline. Error bars represent the standard deviation of triplicate technical replicates.

6.4.4 Manual 2 x 2 Processor Analysis

To characterize the method LOD of the LIF detection module, a standard dilution series of leucine was reacted with fluorescamine dye and quantified in triplicate. Fluorescamine dye was chosen to replace PB dye for this analysis because of the naturally nonfluorescent property of fluorescamine [224]. When reacted with primary amines, fluorescamine forms a highly fluorescent product. While the products of the reaction of PB dye with primary amines are also highly fluorescent, PB dye itself is naturally fluorescent and would, therefore, generate a high background signal if used for total amine quantification.

The reaction products of leucine with fluorescamine dye were manually transferred from a microcentrifuge tube to the automated microfluidic processor for analysis. A discrete 3-valve pumping sequence was used to route the solution to the detection channel. As a result, characteristic pulses of fluorescent material passing through the focused laser beam for excitation and detection were generated. To characterize these results, the peak heights of 10 consecutive pulses were averaged to produce a signal value for each concentration. The calculated noise remained the value of the standard deviation of the baseline. By plotting the log of the average S/N from the three independent dilution series versus the log of their respective concentrations, a linear regression for total leucine content was modeled, and a method LOD was calculated to be 11.8 μM (Figure 6.6). This method LOD value was unsurprisingly higher than that of the raw instrument LOD since the method LOD relies on the reaction between fluorescamine dye and primary amines in the solution and fluorescamine dye has a lower quantum yield compared to PB dye.

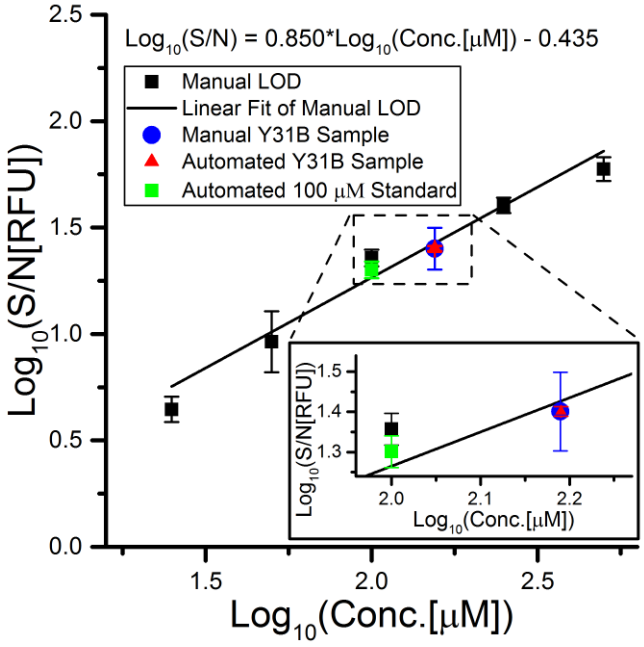

Figure 6.6. Method LOD of the lens tube LIF module using the silicon photomultiplier as the detector. Leucine was reacted with fluorescamine dye in a microcentrifuge tube and transferred to the automated microfluidic processor for detection. A Y31B sample was also reacted with fluorescamine dye in a microcentrifuge tube and transferred to the automated microfluidic processor for detection. A 100 μM solution of leucine and the Y31B sample were reacted with fluorescamine dye using the automated microfluidic processor for comparison to the manually-reacted leucine standards and Y31B sample. Signal was calculated as the average peak height of 10 individual pulses of captured fluorescent light, while noise was calculated as the standard deviation of the baseline. Error bars represent the standard deviation of triplicate technical replicates.

A solid sample (Y31B) was collected from the Atacama Desert in Yungay, Chile. The Atacama Desert is a hyper arid location and contains minimal anthropological contamination and exceptionally limited bacterial biomass [225-227]. This harsh desert region is generally considered an excellent Mars analogue site and has been used to field test multiple instruments and techniques [88, 96, 228, 229]. Since LIF detection is a wet chemistry technique, a liquid extraction was performed to isolate any organic molecules present in the solid sample. The liquid extract was then subjected to the same reaction and quantification procedure to that of the manual LOD analysis. Using the LOD standard

curve, the raw extracted sample was discovered to contain 300 ± 50 µM of primary amines, indicating that this early-stage lens tube LIF detection prototype is capable of detecting trace organics in a Martian environment and potentially in analogue environments of other celestial bodies within the Solar System.

6.4.5 Automated 2 x 2 Processor Analysis

Storage is limited during an outer planetary mission. Limiting size, mass, and power is critical when developing instruments for space flight. The restrictions placed on instrument design can greatly affect the mission criteria even before flight. Specifically, design restraints can dictate the number and frequency of analyses performed, and unforeseen circumstances experienced during a mission can further limit instruments to a few samples for testing. Therefore, an instrument must demonstrate the capability to run a full range of analyses with limited resources. To simulate these conditions, the extract from the manual analysis was used for the automated analysis. The full automated analyses for the Y31B sample was run using the microfluidic processor. Reactions were performed individually on-chip and directly routed to the detection channel for quantification. When quantified using the manual LOD standard curve, the automated Y31B sample was found to contain 289 ± 4 µM of primary amines. The calculated S/N values for the manual Y31B sample were compared to the calculated S/N values for the automated Y31B sample using a 2-tailed paired t-test with a set confidence value of 0.95. The obtained p value of 0.888 was greater than the set alpha value of 0.05 (1.00 - confidence value) (Supplementary Table A.5.6), suggesting that the calculated concentration of 289 ± 4 µM for the automated sample was statistically similar to the calculated concentration of 300 ± 50 µM for the manual sample.

As a control, a 100 μM solution of leucine was quantified using the automated protocol and compared to the manual 100 μM solution of leucine. Like the automated Y31B sample. reactions were performed individually on-chip and directly routed to the detection channel for quantification. When comparing the S/N values using a 2-tailed paired t-test with a set confidence value of 0.95, the obtained p value was 0.358 (Supplementary Table A.5.7), suggesting that the automated protocol did not produce statistically different data than that of the manual protocol. These results have shown promising usability of automated microdevices and portable lens tube LIF detection systems for the analysis of samples taken from restricting environments, like those on Mars, Enceladus, or Europa.

6.5 Conclusions

Not many instruments, particularly those intended to conduct organic analysis, are robust to the high g-loads of a kinetic penetrator mission. The lens tube LIF detection module designed, assembled, and characterized in this study demonstrates an initial step towards the development of a device capable of organic molecule analysis for a kinetic impactor mission. The instrument obtained a 177 nM LOD using a silicon photomultiplier for direct PB quantification, and the method LOD was calculated to be 11.8 μM, a good benchmark for an optical detection system of its unique design. As demonstrated in a similar compact LIF detection system [106], this LOD can be improved with the addition of custom-designed and fabricated optical components. These modifications would reduce the LOD by several orders of magnitude while maintaining the compact size and rigidity of the lens tube structure. This reduced size of the detection system and fixed assembly

style are ideal for an outer-planetary mission, allowing facile integration into any suite of instruments on-board a space craft.

The microdevices used in this study were fabricated using a recently-developed fast-prototyping method [219]. This process permitted an expediated initial design phase and greatly reduced production costs that are normally associated with cleanroom fabrication of microfluidic devices. The automated processor was used to analyze a 100 μM leucine standard and demonstrated mixing capabilities equivalent to traditional manual mixing method using a pipettor and microcentrifuge tubes. The fully integrated microfluidic processor and lens tube LIF detection system was also used to quantify amino acids contained within a Mars analogue sample at 289 ± 4 μM, which was statistically-similar to the manual quantification of primary amines at 300 ± 50 μM. These results represent a great step forward for the development of miniaturized optical devices for the detection of organic molecules, particularly within the scope of a kinetic impactor mission.

CHAPTER 7. CONCLUSIONS AND FUTURE DIRECTIONS

7.1 Concluding Remarks

A benchtop μCE-LIF detection system was built and tested by analyzing standard amino acid samples of valine, serine, alanine, glycine, glutamic acid, and aspartic acid in multiple borate buffered solutions of increasing concentrations from 10-50 millimolar (mM), all pH 9. The limits of detection (LODs) of alanine and glycine using 35 mM borate buffer were found to be 2.12 nanomolar (nM) and 2.91 nM, respectively, comparable to other state-of-the-art μCE-LIF instruments using a spectrometer as a detector. Due to the modularity in design, this system can be adapted to any wavelength excitation/emission required for multiple targets, including enhanced chiral analysis, polycyclic aromatic hydrocarbons (PAH's) , etc…, and serves as an excellent test bed for the fabrication of specialized portable or laboratory-based μCE-LIF systems for trace organic molecule detection for future habitability studies in the Solar System.

Using the benchtop μCE-LIF detection system, a series of icy moon analogue standards was analyzed to evaluate the performance of the instrument towards an icy moon environment. High-resolution separations of an amino acid standard solution, including valine, serine, alanine, glycine, glutamic acid, and aspartic acid, contained within Europa-like solutions of sulfuric acid, carbonic acid, sodium carbonate, and magnesium sulfate were obtained. Separations were improved by diluting the salts in solution, regulating the pH, and sequestering cations with ethylenediaminetetraacetic acid EDTA. When analyzing an icy moon analogue sample taken from Champagne Geyser at Chaffin Ranch, Utah, the amino acids leucine, valine, serine, alanine, and glycine were identified by direct

comparison to spiked standards. Alanine and glycine were quantified via standard curve at 80.1 ± 0.8 µM and 900 ± 100 nM, respectively, while leucine, valine, serine, and glycine were quantified using the spiked sample at 4.4 ± 0.8 µM, 830 ± 80 nM, 780 ± 60 nM, and 1.0 ± 0.2 µM, respectively. These results signify a significant step forward for the liquid-based µCE-LIF analysis of small organic molecules and biopolymers for future space missions to icy bodies like Enceladus and Europa.

The pneumatically-actuated monolithic membrane microvalves within a 10-year-old microdevice were opened successfully under ambient conditions. Using a square wave with a 500 millisecond (ms) actuation pulse width and a 1000 ms period and operating under vacuum at -980 millibar (mbar) from ambient pressure, all microvalves opened in less than 1 hour (hr). Fluidic transfer was characterized at a flow rate of 122 ± 8 microliters/minute (µL/min) right-side up in Earth's gravitational field and 110 ± 10 µL/min upside down in Earth's gravitational field. These results addressed (1) a concern that these systems may have a limited shelf-life and (2) a concern that performance depends specific device orientation in a gravitational field, indicating likely successful implementation of these microfluidic architectures in an orbital microgravity environment after an extended period in storage.

Microdevices were studied through a series of thermocycling tests from -196 °C to 100 °C. No deleterious effects were noted until 3 rounds of temperature cycling, suggesting these devices could survive 3 unlikely critical temperature failures during a space mission. Ten+-year-old PB dye was stored dry with a standard mixture of amino acids exhibited reactivity similar to that of a standard liquid labeling protocol. A slightly lower signal-to-noise (S/N) intensity was noticed for the dry test and was likely due to the hydrolysis of

PB. A 2x excess of PB when stored with amino acids would alleviate any potential loss in S/N, indicating that this labeling process is an acceptable method for future automated μCE-LIF analyses after extended storage of the microdevice in dry conditions.

To minimize mass, size, and power, a portable lens tube LIF detection prototype was developed to quantify bulk organics in a liquid sample. Using a silicon photomultiplier (SiPM) as a detector, a LOD analysis was performed by reacting various concentrations of leucine with fluorescamine dye in 35 mM borate buffer, pH 9. The LOD was found to be 11.8 μM, an excellent benchmark for a prototype LIF detection system of its unique design. A sample (Y31B) collected from the Atacama Desert in Yungay, Chile, was found to contain 300 ± 50 μM of bulk amino acids when quantified manually and 289 ± 4 μM of bulk amino acids when analyzed using an automated fast-prototyped microfluidic processor. These results have shown promising usability of automated microdevices and portable lens tube LIF detection systems in more restricting environments, like those on Europa and Enceladus.

This research has furthered the development of LIF detection techniques for analysis of organic molecule monomers and short polymers for biosignature detection missions to celestial bodies within our Solar System, such as Europa and Enceladus. Plume activity and evidence supporting global subsurface oceans have made Europa and Enceladus high-priority targets for future NASA outer-planetary missions. *In situ* quantitative and compositional analysis of organic molecules in the plumes or subsurface oceans of Europa or Enceladus could provide the first signatures of past or extant life beyond Earth. MicroCE-LIF instruments have the resolution, selectivity, and sensitivity to

provide these analyses. While lander or fly-by missions have largely been the focus for the development of μCE-LIF, as proposed in the Mars Organic Analyzer (MOA) and Enceladus Organic Analyzer (EOA), there has been limited development of LIF detection systems for more extreme environments, like the surfaces of the icy moons Europa and Enceladus. The successful functionality of 10-year-old microdevice, the separation and detection of organic molecules contained within a Europa analogue sample using a μCE-LIF benchtop system, the retained reactivity of 10-year-old PB stored dry with amino acids, and the bulk quantification of amino acids in an icy moon analogue sample using a miniaturized lens tube LIF detection system denote a substantial step forward for the liquid-based analysis of small organic molecules and biopolymers for future space missions to icy bodies like Europa and Enceladus.

7.2 Future Directions and Potential Applications

While this research has effectively demonstrated the advancement of LIF devices for planetary and astrobiological studies, many experiments remain to more completely develop these instruments for future outer-planetary missions. Further PBSE dry-down experiments can be done using a fast-prototyped microfluidic device for comparison to those already done off-chip. Each reaction protocol done for the microcentrifuge tube experiments, including the liquid control, the dry test, and the dry control, should be redone using the fast-prototyped microfluidic device to mix the solutions. Processed solutions can be manually pipetted from the device to a separate glass μCE-LIF microdevice for high resolutions separations as done previously or conducted fully-automated on a more flight-like device. Peak intensities for the on-chip samples should be examined for their statistical similarity to their off-chip counterparts. Statistically similar data sets will support the

conclusion that labeling using dried PBSE on-chip is an acceptable method for future automated μCE-LIF analyses.

While microdevices have been shown to survive multiple extreme temperature cycles, a fast-prototyped, flight-like mixing microdevice and a custom-designed and fabricated Micronit μCE device should be thermocycled at a more mission likely -80 °C to 60 °C in triplicate. After thermocycling, the automated processor should control fluid flow at a rate comparable to its flow rate before thermocycling. MicroCE-LIF analyses should be performed using the thermocycled Micronit μCE device, and electropherogram analyses should prove statistically similar to those done before thermocycling. These experiments will demonstrate the survivability and usability of fast-prototyped mixing microdevices and custom-designed and fabricated Micronit devices after potential extreme temperature swings during outer-planetary mission transit.

Individual components, including the high voltage power supply, the optics, the detection system, and the pneumatics system, have been chosen and tested for a compact, portable μCE-LIF system design. Each component has been tested individually, but component integration and characterization of the assembled system are required. Design and construction of a housing unit for the components is needed. The LabVIEW code used with the modular benchtop μCE-LIF system should be modified to control the miniaturized system. The more compact instrument should be qualified using a set of standard amino acids, like the previous characterization of the modular benchtop μCE-LIF system. An ideal borate buffer concentration and a LOD of the instrument should be determined, and an analogue sample taken from the Holuhraun, Iceland, should be analyzed for amino

acids. This experiment would serve as the capstone for the characterization of the miniaturized μCE-LIF system.

Automation of the benchtop μCE-LIF system for organic molecule analysis is achievable and would decrease sample preparation time and separation analysis time needed for analysis of real samples. Typical set-up and analysis can take days to weeks for one sample. Automation would allow for data interpretation during sample analysis, decreasing the total analysis time to roughly half. Due to the modularity of the benchtop μCE-LIF instrument, targeting different excitation/emission wavelengths of alternate fluorescent dyes can be done by exchanging the dichroic mirror and longpass filter. These components are conveniently held within a magnetically replaceable DFM kinematic fluorescence filter cube. Once exchanged, an alternate fluorescent dye matching the new wavelength profile of the dichroic mirror and longpass filter can be examined, potentially leading to a more powerful assay. Analysis of further real-world analogue samples will fully characterize the efficiency of μCE-LIF for analyzing organic molecules in specific environments. A remote sampling protocol can be created for analyzing unknown samples, simplifying future analyses of real-world samples, like those from the Atacama Desert, Chile, the Rio Tinto, Spain, and Holuhraun, Iceland, fully developing LIF detection techniques for analysis of organic molecules for biosignature detection missions to celestial bodies within the Solar System.

APPENDIX A. SUPPLEMENTARY MATERIAL

A.1. Chapter 2 Supplementary Material

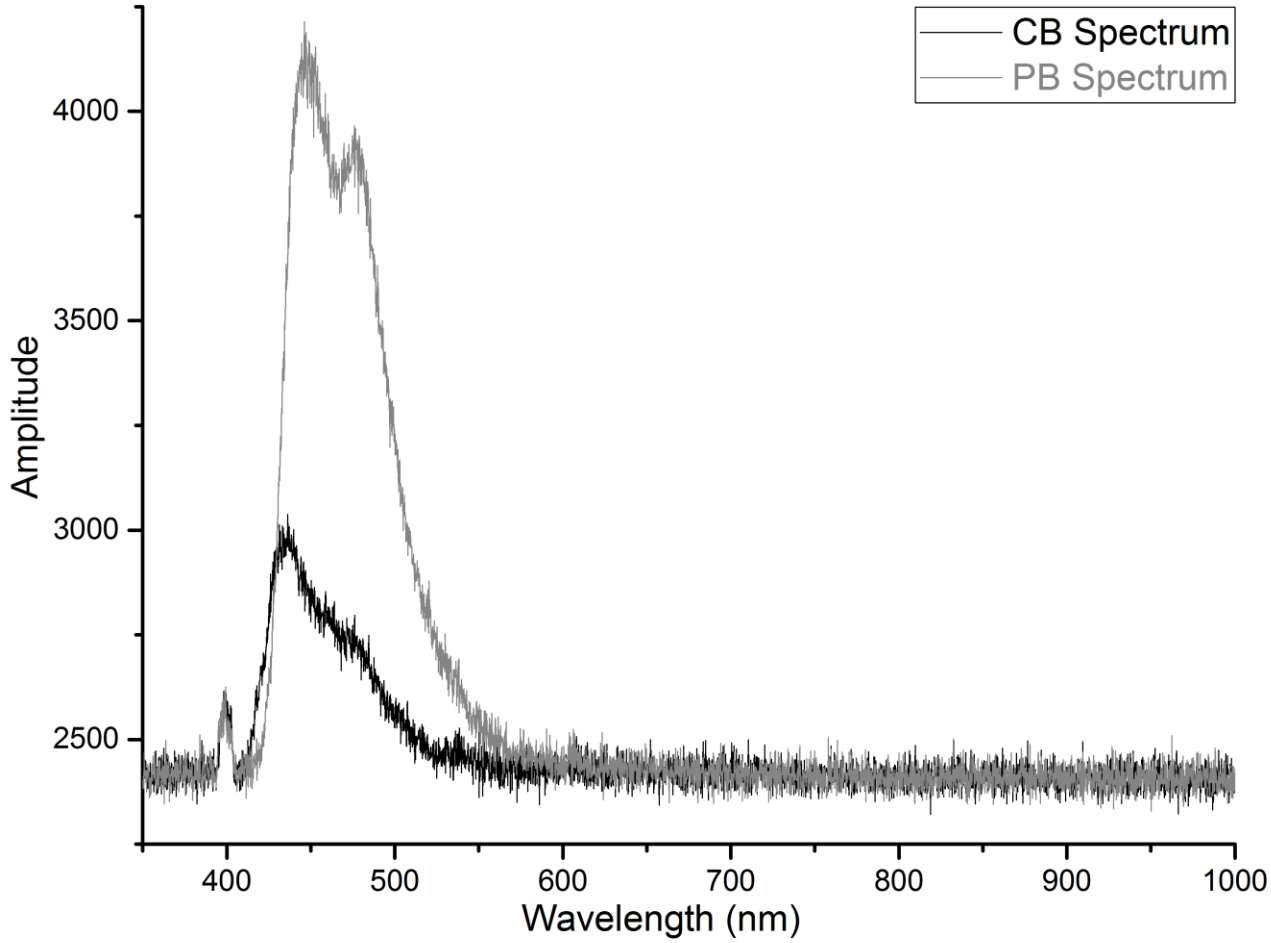

Supplementary Figure A.1.1. Emission spectra of 100 nM Cascade Blue (CB) hydrazide dye and 100 nM Pacific Blue (PB) succinimidyl ester dye each excited at 405 nm and collected using an Ocean Optics Flame spectrometer.

Supplementary Table A.1.1 - Signal-to-noise (S/N; relative fluorescence units – RFU), theoretical plates (N)/m, resolution, and full width at half max (FWHM; seconds - s) of electropherograms from analyses done at 732 V/cm using indicated borate buffer concentrations with an amino acid standard solution containing valine, serine, alanine, glycine, glutamic acid, and aspartic acid each at 20 µM.

Amino Acid	Signal/Noise (RFU)	Theoretical Plates (N)/m	Resolution	FWHM (s)
		10 mM Borate		
Valine	6200 ± 700	230000 ± 40000	-	3.6 ± 0.1
Serine	10000 ± 1000	260000 ± 40000	1.54 ± 0.09	3.56 ± 0.06
Alanine	8000 ± 1000	250000 ± 30000	0.39 ± 0.02	3.66 ± 0.07
Glycine	8700 ± 800	240000 ± 20000	1.58 ± 0.04	4.0 ± 0.2
Glutamic Acid	7400 ± 500	160000 ± 20000	7.3 ± 0.2	6.5 ± 0.1
Aspartic Acid	6300 ± 400	160000 ± 10000	1.75 ± 0.06	7.11 ± 0.05
		20 mM Borate		
Valine	5200 ± 800	178000 ± 4000	-	4.93 ± 0.06
Serine	9000 ± 1000	194000 ± 4000	1.57 ± 0.04	5.0 ± 0.1
Alanine	6300 ± 800	201000 ± 3000	0.44 ± 0.01	5.0 ± 0.1
Glycine	7200 ± 1100	200000 ± 20000	1.64 ± 0.06	5.5 ± 0.3
Glutamic Acid	5900 ± 800	118000 ± 4000	7.2 ± 0.2	9.71 ± 0.07
Aspartic Acid	4900 ± 600	115000 ± 8000	1.76 ± 0.03	10.8 ± 0.4
		30 mM Borate		
Valine	4900 ± 200	159000 ± 7000	-	5.9 ± 0.2
Serine	7600 ± 400	166000 ± 8000	1.60 ± 0.02	6.18 ± 0.07
Alanine	5700 ± 100	167000 ± 3000	0.508 ± 0.002	6.31 ± 0.04
Glycine	6400 ± 300	159000 ± 8000	1.68 ± 0.04	6.9 ± 0.3
Glutamic Acid	4700 ± 200	97000 ± 2000	6.9 ± 0.2	12.6 ± 0.1
Aspartic Acid	4000 ± 200	104000 ± 4000	1.84 ± 0.02	13.5 ± 0.3
		35 mM Borate		
Valine	3800 ± 200	120000 ± 10000	-	7.2 ± 0.5
Serine	5900 ± 300	131000 ± 3000	1.571 ± 0.005	7.5 ± 0.1
Alanine	4200 ± 400	136000 ± 6000	0.53 ± 0.01	7.6 ± 0.1
Glycine	4900 ± 400	130000 ± 10000	1.72 ± 0.06	8.3 ± 0.4
Glutamic Acid	3700 ± 300	81000 ± 3000	7.1 ± 0.2	15.8 ± 0.3
Aspartic Acid	3100 ± 300	72000 ± 6000	1.83 ± 0.02	18.7 ± 0.5
		40 mM Borate		
Valine	4000 ± 200	120000 ± 10000	-	7.8 ± 0.6
Serine	6200 ± 300	130000 ± 10000	1.60 ± 0.06	8.2 ± 0.7
Alanine	4300 ± 400	130000 ± 10000	0.56 ± 0.03	8.3 ± 0.7
Glycine	5000 ± 300	130000 ± 20000	1.7 ± 0.1	9 ± 1
Glutamic Acid	3700 ± 400	78000 ± 8000	7.1 ± 0.3	18 ± 2
Aspartic Acid	2900 ± 400	67000 ± 3000	1.87 ± 0.05	21 ± 1
		50 mM Borate		
Valine	3900 ± 400	123000 ± 7000	-	8.3 ± 0.6
Serine	5600 ± 300	130000 ± 10000	1.69 ± 0.05	8.9 ± 0.9
Alanine	4000 ± 100	140000 ± 20000	0.66 ± 0.04	9 ± 1
Glycine	4600 ± 200	130000 ± 20000	1.87 ± 0.06	10 ± 1
Glutamic Acid	3300 ± 400	70000 ± 6000	7.4 ± 0.2	21 ± 2
Aspartic Acid	2800 ± 600	58000 ± 9000	1.90 ± 0.06	27 ± 4

A.2. Chapter 3 Supplementary Material

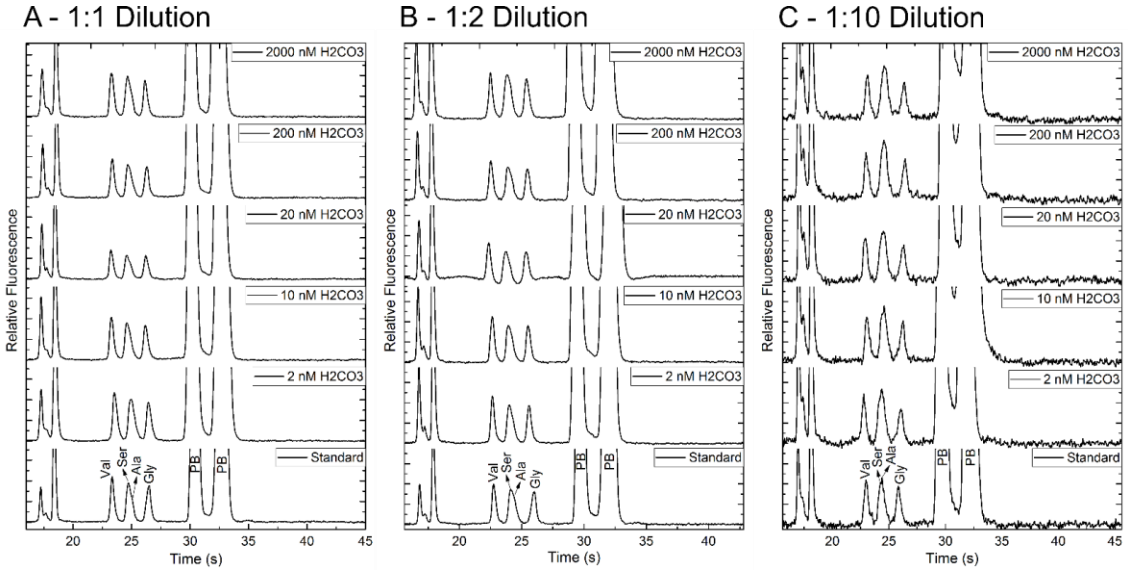

Supplementary Figure A.2.2. MicroCE separations of an amino acid standard (Val, Ser, Ala, Gly, Glu, and Asp - each with a 100 nM starting concentration) in varying starting concentrations of H_2CO_3 diluted (A) 1:1, (B) 1:2, and (C) 1:10 before labeling (732 V/cm separation potential).

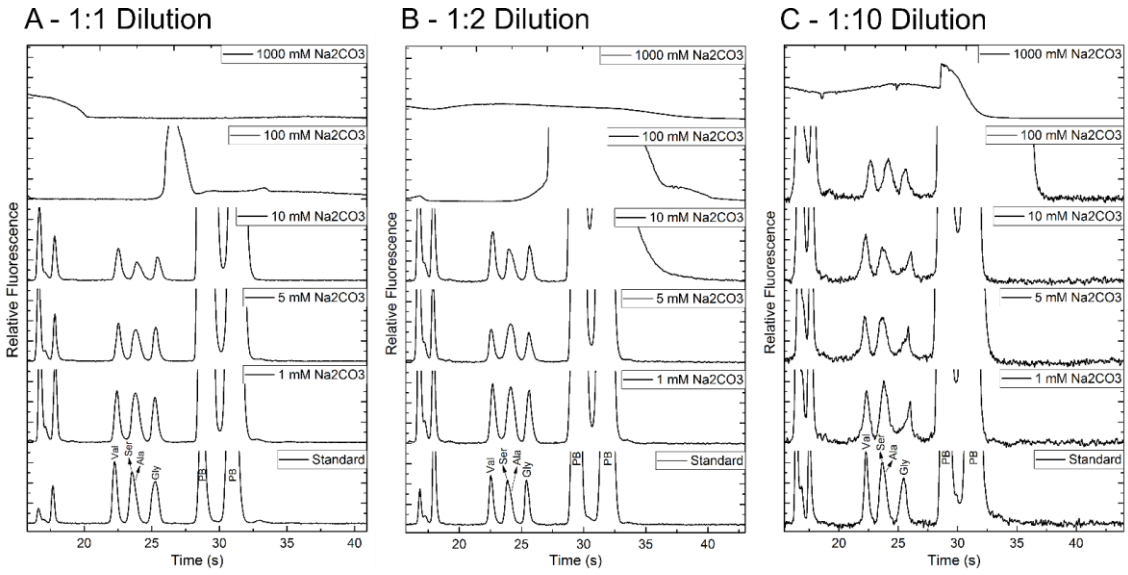

Supplementary Figure A.2.3. MicroCE separations of an amino acid standard (Val, Ser, Ala, Gly, Glu, and Asp - each with a 100 nM starting concentration) in varying starting concentrations of Na_2CO_3 diluted (A) 1:1, (B) 1:2, and (C) 1:10 before labeling (732 V/cm separation potential).

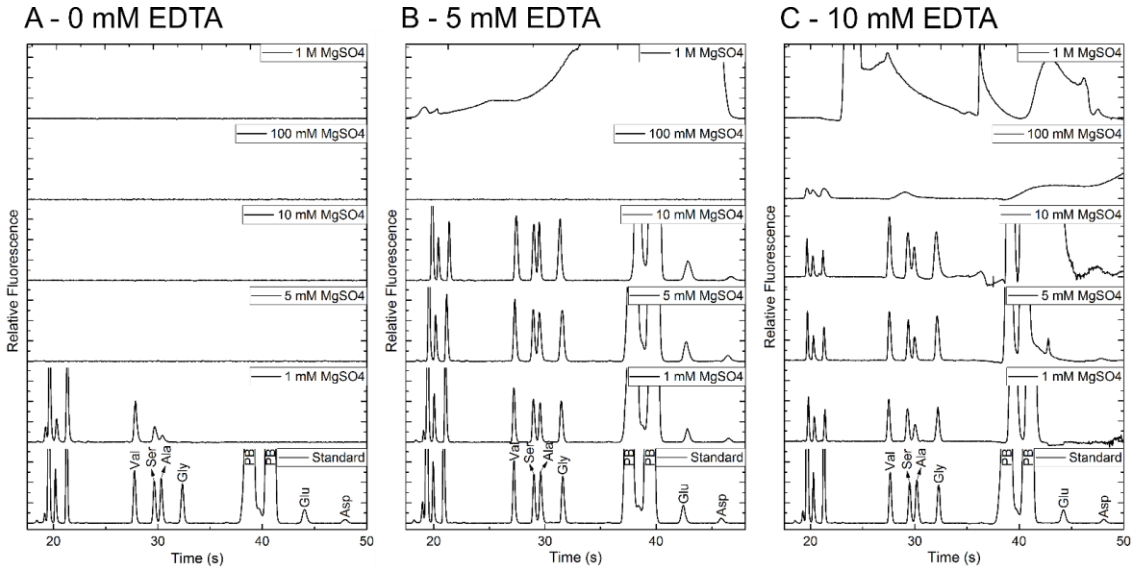

Supplementary Figure A.2.4. MicroCE separations of an amino acid standard (Val, Ser, Ala, Gly, Glu, and Asp - each with a 100 nM starting concentration) in varying starting concentrations of $MgSO_4$ in (A) 0 mM, (B) 5 mM, and (C) 10 mM EDTA (732 V/cm separation potential).

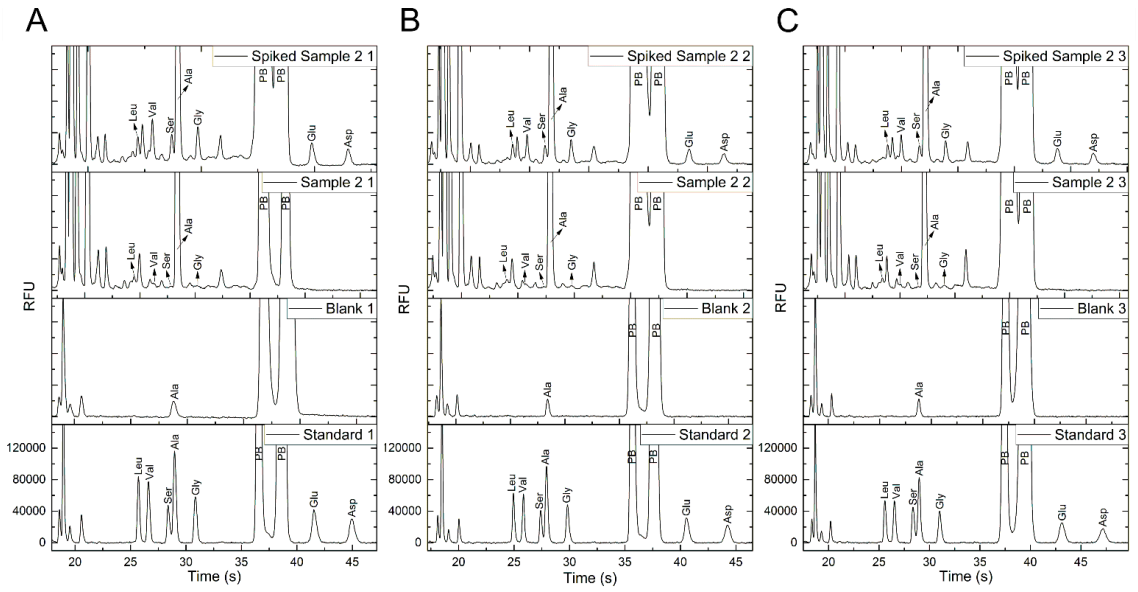

Supplementary Figure A.2.5. Triplicate (A, B, C) electropherogram analyses of a sample taken from Champagne Geyser, an icy moon analogue geyser at Chaffin Ranch in Utah (732 V/cm separation potential).

Supplementary Table A.2.2 - Quantification of Organics Identified using Spiked Standard and Quantified via Standard Curve or Spiked Sample

Amino Acid	Concentration Before Dilution [nM]*
Quantification via Standard Curve	
Alanine	80100 ± 800
Glycine	900 ± 100
Quantification via Spiked Sample	
Leucine	4400 ± 800
Valine	830 ± 80
Serine	780 ± 60
Glycine	1000 ± 200

*Standard deviation represents the average of triplicate technical replicates.

Supplementary Table A.2.3 - Paired Two Sample for Means t-Test

	Spiked Std	*Std Curve*
Mean	1044.726	874.560
Variance	76451.01	19484.84
Observations	3	3
Pearson Correlation	0.846	
Hypothesized Mean Difference	0	
df	2	
t Stat	1.685	
P(T<=t) one-tail	0.117	
t Critical one-tail	2.920	
P(T<=t) two-tail	**0.234**	
t Critical two-tail	4.303	

A.3. Chapter 4 Supplementary Material

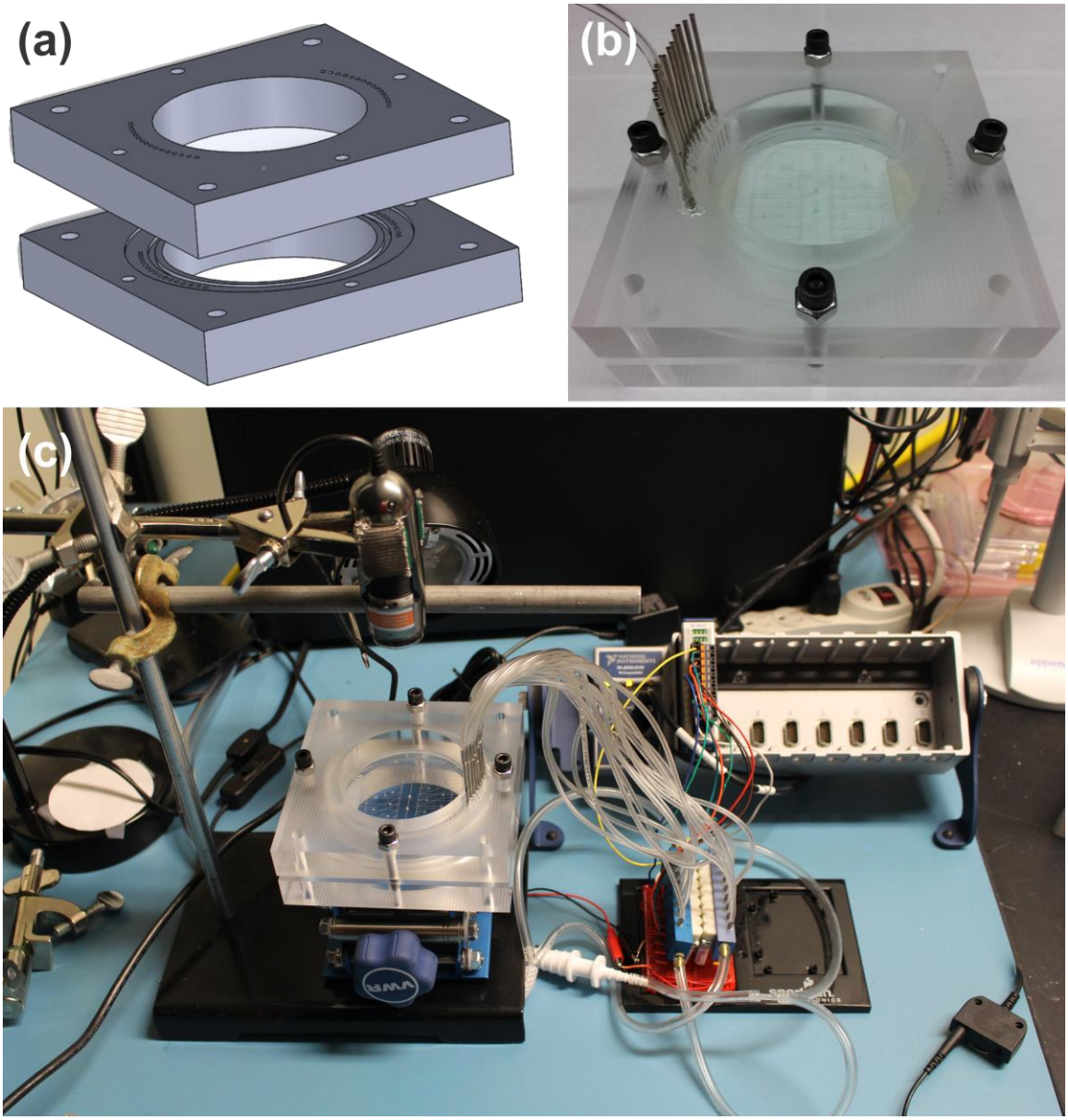

Supplementary Figure A.3.6. (a) Computer-Aided Design (CAD) of the microdevice manifold. (b) Photograph of the microdevice mounted in the manifold. (c) Photograph of experimental setup. The tubing extending from the manifold is connected to the solenoids, which are operated by the cDAQ controller.

Supplementary Table A.3.4 - Summary of factory and current experimental hold pressures of 10-year-old LHLX0500200BB Lee solenoid valves

	Trial 1 (Psid)	Trial 2 (Psid)	Trial 3 (Psid)	Average (Psid)
Experimental	48.72	47.55	49.92	49 ± 1
Factory	-	-	-	15

A.4. Chapter 5 Supplementary Material

Supplementary Table A.4.5 - Obtained p Values for Paired Two Sample for Means t-Tests

Amino Acid	*Liquid Control vs Partial-Liquid Control*	*Liquid Control vs Dry Test*	*Partial-Liquid Control vs Dry Test*
Leucine	0.774	0.269	0.109
Valine	0.794	0.254	0.197
Serine	0.225	0.841	0.210
Alanine	0.664	0.198	0.170
Glycine	0.329	0.591	0.206
Glutamic Acid	0.684	0.0906	0.0635
Aspartic Acid	0.718	**0.0376**	**0.0333**

A.5. Chapter 6 Supplementary Material

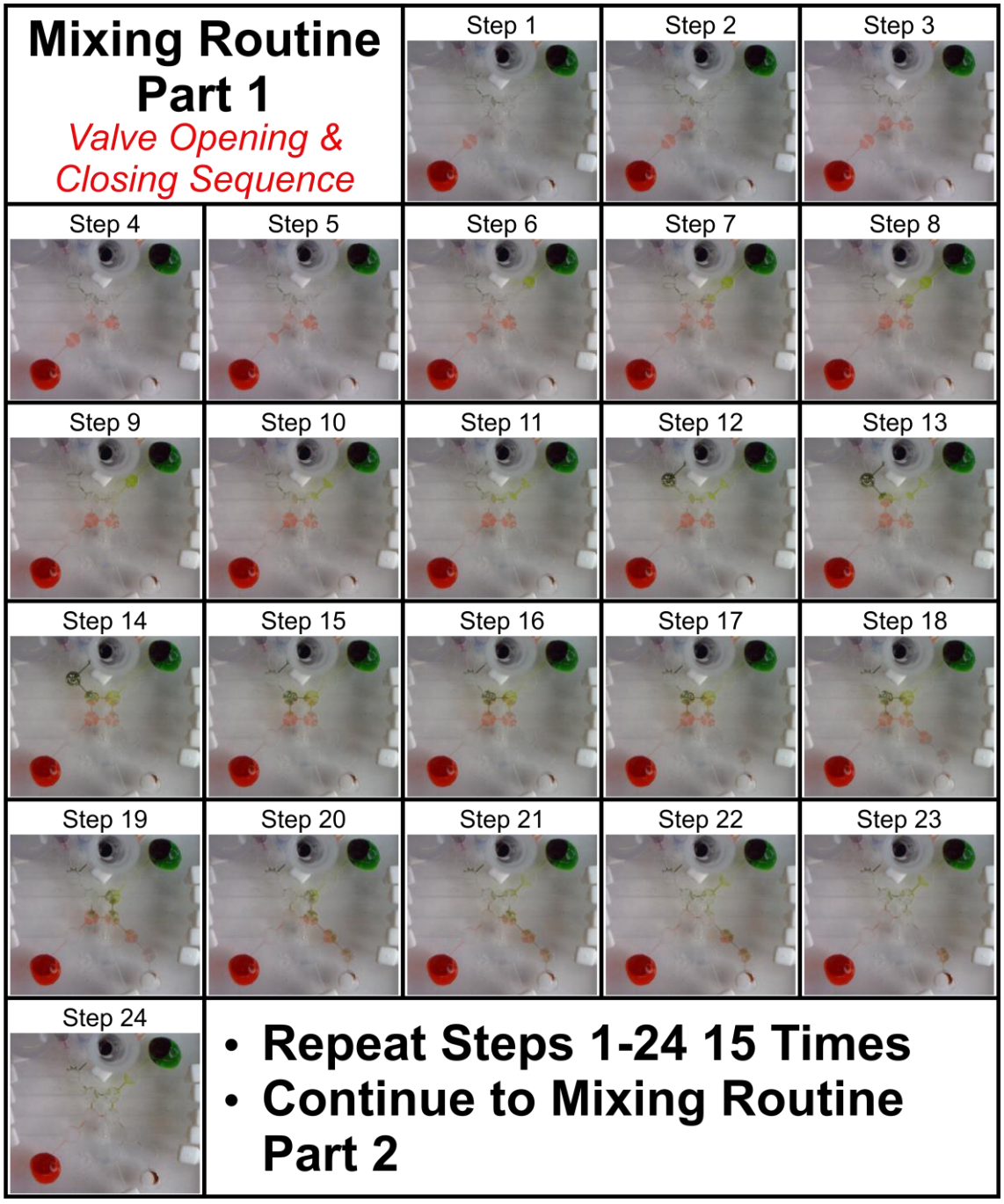

Supplementary Figure A.5.7. The 2x2 microfluidic processor used to perform mixing routine 1. A green, red, and black dye solution (beginning with the red dye solution) are transported, mixed, and routed towards an outlet reservoir, generating a red/brown mixture as a representation of the reaction of primary amines with fluorescamine dye.

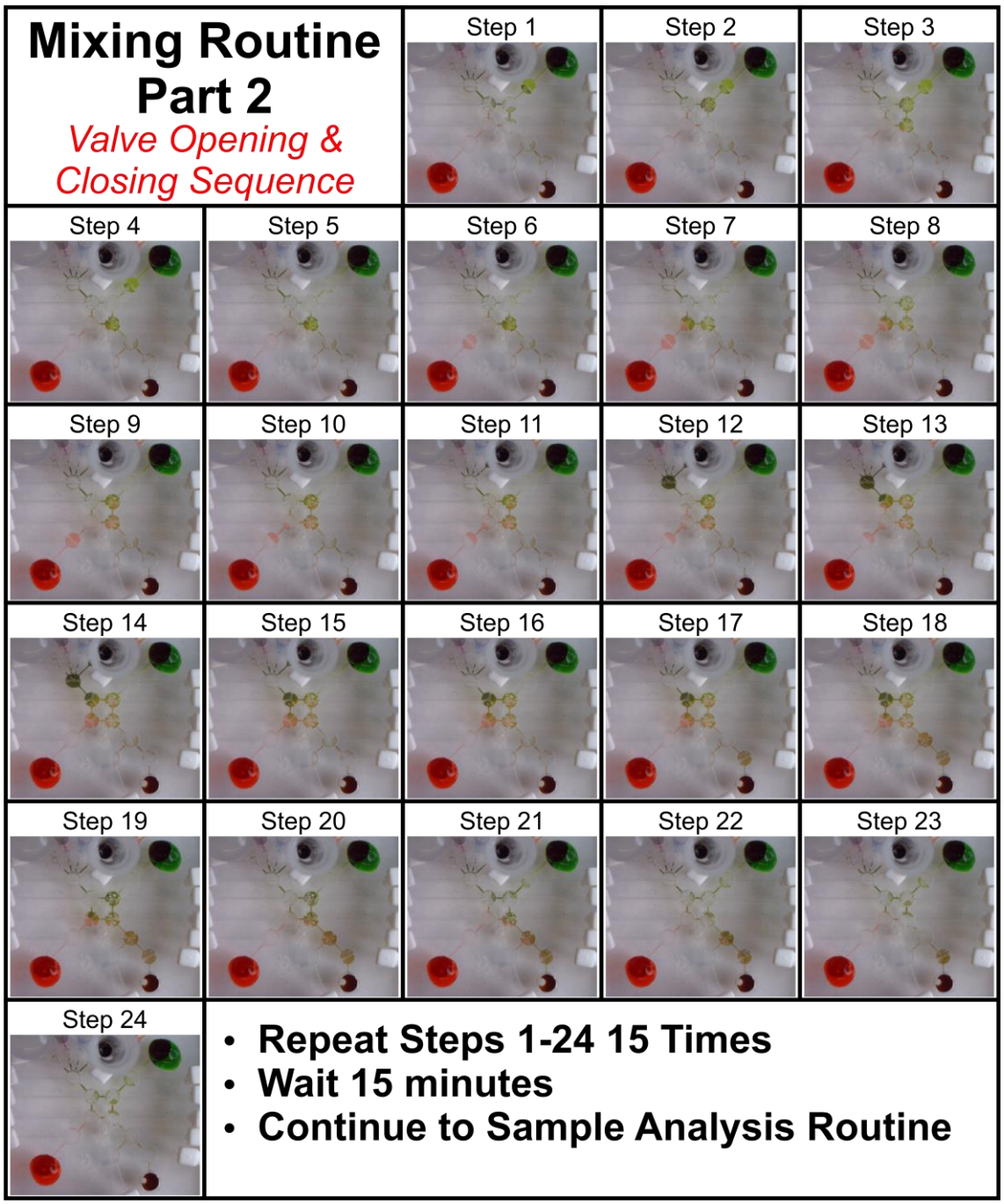

Supplementary Figure A.5.8. The 2x2 microfluidic processor used to perform mixing routine 1. A green, red, and black dye solution (beginning with the green dye solution) are transported, mixed, and routed towards an outlet reservoir, generating a red/brown mixture as a representation of the reaction of primary amines with fluorescamine dye.

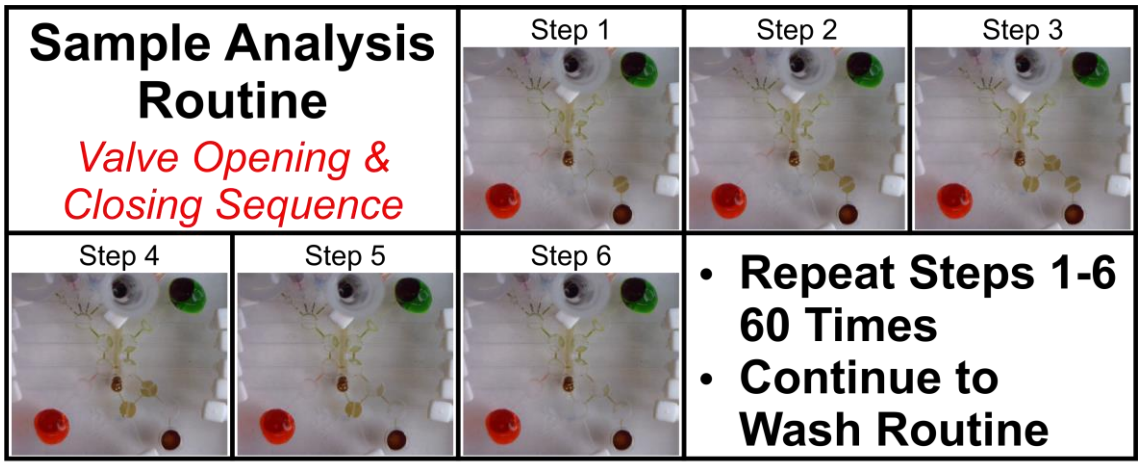

Supplementary Figure A.5.9. The 2x2 microfluidic processor used to perform the sample analysis routine. The red/brown mixture as a representation of the reaction of primary amines with fluorescamine dye is transported to the detection channel for analysis.

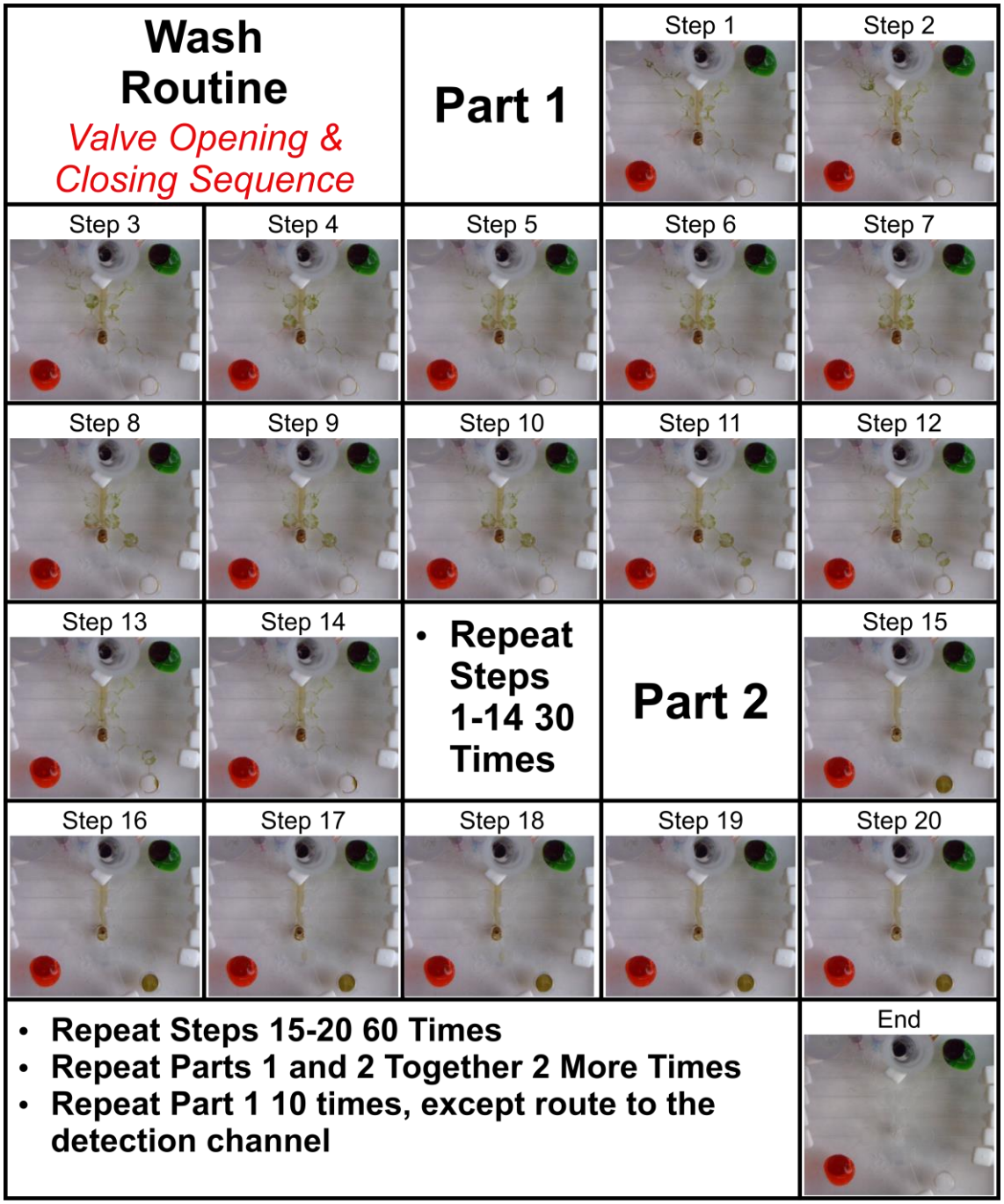

Supplementary Figure A.5.10. The 2x2 microfluidic processor used to perform the wash routine. Water is pumped through all the processor valves, cleaning the residues of dye present from the mixing protocol. After 3 wash cycles, the processor valves are clean and can be used for further analyses.

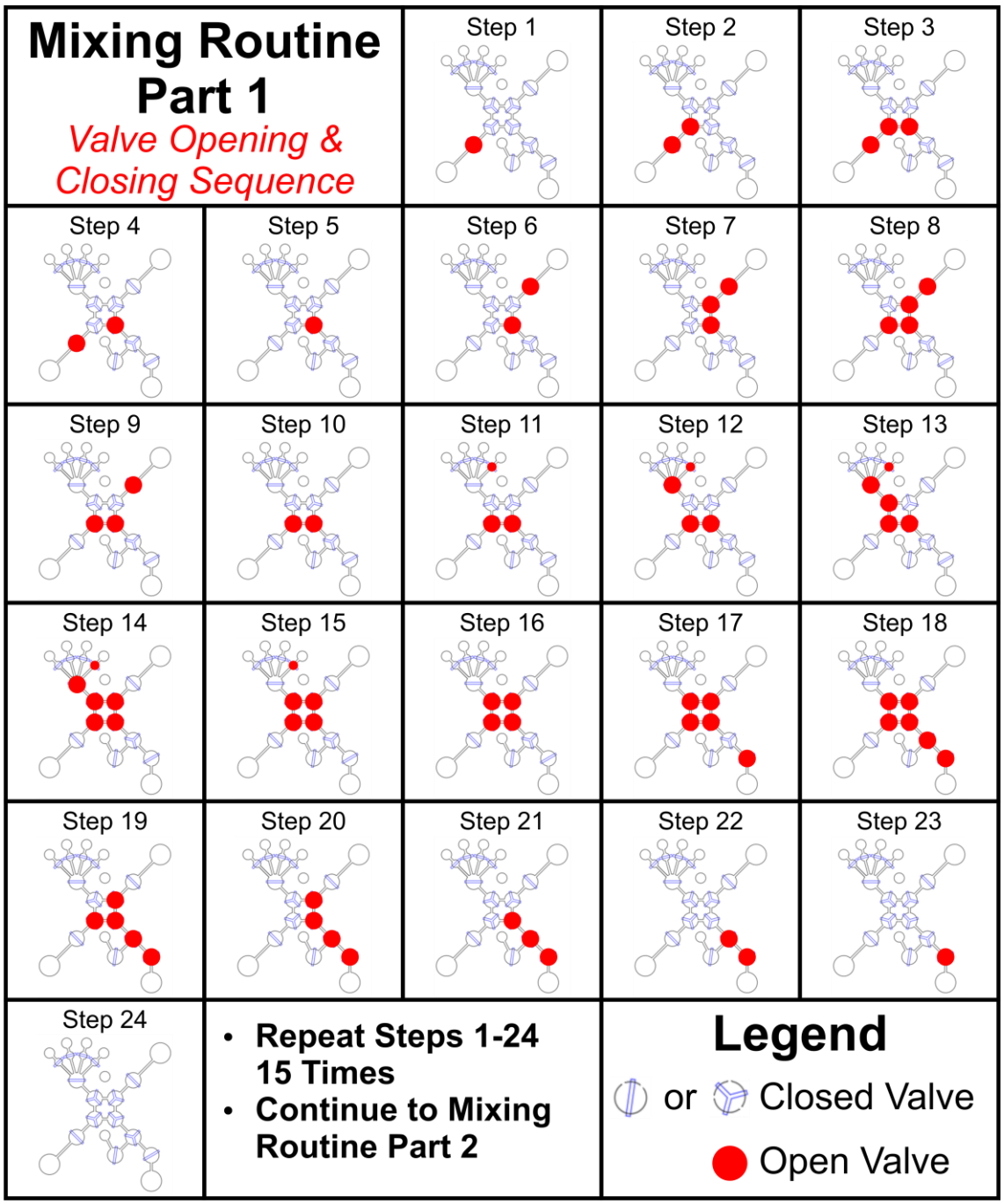

Supplementary Figure A.5.11. A schematic of the 2x2 microfluidic processor used to perform mixing routine 1.

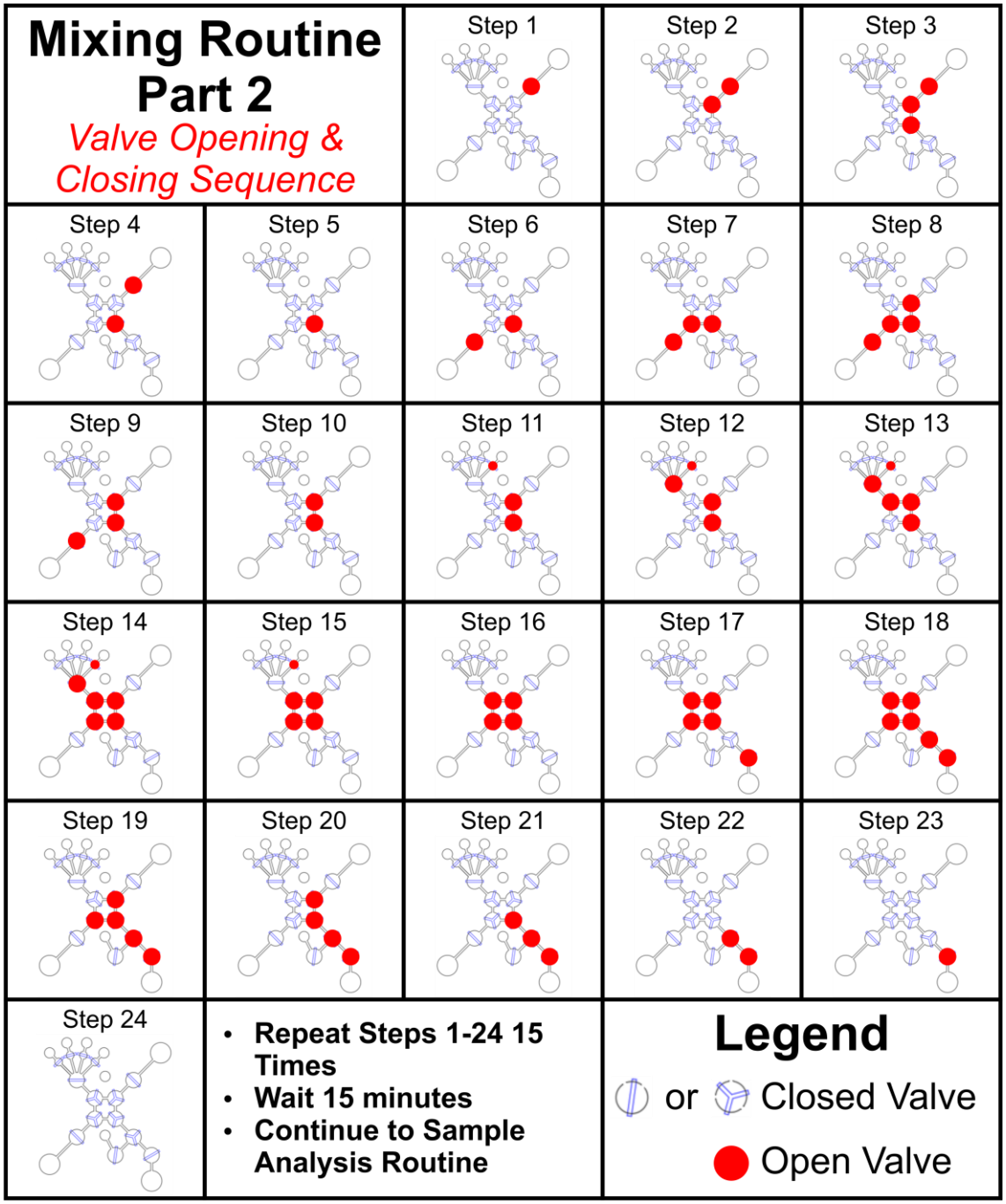

Supplementary Figure A.5.12. A schematic of the 2x2 microfluidic processor used to perform mixing routine 2.

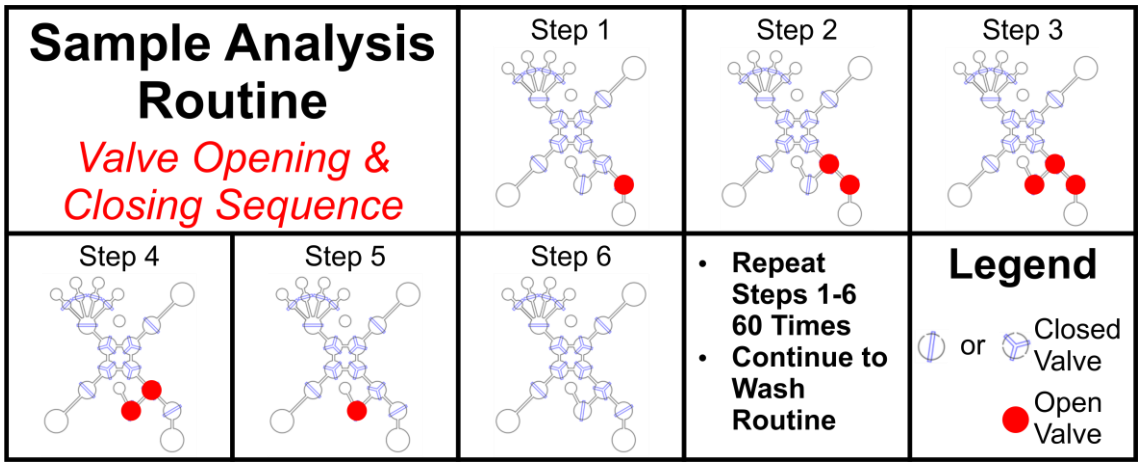

Supplementary Figure A.5.13. A schematic of the 2x2 microfluidic processor used to perform the sample analysis routine.

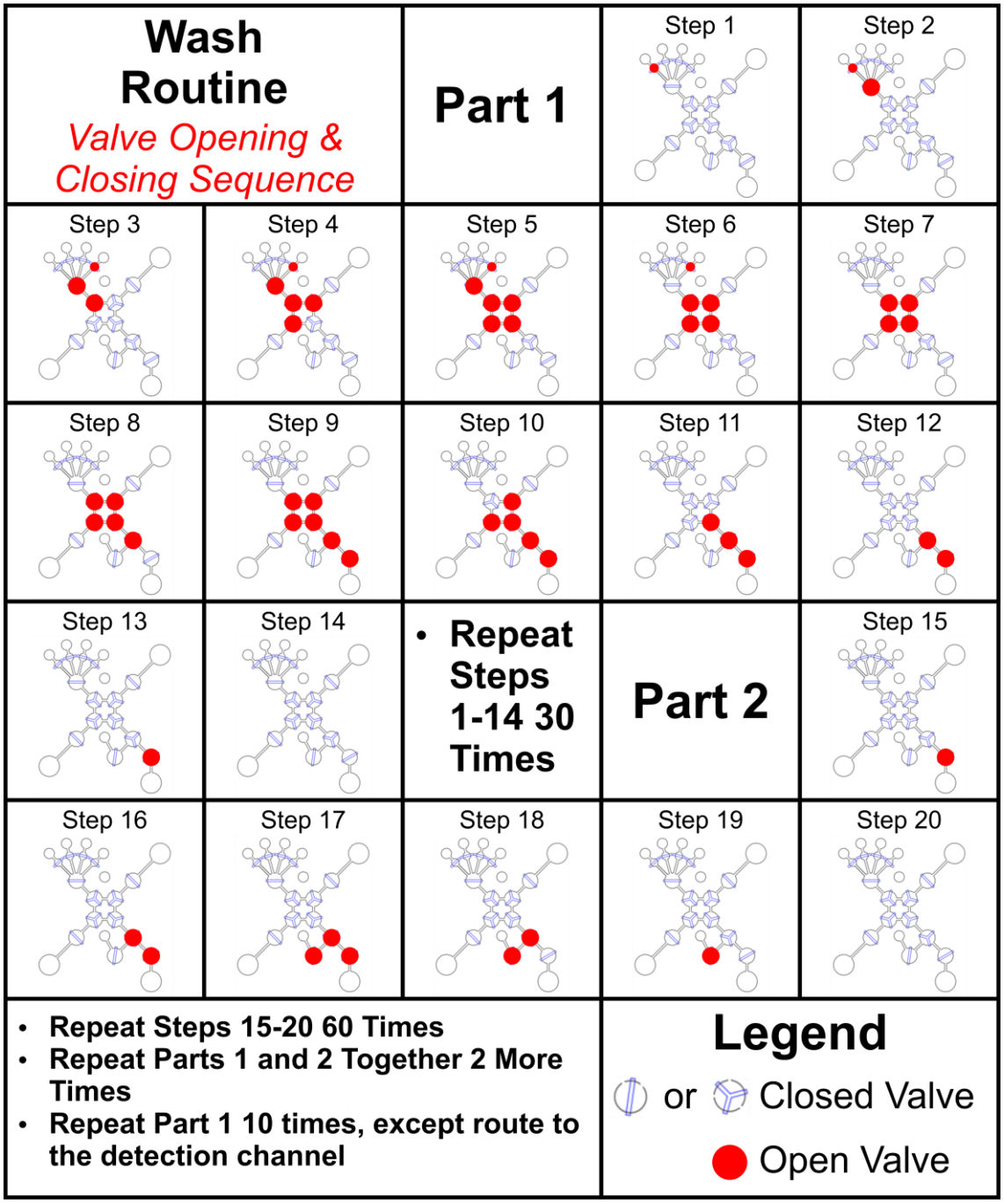

Supplementary Figure A.5.14. A schematic of the 2x2 microfluidic processor used to perform the wash routine.

Supplementary Table A.5.6 - Paired Two Sample for Means t-Test for the Manual and Automated Y31B Sample.

	Manual	*Automated*
Mean	25.785	25.205
Variance	44.782	0.708
Observations	3	3
Pearson Correlation	0.483	
Hypothesized Mean Difference	0	
df	2	
t Stat	0.159	
P(T<=t) one-tail	0.444	
t Critical one-tail	2.920	
P(T<=t) two-tail	**0.888**	
t Critical two-tail	4.303	

Supplementary Table A.5.7 - Paired Two Sample for Means t-Test for the Manual and Automated 100 µM Leucine Standard.

	Manual	*Automated*
Mean	22.842	20.081
Variance	6.193	4.657
Observations	3	3
Pearson Correlation	-0.509	
Hypothesized Mean Difference	0	
df	2	
t Stat	1.184	
P(T<=t) one-tail	0.179	
t Critical one-tail	2.920	
P(T<=t) two-tail	**0.358**	
t Critical two-tail	4.303	

REFERENCES

1. Ptolemy, G.J. Toomer, and O. Gingerich, *Ptolemy's Almagest*. 1998: Princeton University Press.

2. Copernicus, N., *Nicholaus Copernicus*, in *The Tests of Time*, L. M.Dolling, A. F.Gianelli, and G. N.Statile, Editors. 2003, Princeton University Press. p. 38-42.

3. Russell, J.L., *Kepler's Laws of Planetary Motion: 1609-1666.* The British Journal for the History of Science, 1964. **2**(1): p. 1-24.

4. Osserman, R., *Kepler's Laws, Newton's Laws, and the Search for New Planets.* The American Mathematical Monthly, 2001. **108**(9): p. 813-820.

5. Riess, A.G., et al., *Observational Evidence from Supernovae for an Accelerating Universe and a Cosmological Constant.* The Astronomical Journal, 1998. **116**(3): p. 1009-1038.

6. Miller, S.L., *A Production of Amino Acids Under Possible Primitive Earth Conditions.* Science, 1953. **117**(3046): p. 528.

7. Brennan, T., *ASTROBIOLOGY IN THE CLASSROOM.* Science Scope, 2004. **28**(1): p. 45-47.

8. Blaustein, R., *Advances in Astrobiology.* BioScience, 2015. **65**(5): p. 460-465.

9. Rothschild, L.J. and R.L. Mancinelli, *Life in extreme environments.* Nature, 2001. **409**(6823): p. 1092-1101.

10. Rummel, J.D., *Planetary Exploration in the Time of Astrobiology: Protecting against Biological Contamination.* Proceedings of the National Academy of Sciences of the United States of America, 2001. **98**(5): p. 2128-2131.

11. Petrov, A.S., et al., *Evolution of the ribosome at atomic resolution.* Proceedings of the National Academy of Sciences of the United States of America, 2014. **111**(28): p. 10251-10256.

12. Woese, C., *The Universal Ancestor*. Proceedings of the National Academy of Sciences of the United States of America, 1998. **95**(12): p. 6854-6859.

13. Forterre, P. and H. Philippe, *The Last Universal Common Ancestor (LUCA), Simple or Complex?* Biological Bulletin, 1999. **196**(3): p. 373-377.

14. Woellert, K., et al., *Cubesats: Cost-effective science and technology platforms for emerging and developing nations.* Advances in Space Research, 2011. **47**(4): p. 663-684.

15. Horneck, G., et al., *Protection of Bacterial Spores in Space, a Contribution to the Discussion on Panspermia.* Origins of life and evolution of the biosphere, 2001. **31**(6): p. 527-547.

16. Horneck, G., et al., *Resistance of Bacterial Endospores to Outer Space for Planetary Protection Purposes—Experiment PROTECT of the EXPOSE-E Mission.* Astrobiology, 2012. **12**(5): p. 445-456.

17. Shannon, C.C., et al., *Appendix A: Technology Readiness Levels*, in *Finding the Shape of Space*. 2011, Air University Press. p. 111-112.

18. Jaffe, L.D. and L.M. Herrell, *Cassini/Huygens science instruments*. Cassini/Huygens: A Mission to the Saturnian Systems, ed. L. Horn. Vol. 2803. 1996, Bellingham: Spie - Int Soc Optical Engineering. 84-106.

19. Johnson, T.V., *The Galileo Mission.* Scientific American, 1995. **273**(6): p. 44-51.

20. Welch, R., et al., *Mars Science Rovers.* SAE Transactions, 1996. **105**: p. 1013-1019.

21. Grotzinger, J.P., et al., *A Habitable Fluvio-Lacustrine Environment at Yellowknife Bay, Gale Crater, Mars.* Science, 2014. **343**(6169): p. 1242777.

22. Vago, J.L., et al., *Habitability on Early Mars and the Search for Biosignatures with the ExoMars Rover.* Astrobiology, 2017. **17**(6-7): p. 471-510.

23. Biemann, K., et al., *Search for organic and volatile inorganic compounds in two surface samples from the chryse planitia region of Mars.* Science, 1976. **194**(4260): p. 72-6.

24. Levin, G.V. and P.A. Straat, *Viking labeled release biology experiment: interim results.* Science, 1976. **194**(4271): p. 1322-9.

25. Biemann, K., et al., *The search for organic substances and inorganic volatile compounds in the surface of Mars.* Journal of Geophysical Research, 1977. **82**(28): p. 4641-4658.

26. Klein, H.P., *The Viking Biological Investigation: General aspects.* Journal of Geophysical Research, 1977. **82**(28): p. 4677-4680.

27. Levin, G.V. and P.A. Straat, *Recent results from the Viking Labeled Release Experiment on Mars.* Journal of Geophysical Research, 1977. **82**(28): p. 4663-4667.

28. Glavin, D.P., et al., *Evidence for perchlorates and the origin of chlorinated hydrocarbons detected by SAM at the Rocknest aeolian deposit in Gale Crater.* Journal of Geophysical Research: Planets, 2013. **118**(10): p. 1955-1973.

29. Hecht, M.H., et al., *Detection of perchlorate and the soluble chemistry of martian soil at the Phoenix lander site.* Science, 2009. **325**(5936): p. 64-7.

30. Kounaves, S.P., et al., *Wet Chemistry experiments on the 2007 Phoenix Mars Scout Lander mission: Data analysis and results.* Journal of Geophysical Research: Planets, 2010. **115**(E1): p. n/a-n/a.

31. Shimokawabe, M., R. Furuichi, and T. Ishii, *Effect of metal oxide additives on the thermal decomposition of perchlorates, oxalates and hydroxides.* Thermochimica Acta, 1977. **20**(3): p. 347-361.

32. Navarro-González, R., et al., *Reanalysis of the Viking results suggests perchlorate and organics at midlatitudes on Mars.* Journal of Geophysical Research: Planets, 2010. **115**(E12): p. n/a-n/a.

33. Aubrey, A.D., et al., *The Urey instrument: an advanced in situ organic and oxidant detector for Mars exploration.* Astrobiology, 2008. **8**(3): p. 583-95.

34. Carr, M.H., et al., *Evidence for a subsurface ocean on Europa.* Nature, 1998. **391**(6665): p. 363-365.

35. Lowell, R.P. and M. DuBose, *Hydrothermal systems on Europa.* Geophysical Research Letters, 2005. **32**(5): p. n/a-n/a.

36. Vance, S., et al., *Hydrothermal systems in small ocean planets.* Astrobiology, 2007. **7**(6): p. 987-1005.

37. Roth, L., et al., *Transient Water Vapor at Europa's South Pole.* Science, 2014. **343**(6167): p. 171.

38. McCord, T.B., et al., *Salts on Europa's Surface Detected by Galileo's Near Infrared Mapping Spectrometer.* Science, 1998. **280**(5367): p. 1242-1245.

39. McCord, T.B., et al., *Hydrated salt minerals on Europa's surface from the Galileo near-infrared mapping spectrometer (NIMS) investigation.* Journal of Geophysical Research: Planets, 1999. **104**(E5): p. 11827-11851.

40. Greenberg, R., et al., *Chaos on Europa.* Icarus, 1999. **141**(2): p. 263-286.

41. Squyres, S.W., et al., *Liquid water and active resurfacing on Europa.* Nature, 1983. **301**(5897): p. 225-226.

42. Pappalardo, R.T., et al., *Geological evidence for solid-state convection in Europa's ice shell.* Nature, 1998. **391**(6665): p. 365-368.

43. Greenberg, R., et al., *Tectonic Processes on Europa: Tidal Stresses, Mechanical Response, and Visible Features.* Icarus, 1998. **135**(1): p. 64-78.

44. Orlando, T.M., T.B. McCord, and G.A. Grieves, *The chemical nature of Europa surface material and the relation to a subsurface ocean.* Icarus, 2005. **177**(2): p. 528-533.

45. Kelley, D.S., et al., *An off-axis hydrothermal vent field near the Mid-Atlantic Ridge at 30° N.* Nature, 2001. **412**(6843): p. 145-149.

46. Nisbet, E.G. and N.H. Sleep, *The habitat and nature of early life.* Nature, 2001. **409**(6823): p. 1083-1091.

47. Vu, T.H., et al., *Chemistry of Frozen Sodium–Magnesium–Sulfate–Chloride Brines: Implications for Surface Expression of Europa's Ocean Composition.* The Astrophysical Journal, 2016. **816**(2): p. L26.

48. Johnson, P.V., et al., *Insights into Europa's ocean composition derived from its surface expression.* Icarus, 2019. **321**: p. 857-865.

49. Phillips, C.B. and R.T. Pappalardo, *Europa Clipper Mission Concept: Exploring Jupiter's Ocean Moon.* Eos, Transactions American Geophysical Union, 2014. **95**(20): p. 165-167.

50. Grasset, O., et al., *JUpiter ICy moons Explorer (JUICE): An ESA mission to orbit Ganymede and to characterise the Jupiter system.* Planetary and Space Science, 2013. **78**: p. 1-21.

51. Bertotti, B., *An Introduction to the Cassini-Huygens Mission.* Nuovo Cimento Della Societa Italiana Di Fisica C-Geophysics and Space Physics, 1992. **15**(6): p. 1129-1132.

52. Lebreton, J.P. and D.L. Matson, *An overview of the Cassini mission.* Il Nuovo Cimento C, 1992. **15**(6): p. 1137-1147.

53. Carton, C., et al., *The Huygens mission optimization.* Space Technology-Industrial and Commercial Applications, 1995. **15**(5): p. 271-276.

54. Angrilli, F., et al. *First results of performance test of temperature sensors of HASI instrument on Cassini/Huygens mission*. 1996.

55. Gibbs, R., *Cassini spacecraft design*. Cassini/Huygens: A Mission to the Saturnian Systems, ed. L. Horn. Vol. 2803. 1996, Bellingham: Spie - Int Soc Optical Engineering. 246-258.

56. Matson, D.L., *The Cassini/Huygens mission to the Saturnian system*. Cassini/Huygens: A Mission to the Saturnian Systems, ed. L. Horn. Vol. 2803. 1996, Bellingham: Spie - Int Soc Optical Engineering. 22-29.

57. Ruffino, G., et al., *The temperature sensor on the Huygens probe for the Cassini mission: design, manufacture, calibration and tests of the laboratory prototype.* Planetary and Space Science, 1996. **44**(10): p. 1149-1162.

58. Spehalski, R.J., *The Cassini mission to Saturn*. Cassini/Huygens: A Mission to the Saturnian Systems, ed. L. Horn. Vol. 2803. 1996, Bellingham: Spie - Int Soc Optical Engineering. 2-9.

59. Jaffe, L.D. and L.M. Herrell, *Cassini/Huygens Science Instruments, Spacecraft, and Mission.* Journal of Spacecraft and Rockets, 1997. **34**(4): p. 509-521.

60. Bergen, T.F., H. Himelblau, and D.L. Kern, *Development of acoustic test criteria for the Cassini spacecraft.* Journal of the Iest, 1998. **41**(1): p. 26-38.

61. Harri, A.m., et al., *Scientific objectives and implementation of the Pressure Profile Instrument (PPI | HASI) for the Huygens spacecraft.* Planetary and Space Science, 1998. **46**(9–10): p. 1383-1392.

62. Jakel, E., et al., *Drop test of the Huygens Probe from a stratospheric balloon*, in *Active Experiments in Space Plasmas*, W. Riedler and K. Torkar, Editors. 1998, Pergamon Press Ltd: Oxford. p. 1033-1039.

63. Burton, M.E., et al., *The Cassini/Huygens Venus and Earth flybys: An overview of operations and results.* Journal of Geophysical Research: Space Physics, 2001. **106**(A12): p. 30099-30107.

64. Clausen, K.C., et al., *The Huygens Probe System Design.* Space Science Reviews, 2002. **104**(1): p. 155-189.

65. Waite, J.H., et al., *Ion Neutral Mass Spectrometer Results from the First Flyby of Titan.* Science, 2005. **308**(5724): p. 982.

66. Matson, D.L., et al., *Enceladus' plume: Compositional evidence for a hot interior.* Icarus, 2007. **187**(2): p. 569-573.

67. Hsu, H.-W., et al., *Ongoing hydrothermal activities within Enceladus.* Nature, 2015. **519**(7542): p. 207-210.

68. Waite, J.H., et al., *Cassini finds molecular hydrogen in the Enceladus plume: Evidence for hydrothermal processes.* Science, 2017. **356**(6334): p. 155.

69. Thomas, P.C., et al., *Enceladus's measured physical libration requires a global subsurface ocean.* Icarus, 2016. **264**: p. 37-47.

70. Russell, M.J., et al., *The Drive to Life on Wet and Icy Worlds.* Astrobiology, 2014. **14**(4): p. 308-343.

71. Tiselius, A., *A new apparatus for electrophoretic analysis of colloidal mixtures.* Transactions of the Faraday Society, 1937. **33**(0): p. 524-531.

72. Kyhse-Andersen, J., *Electroblotting of multiple gels: a simple apparatus without buffer tank for rapid transfer of proteins from polycrylamide to nitrocellulose.* Journal of Biochemical and Biophysical Methods, 1984. **10**(3): p. 203-209.

73. Kaltschmidt, E. and H.G. Wittmann, *Ribosomal proteins. VII: Two-dimensional polyacrylamide gel electrophoresis for fingerprinting of ribosomal proteins.* Analytical Biochemistry, 1970. **36**(2): p. 401-412.

74. Pappin, D.J.C., P. Hojrup, and A.J. Bleasby, *Rapid identification of proteins by peptide-mass fingerprinting.* Current Biology, 1993. **3**(6): p. 327-332.

75. El-Difrawy, S.A., et al., *High throughput system for DNA sequencing.* Review of Scientific Instruments, 2005. **76**(7): p. 074301.

76. Blazej, R.G., P. Kumaresan, and R.A. Mathies, *Microfabricated bioprocessor for integrated nanoliter-scale Sanger DNA sequencing.* Proceedings of the National Academy of Sciences, 2006. **103**(19): p. 7240-7245.

77. Scherer, J.R., P. Liu, and R.A. Mathies, *Design and operation of a portable scanner for high performance microchip capillary array electrophoresis.* Review of Scientific Instruments, 2010. **81**(11): p. 113105.

78. Dovichi, N.J., *Laser-based microchemical analysis.* Review of Scientific Instruments, 1990. **61**(12): p. 3653-3668.

79. Jorgenson, J.W. and K.D. Lukacs, *Zone electrophoresis in open-tubular glass capillaries.* Analytical Chemistry, 1981. **53**(8): p. 1298-1302.

80. Stockton, A.M., et al., *Capillary electrophoresis analysis of organic amines and amino acids in saline and acidic samples using the Mars organic analyzer.* Astrobiology, 2009. **9**(9): p. 823-31.

81. Stockton, A.M., et al., *Analysis of carbonaceous biomarkers with the Mars Organic Analyzer microchip capillary electrophoresis system: Aldehydes and ketones.* Electrophoresis, 2010. **31**(22): p. 3642-3649.

82. Stockton, A.M., et al., *Analysis of carbonaceous biomarkers with the Mars Organic Analyzer microchip capillary electrophoresis system: carboxylic acids.* Astrobiology, 2011. **11**(6): p. 519-28.

83. Hjertén, S., *High-performance electrophoresis: the electrophoretic counterpart of high-performance liquid chromatography.* Journal of Chromatography A, 1983. **270**: p. 1-6.

84. Thormann, W., et al., *Capillary isoelectric focusing: Effects of capillary geometry, voltage gradient and addition of linear polymer.* Journal of Chromatography A, 1987. **389**: p. 75-86.

85. Zhu, M., et al., *Factors affecting free zone electrophoresis and isoelectric focusing in capillary electrophoresis.* Journal of Chromatography A, 1989. **480**: p. 311-319.

86. Jensen, P.K., et al., *Probing Proteomes Using Capillary Isoelectric Focusing-Electrospray Ionization Fourier Transform Ion Cyclotron Resonance Mass Spectrometry.* Analytical Chemistry, 1999. **71**(11): p. 2076-2084.

87. Foret, F., E. Szoko, and B.L. Karger, *On-column transient and coupled column isotachophoretic preconcentration of protein samples in capillary zone electrophoresis.* Journal of Chromatography A, 1992. **608**(1): p. 3-12.

88. Chiesl, T.N., et al., *Enhanced Amine and Amino Acid Analysis Using Pacific Blue and the Mars Organic Analyzer Microchip Capillary Electrophoresis System.* Analytical Chemistry, 2009. **81**(7): p. 2537-2544.

89. Hjertén, S., J.-L. Liao, and R. Zhang, *High-performance liquid chromatography on continuous polymer beds.* Journal of Chromatography A, 1989. **473**: p. 273-275.

90. Ngola, S.M., et al., *Conduct-as-Cast Polymer Monoliths as Separation Media for Capillary Electrochromatography.* Analytical Chemistry, 2001. **73**(5): p. 849-856.

91. Loo, J.A., H.R. Udseth, and R.D. Smith, *Peptide and protein analysis by electrospray ionization-mass spectrometry and capillary electrophoresis-mass spectrometry.* Analytical Biochemistry, 1989. **179**(2): p. 404-412.

92. Swinney, K. and D.J. Bornhop, *Detection in capillary electrophoresis.* Electrophoresis, 2000. **21**(7): p. 1239-1250.

93. Skoog, D.A., F.J. Holler, and S.R. Crouch, *Principles of instrumental analysis*. Sixth edition. ed. 2007, Belmont, CA: Thomson Brooks/Cole.

94. Reyes, D.R., et al., *Micro Total Analysis Systems. 1. Introduction, Theory, and Technology.* Analytical Chemistry, 2002. **74**(12): p. 2623-2636.

95. Simpson, P.C., A.T. Woolley, and R.A. Mathies, *Microfabrication Technology for the Production of Capillary Array Electrophoresis Chips.* Biomedical Microdevices, 1998. **1**(1): p. 7-26.

96. Skelley, A.M., et al., *Development and evaluation of a microdevice for amino acid biomarker detection and analysis on Mars.* Proceedings of the National Academy of Sciences of the United States of America, 2005. **102**(4): p. 1041-1046.

97. Benhabib, M., et al., *Multichannel Capillary Electrophoresis Microdevice and Instrumentation for in Situ Planetary Analysis of Organic Molecules and Biomarkers.* Analytical Chemistry, 2010. **82**(6): p. 2372-2379.

98. Mora, M.F., A.M. Stockton, and P.A. Willis, *Analysis of thiols by microchip capillary electrophoresis for in situ planetary investigations.* Electrophoresis, 2013. **34**(2): p. 309-316.

99. Petersen, N.J., et al., *Effect of Joule heating on efficiency and performance for microchip-based and capillary-based electrophoretic separation systems: A closer look.* Electrophoresis, 2004. **25**(2): p. 253-269.

100. Mogensen, K.B., H. Klank, and J.P. Kutter, *Recent developments in detection for microfluidic systems.* Electrophoresis, 2004. **25**(21-22): p. 3498-3512.

101. Manz, A., et al., *Miniaturization of separation techniques using planar chip technology.* Journal of High Resolution Chromatography, 1993. **16**(7): p. 433-436.

102. Mathies, R.A., et al., *Laser-excited confocal-fluorescence gel scanner.* Review of Scientific Instruments, 1994. **65**(4): p. 807-812.

103. Skelley, A.M. and R.A. Mathies, *Chiral separation of fluorescamine-labeled amino acids using microfabricated capillary electrophoresis devices for extraterrestrial exploration.* Journal of chromatography. A, 2003. **1021**(1-2): p. 191-199.

104. Weiss, S., *Fluorescence Spectroscopy of Single Biomolecules.* Science, 1999. **283**(5408): p. 1676.

105. Cable, M.L., et al., *Microchip nonaqueous capillary electrophoresis of saturated fatty acids using a new fluorescent dye.* Analytical Methods, 2014. **6**(24): p. 9532-9535.

106. Kamei, T., et al., *Integrated Hydrogenated Amorphous Si Photodiode Detector for Microfluidic Bioanalytical Devices.* Analytical Chemistry, 2003. **75**(20): p. 5300-5305.

107. Krüger, J., et al., *Development of a microfluidic device for fluorescence activated cell sorting.* Journal of Micromechanics and Microengineering, 2002. **12**(4): p. 486-494.

108. Manz, A., et al., *Electroosmotic pumping and electrophoretic separations for miniaturized chemical analysis systems.* Journal of Micromechanics and Microengineering, 1994. **4**(4): p. 257-265.

109. Schwarz, M.A. and P.C. Hauser, *Recent developments in detection methods for microfabricated analytical devices.* Lab on a Chip, 2001. **1**(1): p. 1-6.

110. Kim, J., et al., *Pneumatically actuated microvalve circuits for programmable automation of chemical and biochemical analysis.* Lab on a Chip, 2016. **16**(5): p. 812-819.

111. Bacon, C.P., Y. Mattley, and R. DeFrece, *Miniature spectroscopic instrumentation: Applications to biology and chemistry.* Review of Scientific Instruments, 2003. **75**(1): p. 1-16.

112. Vysetti, B., *Current advances in the miniaturization of analytical instruments-applications in cosmochemistry, geochemistry, exploration, and environmental sciences.* Spectroscopy. Vol. 31. 2016. 40-44.

113. Grover, W.H., et al., *Monolithic membrane valves and diaphragm pumps for practical large-scale integration into glass microfluidic devices.* Sensors and Actuators B: Chemical, 2003. **89**(3): p. 315-323.

114. Paegel, B.M., et al., *Microfluidic Serial Dilution Circuit.* Analytical Chemistry, 2006. **78**(21): p. 7522-7527.

115. Jensen, E.C., et al., *Digitally programmable microfluidic automaton for multiscale combinatorial mixing and sample processing.* Lab on a Chip, 2013. **13**(2): p. 288-296.

116. Skelley, A.M., et al., *Organic amine biomarker detection in the Yungay region of the Atacama Desert with the Urey instrument.* Journal of Geophysical Research: Biogeosciences, 2007. **112**(G4): p. n/a-n/a.

117. Stockton, A.M., et al., *Polycyclic Aromatic Hydrocarbon Analysis with the Mars Organic Analyzer Microchip Capillary Electrophoresis System.* Analytical Chemistry, 2009. **81**(2): p. 790-796.

118. Stockton, A.M., et al. *The Mars Organic Analyzer: Instrumentation and Methods for Detecting Trace Organic Molecules in our Solar System*. in *Eighth International Conference on Mars*. 2014. Pasadena, CA: LPI.

119. Duca, Z.A., et al. *Development of an Extraterrestrial Organic Analyzer (EOA) for Highly Sensitive Organic Detection on a Kinetic Penetrator*. in *Biosignature Preservation and Detection in Mars Analog Environments*. 2016. Lake Tahoe, NV: LPI.

120. Stockton, A.M., et al. *An Organic Analyzer Instrument for Highly Sensitive In Situ Organic Detection on an Ice Shell Impact Penetrator Descent Probe*. in *3rd International Workshop on Instrumentation for Planetary Mission*. 2016. Pasadena: LPI.

121. Butterworth, A., et al. *Instrument for Capturing and Analyzing Trace Organic Molecules from Plumes for Ocean World Missions*. in *3rd International Workshop on Instrumentation for Planetary Missions*. 2016. Pasadena, CA.

122. Manz, A., et al., *Micromachining of monocrystalline silicon and glass for chemical analysis systems A look into next century's technology or just a fashionable craze?* TrAC Trends in Analytical Chemistry, 1991. **10**(5): p. 144-149.

123. Harrison, D.J., et al., *Capillary electrophoresis and sample injection systems integrated on a planar glass chip.* Analytical Chemistry, 1992. **64**(17): p. 1926-1932.

124. Seiler, K., D.J. Harrison, and A. Manz, *Planar glass chips for capillary electrophoresis: repetitive sample injection, quantitation, and separation efficiency.* Analytical Chemistry, 1993. **65**(10): p. 1481-1488.

125. Auroux, P.-A., et al., *Micro Total Analysis Systems. 2. Analytical Standard Operations and Applications.* Analytical Chemistry, 2002. **74**(12): p. 2637-2652.

126. Harrison, D.J., et al., *Micromachining a Miniaturized Capillary Electrophoresis-Based Chemical Analysis System on a Chip.* Science, 1993. **261**(5123): p. 895.

127. Khandurina, J., et al., *Integrated System for Rapid PCR-Based DNA Analysis in Microfluidic Devices.* Analytical Chemistry, 2000. **72**(13): p. 2995-3000.

128. Manz, A., N. Graber, and H.M. Widmer, *Miniaturized total chemical analysis systems: A novel concept for chemical sensing.* Sensors and Actuators B: Chemical, 1990. **1**(1): p. 244-248.

129. Ruha, A., S. Sallinen, and S. Nissila, *A real-time microprocessor QRS detector system with a 1-ms timing accuracy for the measurement of ambulatory HRV.* IEEE Transactions on Biomedical Engineering, 1997. **44**(3): p. 159-167.

130. Shichiri, M., et al., *Wearable Artificial Endocrine Pancreas with Needle-Type Glucose Sensor.* The Lancet, 1982. **320**(8308): p. 1129-1131.

131. Pantridge, J.F. and P.B. Halmos, *Conversion Oof Atrial Fibrllation by Direct Current Counter Shock.* British heart journal, 1965. **27**(1): p. 128-131.

132. Iseki, T., H. Tai, and K. Kimura, *A portable remote methane sensor using a tunable diode laser.* Measurement Science and Technology, 2000. **11**(6): p. 594-602.

133. Ramsey, J.M., S.C. Jacobson, and M.R. Knapp, *Microfabricated chemical measurement systems.* Nature Medicine, 1995. **1**(10): p. 1093-1095.

134. Goss, L.P., A.A. Smith, and M.E. Post, *Surface thermometry by laser-induced fluorescence.* Review of Scientific Instruments, 1989. **60**(12): p. 3702-3706.

135. Combs, C.A., *Fluorescence microscopy: a concise guide to current imaging methods.* Current protocols in neuroscience, 2010. **Chapter 2**: p. Unit2.1-Unit2.1.

136. Sanderson, M.J., et al., *Fluorescence microscopy.* Cold Spring Harbor protocols, 2014. **2014**(10): p. pdb.top071795-pdb.top071795.

137. Jacobson, S.C., et al., *High-Speed Separations on a Microchip.* Analytical Chemistry, 1994. **66**(7): p. 1114-1118.

138. Bliss, C.L., J.N. McMullin, and C.J. Backhouse, *Rapid fabrication of a microfluidic device with integrated optical waveguides for DNA fragment analysis.* Lab on a Chip, 2007. **7**(10): p. 1280-1287.

139. Kaigala, G.V., et al., *An inexpensive and portable microchip-based platform for integrated RT–PCR and capillary electrophoresis.* Analyst, 2008. **133**(3): p. 331-338.

140. Tian, J.-h., et al., *Real time detection and characterisation of bioaerosol emissions from wastewater treatment plants.* Science of The Total Environment, 2020. **721**: p. 137629.

141. Könemann, T., et al., *Spectral Intensity Bioaerosol Sensor (SIBS): An instrument for spectrally resolved fluorescence detection of single particles in real time.* Atmospheric Measurement Techniques, 2019. **12**(2): p. 1337-1363.

142. Cheng, B., et al., *Summertime fluorescent bioaerosol particles in the coastal megacity Tianjin, North China.* Science of The Total Environment, 2020. **723**: p. 137966.

143. Perquis, L., et al., *Capillary electrophoresis/visible-LED induced fluorescence of tryptophan: What's new?* ELECTROPHORESIS, 2019. **40**(18-19): p. 2342-2348.

144. Cable, M.L., et al., *Low-Temperature Microchip Nonaqueous Capillary Electrophoresis of Aliphatic Primary Amines: Applications to Titan Chemistry.* Analytical Chemistry, 2013. **85**(2): p. 1124-1131.

145. Spierings, G.A.C.M., *Wet chemical etching of silicate glasses in hydrofluoric acid based solutions.* Journal of Materials Science, 1993. **28**(23): p. 6261-6273.

146. Lagally, E.T., P.C. Simpson, and R.A. Mathies, *Monolithic integrated microfluidic DNA amplification and capillary electrophoresis analysis system.* Sensors and Actuators B: Chemical, 2000. **63**(3): p. 138-146.

147. Shultz-Lockyear, L.L., et al., *Effects of injector geometry and sample matrix on injection and sample loading in integrated capillary electrophoresis devices.* Electrophoresis, 1999. **20**(3): p. 529-538.

148. Paegel, B.M., et al., *High throughput DNA sequencing with a microfabricated 96-lane capillary array electrophoresis bioprocessor.* Proceedings of the National Academy of Sciences of the United States of America, 2002. **99**(2): p. 574-579.

149. Jacobson, S.C., et al., *Effects of Injection Schemes and Column Geometry on the Performance of Microchip Electrophoresis Devices.* Analytical Chemistry, 1994. **66**(7): p. 1107-1113.

150. Kašička, V., et al., *Contribution of capillary coiling to zone dispersion in capillary zone electrophoresis.* Electrophoresis, 1995. **16**(1): p. 2034-2038.

151. Paegel, B.M., et al., *Turn Geometry for Minimizing Band Broadening in Microfabricated Capillary Electrophoresis Channels.* Analytical Chemistry, 2000. **72**(14): p. 3030-3037.

152. Mora, M.F., et al., *Toward Total Automation of Microfluidics for Extraterrestial In Situ Analysis.* Analytical Chemistry, 2011. **83**(22): p. 8636-8641.

153. Stockton, A.M., et al., *Hydrolysis of 3-carboxy-6,8-difluoro-7-hydroxycoumarin (Pacific Blue™) succinimidyl ester under acidic and basic conditions.* Dyes and Pigments, 2013. **96**(1): p. 148-151.

154. Sun, W.-C., K.R. Gee, and R.P. Haugland, *Synthesis of novel fluorinated coumarins: Excellent UV-light excitable fluorescent dyes.* Bioorganic & Medicinal Chemistry Letters, 1998. **8**(22): p. 3107-3110.

155. Abrams, B., et al., *3-Carboxy-6-chloro-7-hydroxycoumarin: A highly fluorescent, water-soluble violet-excitable dye for cell analysis.* Analytical Biochemistry, 2009. **386**(2): p. 262-269.

156. Bruin, G.J.M., et al., *Capillary zone electrophoretic separations of proteins in polyethylene glycol-modified capillaries.* Journal of Chromatography A, 1989. **471**(C): p. 429-436.

157. Nashabeh, W. and Z. El Rassi, *Capillary zone electrophoresis of pyridylamino derivatives of maltooligosaccharides.* Journal of Chromatography A, 1990. **514**(C): p. 57-64.

158. Issaq, H.J., et al., *The effect of electric field strength, buffer type and concentration on separation parameters in capillary zone electrophoresis.* Chromatographia, 1991. **32**(3-4): p. 155-161.

159. Creamer, J.S., M.F. Mora, and P.A. Willis, *Enhanced Resolution of Chiral Amino Acids with Capillary Electrophoresis for Biosignature Detection in Extraterrestrial Samples.* Analytical Chemistry, 2017. **89**(2): p. 1329-1337.

160. Kim, J., et al., *Universal Microfluidic Automaton for Autonomous Sample Processing: Application to the Mars Organic Analyzer.* Analytical Chemistry, 2013. **85**(16): p. 7682-7688.

161. Dittrich, P.S. and P. Schwille, *An Integrated Microfluidic System for Reaction, High-Sensitivity Detection, and Sorting of Fluorescent Cells and Particles.* Analytical Chemistry, 2003. **75**(21): p. 5767-5774.

162. Flores Martinez, C.L., *Convergent evolution and the search for biosignatures within the solar system and beyond.* Acta Astronautica, 2015. **116**: p. 394-402.

163. Pang, K.D., et al., *The E ring of Saturn and satellite Enceladus.* Journal of Geophysical Research: Solid Earth, 1984. **89**(B11): p. 9459-9470.

164. Showalter, M.R., J. N. Cuzzi, and S.M. Larson, *Structure and particle properties of Saturn's E Ring.* Icarus, 1991. **94**(2): p. 451-473.

165. Hamilton, D.P. and J.A. Burns, *Origin of Saturn's E Ring: Self-Sustained, Naturally.* Science, 1994. **264**(5158): p. 550.

166. Porco, C.C., et al., *Cassini Observes the Active South Pole of Enceladus.* Science, 2006. **311**(5766): p. 1393.

167. Spahn, F., et al., *Cassini Dust Measurements at Enceladus and Implications for the Origin of the E Ring.* Science, 2006. **311**(5766): p. 1416.

168. Waite, J.H., et al., *Cassini Ion and Neutral Mass Spectrometer: Enceladus Plume Composition and Structure.* Science, 2006. **311**(5766): p. 1419.

169. Postberg, F., et al., *Macromolecular organic compounds from the depths of Enceladus.* Nature, 2018. **558**(7711): p. 564-568.

170. Khurana, K.K., et al., *Induced magnetic fields as evidence for subsurface oceans in Europa and Callisto.* Nature, 1998. **395**(6704): p. 777-780.

171. Kivelson, M.G., et al., *Galileo Magnetometer Measurements: A Stronger Case for a Subsurface Ocean at Europa.* Science, 2000. **289**(5483): p. 1340.

172. Smith, B.A., et al., *The Jupiter System Through the Eyes of Voyager 1.* Science, 1979. **204**(4396): p. 951.

173. Smith, B.A., et al., *The Galilean Satellites and Jupiter: Voyager 2 Imaging Science Results.* Science, 1979. **206**(4421): p. 927.

174. Wu, F.M., P. Gangopadhyay, and D.L. Judge, *Pioneer 10 ultraviolet photometer observations of Jovian UV emission in 1973.* Journal of Geophysical Research: Space Physics, 1995. **100**(A3): p. 3481-3493.

175. Null, G.W., *Gravity field of Jupiter and its satellites from Pioneer 10 and Pioneer 11 tracking data.* The Astronomical Journal, 1976. **81**: p. 1153.

176. Belton, M.J.S., et al., *Galileo's First Images of Jupiter and the Galilean Satellites.* Science, 1996. **274**(5286): p. 377.

177. Zahnle, K., et al., *Cratering rates in the outer Solar System.* Icarus, 2003. **163**: p. 263.

178. Cooper, J.F., et al., *Energetic Ion and Electron Irradiation of the Icy Galilean Satellites.* Icarus, 2001. **149**(1): p. 133-159.

179. Paranicas, C., R.W. Carlson, and R.E. Johnson, *Electron bombardment of Europa.* Geophysical Research Letters, 2001. **28**(4): p. 673-676.

180. Nordheim, T.A., K. Hand, and C. Paranicas, *Preservation of potential biosignatures in the shallow subsurface of Europa.* Nature Astronomy, 2018. **2**.

181. O'Brien, D.P., P. Geissler, and R. Greenberg, *A Melt-through Model for Chaos Formation on Europa.* Icarus, 2002. **156**(1): p. 152-161.

182. Schmidt, B.E., et al., *Active formation of 'chaos terrain' over shallow subsurface water on Europa.* Nature, 2011. **479**(7374): p. 502-505.

183. Sparks, W.B., et al., *Active Cryovolcanism on Europa?* The Astrophysical Journal, 2017. **839**(2): p. L18.

184. Hand, K.P., et al., *Report of the Europa Lander Science Definition Team*. 2017.

185. Kargel, J.S., et al., *Europa's Crust and Ocean: Origin, Composition, and the Prospects for Life.* Icarus, 2000. **148**(1): p. 226-265.

186. Tavares, M.F.M. and V.L. McGuffin, *Theoretical Model of Electroosmotic Flow for Capillary Zone Electrophoresis.* Analytical Chemistry, 1995. **67**(20): p. 3687-3696.

187. Green, J.S. and J.W. Jorgenson, *Minimizing adsorption of proteins on fused silica in capillary zone electrophoresis by the addition of alkali metal salts to the buffers.* Journal of Chromatography A, 1989. **478**: p. 63-70.

188. Chen, S. and D.J. Pietrzyk, *Separation of sulfonate and sulfate surfactants by capillary electrophoresis: effect of buffer cation.* Analytical Chemistry, 1993. **65**(20): p. 2770-2775.

189. Pietrzyk, D.J., S. Chen, and B. Chanthawat, *Enhanced capillary zone electrophoretic separation of dinitrophenyl-amino acid derivatives through control of electroosmotic flow by the buffer cation.* Journal of Chromatography A, 1997. **775**(1): p. 327-338.

190. Heath, J., et al., *Hydrogeochemical characterization of leaking, carbon dioxide-charged fault zones in east-central Utah, with implications for geologic carbon*

storage. Washington DC American Geophysical Union Geophysical Monograph Series, 2009. **183**: p. 147-158.

191. Han, W.S., et al., *Characteristics of CO2-driven cold-water geyser, Crystal Geyser in Utah: experimental observation and mechanism analyses.* Geofluids, 2013. **13**(3): p. 283-297.

192. Glennon, A. and R.M. Pfaff, *The operation and geography of carbon-dioxide-driven cold-water geysers.* GOSA Transactions, 2005. **9**: p. 184-192.

193. Shipton, Z., et al., *Analysis of CO2 leakage through 'low-permeability' faults from natural reservoirs in the Colorado Plateau, east-central Utah.* Geological Society, London, Special Publications, 2004. **233**: p. 43-58.

194. Mayo, A.L., D.B. Shrum, and T.C. Chidsey Jr., *Factors contributing to exsolving carbon dioxide in ground watersystems in the Colorado Plateau, Utah*, in *Geology of East-Central Utah*, T.C. Chidsey Jr., Editor. 1991, Utah Geology Associated Publications: Salt Lake City. p. 335-342.

195. [NRC], N.R.C., *Vision and Voyages for Planetary Science in the Decade 2013-2022*. 2011, Washington, D.C.: The National Academies Press.

196. Seewald, J.S., *Detecting molecular hydrogen on Enceladus.* Science, 2017. **356**(6334): p. 132.

197. Liu, C.N., N.M. Toriello, and R.A. Mathies, *Multichannel PCR-CE Microdevice for Genetic Analysis.* Analytical Chemistry, 2006. **78**(15): p. 5474-5479.

198. Jensen, E.C., et al., *Microvalve Enabled Digital Microfluidic Systems for High Performance Biochemical and Genetic Analysis.* JALA (Charlottesville, Va.), 2010. **15**(6): p. 455-463.

199. Toriello, N.M., et al., *Integrated microfluidic bioprocessor for single-cell gene expression analysis.* Proceedings of the National Academy of Sciences, 2008. **105**(51): p. 20173-20178.

200. Abbasi, F., H. Mirzadeh, and A.-A. Katbab, *Modification of polysiloxane polymers for biomedical applications: a review.* Polymer International, 2001. **50**(12): p. 1279-1287.

201. Makamba, H., et al., *Surface modification of poly(dimethylsiloxane) microchannels.* ELECTROPHORESIS, 2003. **24**(21): p. 3607-3619.

202. Zhou, J., A.V. Ellis, and N.H. Voelcker, *Recent developments in PDMS surface modification for microfluidic devices.* ELECTROPHORESIS, 2010. **31**(1): p. 2-16.

203. Stockton, A.M., et al., *Design rules and operational optimization for rapid, contamination-free microfluidic transfer using monolithic membrane valves.* Sensors and Actuators B: Chemical, 2013. **177**: p. 668-675.

204. Ferri, P., *Mission operations for the new Rosetta.* Acta Astronautica, 2006. **58**(2): p. 105-111.

205. Vargaftik, N.B., B.N. Volkov, and L.D. Voljak, *International Tables of the Surface Tension of Water.* Journal of Physical and Chemical Reference Data, 1983. **12**(3): p. 817-820.

206. Efimenko, K., W.E. Wallace, and J. Genzer, *Surface Modification of Sylgard-184 Poly(dimethyl siloxane) Networks by Ultraviolet and Ultraviolet/Ozone Treatment.* Journal of Colloid and Interface Science, 2002. **254**(2): p. 306-315.

207. Graubner, V.-M., et al., *Photochemical Modification of Cross-Linked Poly(dimethylsiloxane) by Irradiation at 172 nm.* Macromolecules, 2004. **37**(16): p. 5936-5943.

208. Meléndez-Zamudio, M., et al., *Study of a Polydimethylsiloxane (PDMS) Elastomer Generated by $gamma$ Irradiation: Correlation Between Properties (Thermal and Mechanical) and Structure (Crosslink Density Value).* Vol. 27. 2017. 1-11.

209. Duca, Z.A., et al., *Operation of pneumatically-actuated membrane-based microdevices for in situ analysis of extraterrestrial organic molecules after prolonged storage and in multiple orientations with respect to Earth's gravitational field.* Sensors and Actuators B: Chemical, 2018. **272**: p. 229-235.

210. Botta, O. and J.L. Bada, *Extraterrestrial Organic Compounds in Meteorites.* Surveys in Geophysics, 2002. **23**(5): p. 411-467.

211. Ehrenfreund, P. and S.B. Charnley, *Organic Molecules in the Interstellar Medium, Comets, and Meteorites: A Voyage from Dark Clouds to the Early Earth.* Annual Review of Astronomy and Astrophysics, 2000. **38**(1): p. 427-483.

212. Campagnola, S., B.B. Buffington, and A.E. Petropoulos, *Jovian tour design for orbiter and lander missions to Europa.* Acta Astronautica, 2014. **100**: p. 68-81.

213. Gershman, R. and R.A. Wallace, *Technology needs of future planetary missions.* Acta Astronautica, 1999. **45**(4): p. 329-335.

214. Wurz, P., et al., *An Impacting Descent Probe for Europa and the Other Galilean Moons of Jupiter.* Earth, Moon, and Planets, 2017. **120**(2): p. 113-146.

215. Stockton, A.M., et al. *An Ice Shell Impact Penetrator (IceShIP) for Organic Analysis on Europa*. in *American Geophysical Union*. 2015. San Fransisco, CA: AGU.

216. Morkoç, H., et al., *Large-band-gap SiC, III-V nitride, and II-VI ZnSe-based semiconductor device technologies.* Journal of Applied Physics, 1994. **76**(3): p. 1363-1398.

217. Broennimann, C., et al., *Development of an Indium bump bond process for silicon pixel detectors at PSI.* Nuclear Instruments and Methods in Physics Research Section A: Accelerators, Spectrometers, Detectors and Associated Equipment, 2006. **565**(1): p. 303-308.

218. Jiang, J., et al., *Fabrication of indium bumps for hybrid infrared focal plane array applications.* Infrared Physics & Technology, 2004. **45**(2): p. 143-151.

219. Speller, N.C., et al., *Green, Low-Cost, User-Friendly, and Elastomeric (GLUE) Microfluidics.* ACS Applied Polymer Materials, 2020. **2**(3): p. 1345-1355.

220. Ali, T., et al. *In vivo analysis of tissue by Raman microprobe: examination of human skin lesions and esophagus Barrett's mucosa on an animal model*. in *Proc.SPIE*. 2006.

221. Ho Mer Lin, D., et al., *The use of different dispersive Raman spectrometers for the analysis of uranium compounds.* Vibrational Spectroscopy, 2014. **73**: p. 102-110.

222. Castro-Esau, K.L., G.A. Sánchez-Azofeifa, and B. Rivard, *Comparison of spectral indices obtained using multiple spectroradiometers.* Remote Sensing of Environment, 2006. **103**(3): p. 276-288.

223. Luhung, I., et al., *Protocol Improvements for Low Concentration DNA-Based Bioaerosol Sampling and Analysis.* PLOS ONE, 2015. **10**(11): p. e0141158.

224. Udenfriend, S., et al., *Fluorescamine: A Reagent for Assay of Amino Acids, Peptides, Proteins, and Primary Amines in the Picomole Range.* Science, 1972. **178**(4063): p. 871.

225. Navarro-González, R., et al., *Mars-Like Soils in the Atacama Desert, Chile, and the Dry Limit of Microbial Life.* Science, 2003. **302**(5647): p. 1018.

226. Ewing, S.A., et al., *Rainfall limit of the N cycle on Earth.* Global Biogeochemical Cycles, 2007. **21**(3).

227. McKay, C.P., et al., *Temperature and Moisture Conditions for Life in the Extreme Arid Region of the Atacama Desert: Four Years of Observations Including the El Niño of 1997–1998.* Astrobiology, 2003. **3**(2): p. 393-406.

228. Parro, V., et al., *A Microbial Oasis in the Hypersaline Atacama Subsurface Discovered by a Life Detector Chip: Implications for the Search for Life on Mars.* Astrobiology, 2011. **11**(10): p. 969-996.

229. Quinn, R.C., et al., *Detection and characterization of oxidizing acids in the Atacama Desert using the Mars Oxidation Instrument.* Planetary and Space Science, 2005. **53**(13): p. 1376-1388.

VITA

Zachary A. Duca was born on August 17, 1992, in Lynn, MA, to Darol and Judith Duca and is a sibling to his brother Wesley Duca and his late sister Julia Seide. He graduated from Saugus Middle School in 2006 and from Malden Catholic High School (MCHS) 6th in his class in 2010. During his time at MCHS, Zachary participated in the KISS Institute for Practical Robotics Botball robotics program and aided in securing multiple regional victories with his team. Zachary attended Worcester Polytechnic Institute (WPI) in Worcester, MA, and was awarded the WPI Scholarship and a Chemistry and Biochemistry Scholarship. In 2014, he received his Bachelor of Science as a dual major in chemistry and biology & biotechnology. He became a member of the Delta Sigma Phi chapter of Alpha Chi Rho fraternity while attending WPI and served individual one-year terms as the organization's Recruitment Chair and President. He was also inducted into the fraternal honor society Order of Omega for his academic excellence. Zachary was accepted into the chemistry graduate program in the Department of Chemistry and Biochemistry at Georgia Institute of Technology (GT) in 2014 and was awarded a Cherry Emerson Scholarship. He joined the Stockton Group at the end of his first year and was awarded a NASA Space Technology Research Fellowship during his second year, as well as multiple other travel grants throughout his time at GT, including the Georgia Tech SGA Conference Fund, the Georgia Tech College of Sciences Travel Supplement, the NAI 2015 Astrobiology Summer School Scholarship, the CRIDC Travel Grant, and the 12th Rencontres du Vietnam Accommodation Fund. He is continuing his career in science as a

Savannah River National Laboratory (SRNL) Postdoctoral Research Associate at Savannah River Nuclear Solutions (SRNS), LLC, in September, 2020.